

Experimental investigation of ventilation effectiveness and dispersion of tracer gas in aircraft
cabin mockups

by

Jignesh Arvind Patel

B.S., University of Mumbai, 2010

A THESIS

submitted in partial fulfillment of the requirements for the degree

MASTER OF SCIENCE

Department of Mechanical & Nuclear Engineering
College of Engineering

KANSAS STATE UNIVERSITY
Manhattan, Kansas

2017

Approved by:

Co-Major Professor
Dr. Mohammad H.Hosni

Approved by:

Co-Major Professor
Dr. Byron W.Jones

Copyright

© Jignesh Patel 2017.

Abstract

The 2015 Airline Traffic Data released by the Bureau of Transportation Statistics (BTS 2016), shows that the commercial flights serving the United States carried an all-time high of 895.5 million passengers in 2015, which represents an approximate 5 % increase in number of passengers from 2014. There is a potential for disease and/or contaminants spreading throughout the airliner cabin raising health risks for passengers and crewmembers onboard flight. In order to limit health risks caused by spread of disease and/or contaminants, it is necessary to understand the various factors affecting the airliner cabin environment. Ventilation effectiveness is one such factor investigated in this study. In addition, experiments were conducted using tracer gas to study the dispersion of tracer gas inside an airliner cabin.

Experimental investigations were carried out inside a wide body, eleven-row Boeing 767 mockup cabin and a narrow body, five-row Boeing 737 mockup cabin. The Boeing 767 mockup cabin was constructed with actual aircraft components for air distribution to represent a real aircraft cabin, while the Boeing 737 mockup cabin is a fuselage section from an actual Boeing 737 aircraft. Thermal manikins occupied each seat of both the cabins to simulate thermal load from an average seated person. Four sets of experiments were conducted to evaluate the ventilation effectiveness and dispersion of tracer gas inside the aircraft cabin mockups. The first set of experiments investigated the ventilation effectiveness in a Boeing 767 mockup cabin. The second set of experiments determined the ventilation effectiveness at various heights and locations in a Boeing 737 mockup cabin. The third set of experiments focused on the study of dispersion of tracer gas inside a Boeing 737 mockup cabin with ventilation air. The last set of experiments aimed to study the dispersion of tracer gas inside a Boeing 737 mockup cabin with no ventilation air.

The ventilation effectiveness studies were performed by using Carbon Dioxide (CO₂) as a tracer gas and applying the tracer gas decay method. The conclusion for the first set of experiments was that air is efficiently and uniformly supplied to all seat locations inside the Boeing 767 mockup cabin with no clear patterns with respect to seat locations, i.e. window versus center versus aisle observed. From the second set of experiments, it was concluded that the ventilation effectiveness is uniform throughout the Boeing 737 mockup cabin irrespective of seat locations and elevations from cabin floor. In order to determine the spread of disease and/or

contaminants, a mixture of CO₂ and Helium (He) was used as a tracer gas. Tracer gas was released from particular locations inside the cabin to simulate gaseous contaminants released by a passenger and sampled at various locations throughout the cabin. The third set of experiments revealed that transport of tracer gas inside an aircraft cabin depends on the source location as well as on the relative distance of the sampling point from the source. Dispersion of tracer gas in the longitudinal direction was also observed inside the cabin. From the fourth set of experiments, it was concluded that even in the absence of ventilation air, considerable dispersion of tracer gas occurred in both the longitudinal and lateral directions.

Table of Contents

List of Figures	viii
List of Tables	xii
Acknowledgements	xiv
Dedication	xv
Chapter 1 - Introduction	1
Chapter 2 - Background and Literature Review	3
2.1 Standard Conditions inside an Aircraft Cabin	3
2.1.1 Aircraft Air Quality Standard	3
2.1.2 Ventilation Standard	4
2.2 Airflow Design	4
2.3 Ventilation Effectiveness	6
2.4 Pollutant and/or Contaminant Movement	7
Chapter 3 - Experimental Test Facility	8
3.1 Aircraft Mockup Cabins	8
3.1.1 Boeing 767 Mockup Cabin	8
3.1.1.1 Cabin Geometry	10
3.1.1.2 Seat Geometry	13
3.1.2 Boeing 737 Mockup Cabin	15
3.1.2.1 Cabin Geometry	15
3.1.2.2 Seat Geometry	19
3.1.3 Thermal Manikins	20
3.2 Air Supply System	21
3.2.1 Ductwork	22
3.2.1.1 Boeing 767 Mockup Cabin Ductwork	23
3.2.1.2 Boeing 737 Mockup Cabin Ductwork	23
3.2.2 Supply Air Conditioning System	24
3.2.3 Control System	26
3.3 Tracer Gas Supply and Measurement System	29
3.3.1 Tracer Gas Supply System	29

3.3.2 Tracer Gas Measurement System	30
3.3.3 Control System.....	33
Chapter 4 - Test Procedure	36
4.1 Ventilation Effectiveness Study.....	36
4.1.1 Tracer Gas Injection.....	36
4.1.2 Tracer Gas Measurement	37
4.1.3 Testing Procedure	41
4.1.4 Data Analysis Method.....	43
4.2 Dispersion of Tracer Gas Study	45
4.2.1 Testing with Ventilation Air	45
4.2.1.1 Tracer Gas Injection.....	45
4.2.1.2 Tracer Gas Measurement	47
4.2.1.3 Testing Procedure	48
4.2.1.4 Data Analysis Method.....	50
4.2.2 Testing with No Ventilation Air	52
4.2.2.1 Tracer Gas Injection.....	53
4.2.2.2 Tracer Gas Measurement	54
4.2.2.3 Testing Procedure	54
4.2.2.4 Data Analysis Method.....	56
4.3 Repeatability of CO ₂ Analyzers.....	57
4.4 Effect of Transient Response	57
4.5 Time Response of CO ₂ Analyzers	58
Chapter 5 - Results and Discussions	59
5.1 Ventilation Effectiveness	59
5.1.1 Ventilation Effectiveness Study inside the Boeing 767 Cabin	59
5.1.2 Ventilation Effectiveness Study inside the Boeing 737 Cabin	64
5.2 Dispersion of Tracer Gas with Ventilation Air.....	72
5.3 Dispersion of Tracer Gas with No Ventilation Air.....	85
5.4 Verification Experiments	92
5.4.1 Experiment Repeatability.....	93
5.4.2 Effect of Transient Response of Sampling System.....	93

5.4.3 Time Response of CO ₂ Analyzers	94
Chapter 6 - Summary and Conclusions	95
6.1 Ventilation Effectiveness	95
6.2 Dispersion of Tracer Gas with Ventilation Air.....	96
6.3 Dispersion of Tracer Gas with No Ventilation Air.....	96
Chapter 7 - Recommendations.....	97
References.....	98
Appendix A - Uncertainty Analysis.....	100
A.1 Supply Air Uncertainty	100
A.2 Tracer Gas Injection Uncertainty.....	102
A.3 Tracer Gas Sampling Uncertainty.....	105
A.4 Overall Uncertainty.....	107
Appendix B - Electronic Appendix Manual	110
B.1 Ventilation Effectiveness Folder Instructions	110
B.2 Dispersion of Tracer Gas with Ventilation Air Folder Instructions.....	111
B.3 Dispersion of Tracer Gas with No Ventilation Air Folder Instructions.....	111
Appendix C - The Effect of Recirculation on Local Ventilation Effectiveness	112
Introduction.....	112
Derivation	112
Discussion.....	114

List of Figures

Figure 2.1 Design Airflow Pattern Inside a Boeing 737 Cabin	5
Figure 2.2 Design Airflow Inside a Boeing 767 Cabin (Hunt & Space, 1994)	5
Figure 3.1 Southeast Face of the Wooden Enclosure (Beneke, 2010).....	9
Figure 3.2 East and West Hallways and Crawl Space (Beneke, 2010)	9
Figure 3.3 Boeing 767 Cabin Cross-Sectional View (Trupka, 2011).....	10
Figure 3.4 Boeing 767 Cabin Layout (Trupka, 2011)	11
Figure 3.5 Ventilation Gaps Inside the Boeing 767 Cabin	12
Figure 3.6 Linear Diffuser Slots Inside the Boeing 767 Cabin.....	12
Figure 3.7 Boeing 767 Center Seat Dimensions (Trupka, 2011).....	13
Figure 3.8 Boeing 767 Side Seat Dimensions (Trupka, 2011)	14
Figure 3.9 Side View Dimensions of the Seats (Trupka, 2011)	14
Figure 3.10 Boeing 737 Mockup Cabin.....	15
Figure 3.11 Boeing 737 Cabin Cross-Sectional View (Mo, 2012).....	16
Figure 3.12 Boeing 737 Cabin Layout.....	17
Figure 3.13 Linear Diffuser and Connectors Inside the Boeing 737 Cabin.....	18
Figure 3.14 Ventilation Grills Inside the Boeing 737 Cabin	18
Figure 3.15 Dimensions of the Boeing 737 Cabin Triple Seats	19
Figure 3.16 Side View of the Triple Seats.....	20
Figure 3.17 Thermal Manikins Occupying All Seats Inside the Boeing 767 Mockup Cabin	21
Figure 3.18 Ductwork for the Boeing 737 Mockup Cabin	22
Figure 3.19 Boeing 767 Cabin Supply Duct with Flexible Tubes Connected to Diffuser	23
Figure 3.20 Boeing 737 Cabin Supply Duct with Connection to the Diffuser	24
Figure 3.21 Schematic Flow Diagram of the Air Supply and Conditioning System.....	24
Figure 3.22 Graphical User Interface of the Supply Air Control System (Madden, 2015).....	27
Figure 3.23 Mass Flow Controllers Along with the Two Flow Meters.....	30
Figure 3.24 A Sampling Port Along With Tube Connections to a CO ₂ Analyzer.....	31
Figure 3.25 WMA-4 Infrared CO ₂ Gas Analyzers	31
Figure 3.26 Interior View of the Custom Made CO ₂ Gas Analyzer.....	32
Figure 3.27 The Flow Balancing System.....	33

Figure 3.28 DAQ System Along With the Power Supply	34
Figure 3.29 Screenshot of the LabVIEW Program (Madden, 2015)	35
Figure 4.1 Tracer Gas Injection Location For Ventilation Effectiveness Study.....	37
Figure 4.2 Sampling Ports Used for Testing at Breathing Level of Seated Adult Passengers	38
Figure 4.3 Sampling Ports Used for Testing at Breathing Level of Seated Infant Passengers.....	39
Figure 4.4 Measurement Locations for the Second and Third Series of Experiments	39
Figure 4.5 Sampling Ports Used for Testing at Breathing Level of Standing Passengers.....	40
Figure 4.6 Measuerment Locations for the Fourth Series of Experiments	41
Figure 4.7 Steady State Test Results for Boeing 767 Mockup Cabin	42
Figure 4.8 Steady State Test Results for Boeing 737 Mockup Cabin	43
Figure 4.9 Comparison Between Raw and Smoothened CO ₂ Concentration Data	45
Figure 4.10 Tracer Gas Injection Apparatus for Tracer Gas Dispersion Study.....	46
Figure 4.11 Tracer Gas Injection Locations for Dispersion Study With Ventilation Air.....	47
Figure 4.12 Sampling Locations for Various Injection Locations.....	48
Figure 4.13 Steady State Results for Point Source Injection	49
Figure 4.14 Setup for Calibration Process	50
Figure 4.15 Results from One of the Calibrations	51
Figure 4.16 Comparison of Suppy Air CO ₂ Concentration Data.....	52
Figure 4.17 Tracer Gas Injection Locations for Dispersion Study with No Ventilation Air.....	53
Figure 4.18 Result for Thermal Equilibrium Testing	55
Figure 4.19 CO ₂ Concentration Data	55
Figure 5.1 Result for Optimal Time Period Analysis	60
Figure 5.2 Seat-to-Seat Variation of e_L Rates.....	61
Figure 5.3 Seat-to-Seat Variation of E_L Values	63
Figure 5.4 Comparison Plot of Variation of E_L Rates from Mean for Set One Repeats	64
Figure 5.5 Result for Optimal Time Period Analysis	64
Figure 5.6 Location-to-Location Variation of e_L Rates	65
Figure 5.7 Location-to-Location Variation of E_L Values	66
Figure 5.8 Location-to-Location Variation of e_L Rates	67
Figure 5.9 Location-to-Location Variation of E_L Values	68
Figure 5.10 Location-to-Location Variation of e_L Rates	69

Figure 5.11 Location-to-Location Variation of E_L Values	69
Figure 5.12 Location-to-Location Variation of e_L Rates	70
Figure 5.13 Location-to-Location Variation of E_L Values	71
Figure 5.14 Comparison Plot of Variation of E_L Values from Mean for Series One Repeats	72
Figure 5.15 Longitudinal Dispersion of Tracer Gas	73
Figure 5.16 Lateral Dispersion of Tracer Gas	74
Figure 5.17 Average Normalized CO ₂ Counts for Seats 1A, 3A and 5A	74
Figure 5.18 Average Normalized CO ₂ Counts for Seats 1C, 3C and 5C.....	75
Figure 5.19 Average Normalized CO ₂ Counts for Seats 1D, 3D and 5D.....	75
Figure 5.20 Average Normalized CO ₂ Counts for Seats 1F, 3F and 5F.....	76
Figure 5.21 Longitudinal Dispersion of Tracer Gas	77
Figure 5.22 Lateral Dispersion of Tracer Gas	77
Figure 5.23 Longitudinal Dispersion of Tracer Gas	78
Figure 5.24 Lateral Dispersion of Tracer Gas	79
Figure 5.25 Lateral Dispersion of Tracer Gas	80
Figure 5.26 Longitudinal Dispersion of Tracer Gas	80
Figure 5.27 Average Normalized CO ₂ Counts for Seats 1B, 2A and 2C	81
Figure 5.28 Average Normalized CO ₂ Counts for Seats 1E, 4D and 4F	81
Figure 5.29 Average Normalized CO ₂ Counts for Seats 2D, 2E and 2F	82
Figure 5.30 Average Normalized CO ₂ Counts for Seats 3B, 4B and 5B.....	82
Figure 5.31 Average Normalized CO ₂ Counts for Seats 3E, 4E and 5E	83
Figure 5.32 Average Normalized CO ₂ Counts for Seats 4A and 4C	83
Figure 5.33 Lateral Dispersion of Tracer Gas	84
Figure 5.34 Longitudinal Dispersion of Tracer Gas	85
Figure 5.35 Lateral Dispersion of Tracer Gas	86
Figure 5.36 Longitudinal Dispersion of Tracer Gas	87
Figure 5.37 Average Normalized CO ₂ Counts for Seats 1B, 2A, 3B and 2C.....	87
Figure 5.38 Average Normalized CO ₂ Counts for Seats 2D and 2E	88
Figure 5.39 Average Normalized CO ₂ Counts for Seats 4A, 4C, 2F and 3E	88
Figure 5.40 Average Normalized CO ₂ Counts for Seats 4B, 5B and 1E.....	89
Figure 5.41 Average Normalized CO ₂ Counts for Seats 4D, 4E, 4F and 5E.....	89

Figure 5.42 Longitudinal Dispersion of Tracer Gas	90
Figure 5.43 Lateral Dispersion of Tracer Gas	91
Figure 5.44 Lateral Dispersion of Tracer Gas	92
Figure 5.45 Longitudinal Dispersion of Tracer Gas	92

List of Tables

Table 3.1 Temperature Probes Locations Along with Feedback and Control Parameters	28
Table 4.1 Test Procedure for Ventilation Effectiveness Testing	43
Table 4.2 Test Procedure for Tracer Gas Dispersion Study with Ventilation Air	49
Table 4.3 Test Procedure for Tracer Gas Dispersion Study with No Ventilation Air	56
Table 5.1 Average e_L Rates for Entire Cabin (min^{-1})	61
Table 5.2 Average E_L Values for Entire Cabin.....	62
Table 5.3 Comparison of Experimental Repeats for Boeing 767 Mockup Cabin	63
Table 5.4 Average e_L Rates for First Series of Experiments (min^{-1})	65
Table 5.5 Average E_L Values for First Series of Experiments	66
Table 5.6 Average e_L Rates for Second Series of Experiments (min^{-1}).....	67
Table 5.7 Average E_L Values for Second Series of Experiments	67
Table 5.8 Average e_L Rates for Third Series of Experiments (min^{-1}).....	68
Table 5.9 Average E_L Values for Third Series of Experiments.....	69
Table 5.10 Average e_L Rates for Fourth Series of Experiments (min^{-1}).....	70
Table 5.11 Average E_L Values for Fourth Series of Experiments	70
Table 5.12 Comparison of Experimental Repeats for Boeing 737 Mockup.....	71
Table 5.13 Average Normalized CO_2 Count for Injection at Centerline of Aisle at Row 1	73
Table 5.14 Average Normalized CO_2 Count for Injection at Centerline of Aisle at Row 3.....	76
Table 5.15 Average Normalized CO_2 Count for Injection at Centerline of Aisle at Row 5.....	78
Table 5.16 Average Normalized CO_2 Count for Injection at 2B	80
Table 5.17 Average Normalized CO_2 Count for Injection at 4E	84
Table 5.18 Average Normalized CO_2 Count for Injection at 2B	86
Table 5.19 Average Normalized CO_2 Count for Injection at Centerline of Aisle at Row 3.....	90
Table 5.20 Average Normalized CO_2 Count for Injection at 4E	91
Table 5.21 Experimental Repeatability Testing Results (min^{-1}).....	93
Table 5.22 Variation in e_L with Varying Sampling Tube Lengths (min^{-1}).....	94
Table 5.23 Time Response of CO_2 Analyzers (seconds).....	94
Table A.1 Supply Air Instruments Uncertainties.....	100
Table A.2 Calibration Gas and Tracer Gas Mixture Uncertainty	103

Table A.3 Mass Flow Controllers Uncertainty	103
Table A.4 Tracer Gas Injection Repeatability	104
Table A.5 Tracer Gas Sampling System Uncertainty	105
Table A.6 R-Squared and Linearity Values of Analyzers	105
Table A.7 Sampling Uncertainty for Dispersion Study With Ventilation Air.....	106
Table A.8 CO ₂ Analyzers Total Uncertainty for Dispersion Study With Ventilation Air	106
Table A.9 Sampling Uncertainty for Dispersion Study With No Ventilation Air.....	106
Table A.10 CO ₂ Analyzers Total Uncertainty for Dispersion Study With No Ventilation Air..	107

Acknowledgements

I would like to thank my mother, my sisters and the rest of my family for their constant support and encouragement throughout the pursuit of my Master's Degree. I would also like to thank my friends for always being there and for being patient with me.

I would like to thank Dr. Hosni and Dr. Jones for believing in me and giving me the opportunity to work on this project. Special thanks to Dr. Hosni for his constant encouragement and support throughout my graduate study. Heartfelt thanks to Dr. Jones for providing me with excellent technical guidance and always helping with any difficulties I faced throughout my Master's program.

I would also like to thank Dr. Eckels and Dr. Bennett for serving on my supervisory committee and providing me with their valuable guidance and suggestions.

Dedication

To
My Mother
&
My Grandmother

Chapter 1 - Introduction

There are continued interests regarding effects of aircraft air quality on the health of passengers and crewmembers. With an increasing number of passengers travelling both domestically and internationally, it has become essential to address aircraft air quality concerns. Inside an aircraft cabin, passengers and crewmembers are exposed to various environmental factors like reduced pressure, low humidity levels, high occupant density and contamination of air. It is the responsibility of the environmental control system (ECS) of an aircraft to maintain a healthy and comfortable cabin environment. In order to reduce health risks, the ECS needs to efficiently remove contaminants from the cabin.

To address concerns related to aircraft air quality as well as to investigate transport phenomena in aircraft cabins, the Air Transportation Center of Excellence for Airliner Cabin Environment Research (ACER) team was formed. ACER employs experimental data collection in aircraft cabin mockups, computational fluid dynamic (CFD) analysis as well as other investigation methods. Many experimental and numerical studies have been done by the previous ACER team members to examine airflow distribution and turbulence in the longitudinal direction of the cabin mockups (Shehadi, 2015), ventilation air and passenger loading effects on airflow patterns (Madden, 2015), effect of gaspers on airflow patterns (Anderson, 2012), beverage cart wake effects (Trupka, 2011), longitudinal particulate dispersion (Beneke, 2010), numerical models for predicting transport (Jones, 2009), movement of tracer gas and particulate contaminants (Lebbin, 2006).

Effectiveness of the ventilation system in the aircraft cabin mockups is one of the topics focused on in the research documented in this thesis. Carbon Dioxide (CO₂) is used as a tracer for this study. Tracer gas is introduced into the cabin mockups by directly injecting it into the supply air. The gas concentration is then sampled at various locations of interest inside the cabin mockups. Another topic studied in this research is the spread of contaminants inside an aircraft cabin mockup with and without ventilation air. To simulate the gaseous or fine particulate contaminants, a mixture of CO₂ and Helium (He) was used as a tracer gas. Tracer gas is injected at particular locations inside the cabin. The tracer gas concentration is then sampled at various locations of interest throughout the cabin for each injection location to determine the flow characteristics. To study the dispersion of contaminants with no ventilation air, the cabin is

supplied with conditioned air for three hours to bring it to uniform steady state thermal conditions. Tracer gas mixture is then injected at particular locations inside the cabin until steady state CO₂ concentration is reached. The air supply is then cut-off with continued CO₂ injection and CO₂ concentration measurements are taken at various seat locations for each injection location.

Chapter 2 - Background and Literature Review

Because of frequent air travel and long flight durations, disease and/or contaminants transmission is an issue of major concern. As passengers occupy the same space for the entire flight duration, the air quality inside the cabin could have a major impact on the health of the passengers. The ECS of an aircraft controls the ventilation, pressure, temperature and filtration to ensure a safe cabin environment. In addition, rigorous regulations are set to make the cabin environment safe.

2.1 Standard Conditions inside an Aircraft Cabin

In order to ensure the protection and comfort of onboard passengers and crewmembers, the Federal Aviation Administration (FAA) has set regulations for the quality of air supplied to the aircraft cabin. The properties usually associated with the air quality include relative humidity, temperature, pressure, contaminants level and ventilation rates.

2.1.1 Aircraft Air Quality Standard

Physiological problems such as hypoxia, decompression sickness and altitude sickness associated with low outside pressure at average flight altitudes of 10,970 m (36,000 ft) necessitate pressurization of an aircraft cabin. According to FAA regulations section 25.841, the cabin pressure altitude should not exceed 2,440 m (8,000 ft) at any time during flight, except in case of an emergency (FAA 2010). In order to comply with these regulations most modern aircraft are pressurized to an equivalent altitude of 1,524 m (5,000 ft) to 2,440 m (8,000 ft). According to FAA, the acceptable range for temperature of the cabin is 18.3 °C (65 °F) to 26.7 °C (80 °F) (FAA 2010). In addition, according to FAA regulations section 25.831 the maximum allowable temperature difference between various zones of the cabin is 2.8 °C (5 °F) (FAA 2010). Both low humidity and high humidity can cause discomfort and may have an impact on the health of the passengers and crewmembers (Shehadi 2010). Although FAA does not impose any regulations on the humidity level, it recommends that the relative humidity of cabin air be maintained within the range of 20 % to 70 %. According to FAA regulations section 25.831, CO₂ concentration in the cabin must not exceed 5,000 parts per million. Additionally, Carbon Monoxide (CO) concentration is not to exceed 50 parts per million at any time (FAA 2010).

2.1.2 Ventilation Standard

In order to remove contaminants and heat from the cabin, fresh air needs to be supplied to the cabin at an optimal rate. The FAA regulations section 25.841 requires each occupant be supplied with at least 0.25 kg/min (0.55 lb/min) of fresh air (FAA 2010), which is equivalent to 0.283 m³/min (10 ft³/min) at an approximate height of 2,440 m (8,000 ft) cabin altitude (ASHRAE, 2007). In compliance with this regulation, up until the 1980's most commercial aircraft supplied 0.57 m³/min (20 ft³/min) of outside/fresh air per occupant (Shehadi, 2010). However, most modern aircraft in service today supply ventilation air to the cabin at the same rate, but with 50 % of it being fresh air and 50 % being recirculated air while still complying with the FAA regulation. High efficiency particulate air (HEPA) filters are used to remove bacteria, fungi and other contaminants from the recirculated air. Although FAA does not necessitate the use of HEPA filters, they play a vital role in mitigating the spread of disease and/or contaminants by filtering out most of the impurities from the recirculation air before it is mixed with fresh outside air to be supplied to the cabin.

2.2 Airflow Design

In both the twin-aisle and single-aisle aircraft cabin types used in this research, the conditioned air is supplied to the cabin through linear diffusers mounted along the length of supply duct bottom, which is located above the ceiling at the center of the cabin. In addition, air flows through gaspers located over each passenger seat to provide personal ventilation. The air circulates through the cabin and exits through the exhaust grills located at the cabin walls near the floor as shown in Figure 2.1 and Figure 2.2. The ventilation system is designed in such a manner with an expectation of creating circulation in the lateral direction throughout the cabin length. The main purpose of having a dominant lateral flow is to restrict the spread of disease and/or contaminants to rows adjacent to the source thus preventing its spread in the longitudinal direction (Madden, 2015). However previous research conducted to study the airflow in aircraft cabins suggest that the flow is highly chaotic and turbulent resulting in considerable flow in both the lateral and longitudinal directions (Shehadi 2015, Wang et al. 2006, Beneke, 2010).

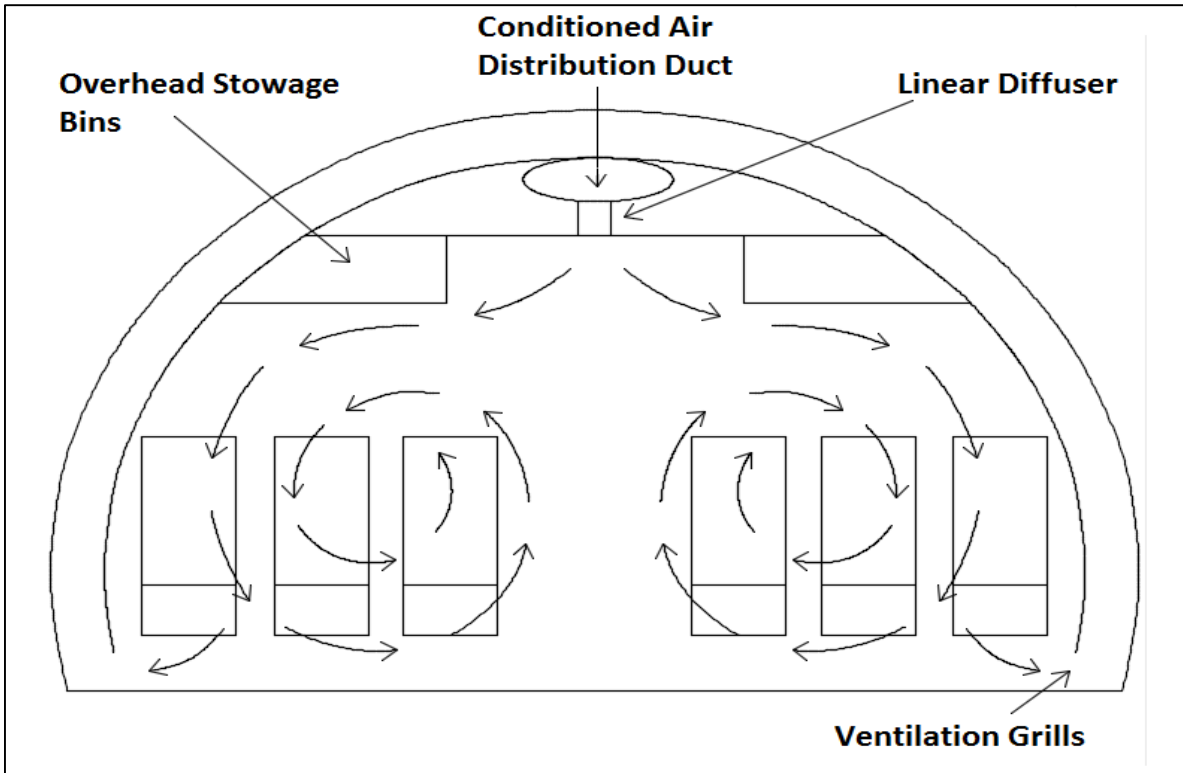


Figure 2.1 Design Airflow Pattern Inside a Boeing 737 Cabin

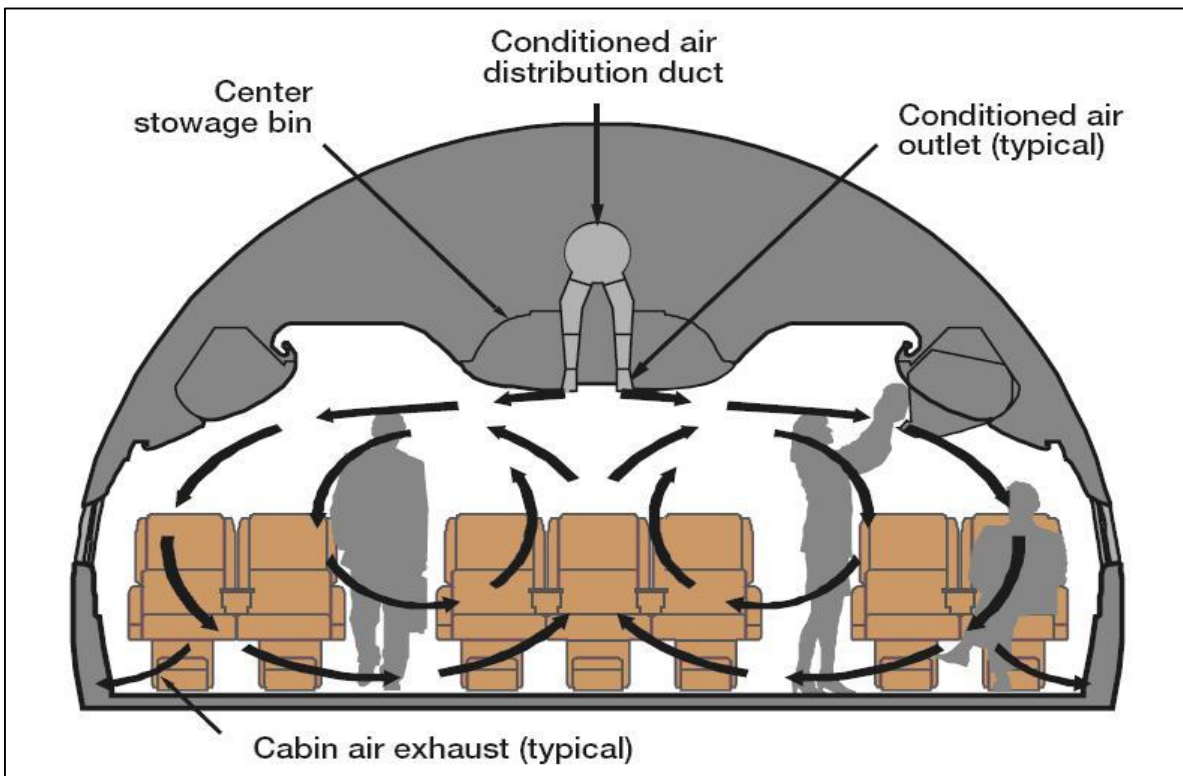


Figure 2.2 Design Airflow Inside a Boeing 767 Cabin (Hunt & Space, 1994)

2.3 Ventilation Effectiveness

During flight, fresh air is bled from the compressor of the gas turbine engine and is heated, compressed, cooled and mixed with the filtered recirculated air before being supplied to the cabin. On ground, an auxiliary power unit (APU) is used to supply fresh air. The cabin space should be well ventilated to ensure efficient removal of contaminants and to maintain thermal uniformity for human comfort, thus, making study of the ventilation system of an aircraft cabin imperative. Ventilation effectiveness is one of the major factors affecting the quality of air inside the cabin. Ventilation effectiveness is defined as the ability of the air distribution system to remove internally generated pollutants or contaminants from a building, zone or space (ASHRAE, 2013).

Not much published study has been done to evaluate the effectiveness of the ventilation system of an aircraft. In the study conducted by Wang et al. (2008), they experimentally evaluated the ventilation effectiveness and examined the air velocity distribution in a five-row Boeing 767-300 cabin mockup. They used the tracer gas technique to evaluate the local mean age of air and the ventilation effectiveness factor. To determine the velocity distribution inside the cabin, they used the volumetric particle tracking velocimetry technique. From their study, they concluded that the ventilation effectiveness factor at most seat locations was better than a perfect mixing model indicating efficient removal of contaminants. They reported that the ventilation effectiveness factor was within the 1 to 1.4 range while the local mean age of air ranged from approximately 2 to 6 minutes. These ventilation effectiveness values are higher than the values measured in the study reported in this thesis, where ventilation effectiveness ranged from 0.78 to 0.93 for the Boeing 767 cabin, and for the Boeing 737 cabin, it ranged from 0.77 to 0.83. Wang et al. also carried out experiments to study the relation of the air supply rate with the local mean age of air and ventilation effectiveness factor. Their results suggested that the ventilation effectiveness factor was unaffected by the air supply rate whereas the local mean age of air decreased linearly with the increase in air supply rate. From their velocity distribution study, they found that the flow inside the cabin was highly lateral and that local mean age of air at a particular area was affected by the velocity magnitude along with the air flow patterns in that area.

2.4 Pollutant and/or Contaminant Movement

Contaminants inside an aircraft cabin can originate from various sources. An infected passenger may be one of the sources of contaminants. Contaminants may enter the cabin from outside the aircraft, as the fresh air supplied to the cabin is not filtered. The bleed air from the engine may also be contaminated with oil particles or hazardous contaminants may be released inside the cabin with malicious intents. In order to mitigate the spread of contaminants it is important to study the movement of contaminants inside an aircraft cabin.

Many experimental and numerical studies have been carried out previously to study the airflow characteristics and transport of contaminants inside an aircraft cabin. Zang et al. (2009) carried out CFD simulations to determine the airflow, temperature field and dispersion of gaseous and particulate contaminants inside a Boeing 767 aircraft cabin and collected experimental data to validate these results. They used 0.7- μm di-ethyl-hexafluoride particles to evaluate particulate contaminants and sulfur hexafluoride gas to simulate gaseous contaminants. From their study, they noticed two large lateral circulations, which were asymmetric about the center of the cabin. Their results from CFD simulations agreed reasonably with the experimental data for the velocity field, temperature field and particulate and gaseous contaminants. Singh et al. (2002) conducted experimental and numerical analysis to determine the effects of occupant density on air distribution inside a Boeing 737 cabin. They concluded from their study that occupant density inside an aircraft cabin has a significant effect on the airflow patterns. Beneke (2010) studied the dispersion of fine particles in a Boeing 767 mockup cabin. He concluded that the fine particles concentration decreased exponentially moving away from the source along the longitudinal direction. Anderson (2012) studied the effects of personal ventilation system on airflow and on transmission of contaminants inside a Boeing 767 mockup cabin. He found that gaspers created an air curtain significantly disrupting the longitudinal transport of contaminants and based on the orientation of the gaspers, they can have a significant or negligible impact on the transport of contaminants inside an aircraft cabin.

Chapter 3 - Experimental Test Facility

The experimental test facility used for testing consists of the aircraft cabin mockups, equipment to condition the air supplied to the mockup cabins, thermal manikins to generate thermal load, a tracer gas injection and an air sampling system. This chapter provides detailed description of each of these components.

3.1 Aircraft Mockup Cabins

As mentioned previously, all the experiments for this research were conducted inside a Boeing 767 and a Boeing 737 mockup cabins. The aircraft cabin mockups are located at the Airliner Cabin Environment Research Lab (ACER) at Kansas State University located in Manhattan, Kansas. The following sections provide detailed information about each of the cabin mockups used for testing.

3.1.1 Boeing 767 Mockup Cabin

The Boeing 767 mockup cabin was constructed to simulate an actual Boeing 767 aircraft cabin environment. The mockup cabin was built inside a large wooden enclosure, which is 9.75 m (32 ft) long, 7.32 m (24 ft) wide and 4.88 m (16 ft) tall as seen in Figure 3.1. The enclosure houses the cabin mockup, two hallways one on each side of the cabin, crawl space below the cabin and space above the cabin as shown in Figure 3.2. The two hallways, space above the cabin and crawl space act as a plenum for the cabin. The east hallway contains the tracer gas injection system and the data acquisition system (DAQ). The space above the cabin contains the air distribution system for the cabin. There are doors on each end of both the hallways. Two exhaust fans are installed at the top south face of the enclosure to maintain the cabin enclosure at neutral pressure. In order to maintain a safe O₂ concentration level inside the laboratory, a CellarSafe CS100 O₂ detector/alarm was installed in the east hallway of the enclosure.



Figure 3.1 Southeast Face of the Wooden Enclosure (Beneke, 2010)



Figure 3.2 East and West Hallways and Crawl Space (Beneke, 2010)

3.1.1.1 Cabin Geometry

The cabin space inside the wooden enclosure is 9.41 m (30.87 ft) long and 4.72 m (15.45 ft) wide. The cross-sectional cabin profile along with detailed dimensions of the Boeing 767 mockup cabin is shown in Figure 3.3. Lebbin (2006) derived the equations to generate the cabin's detailed interior profile.

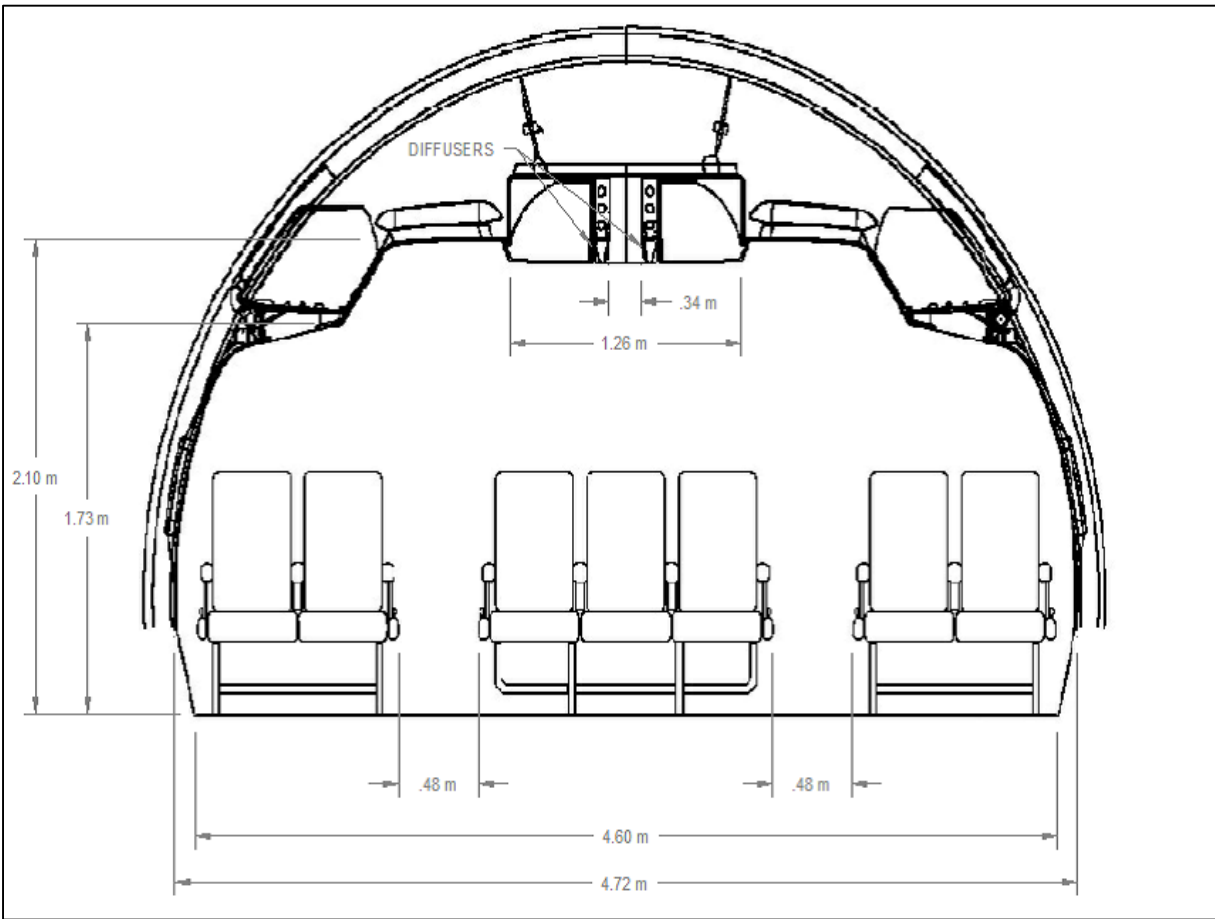


Figure 3.3 Boeing 767 Cabin Cross-Sectional View (Trupka, 2011)

The front of the cabin is towards the south face of the enclosure. The back of the cabin at the north face of the enclosure has two doors for access to the cabin space as can be seen in Figure 3.4. The Boeing 767 cabin has a 2-3-2 seat configuration. The mockup cabin contains eleven rows and seven seats per row for a total of seventy-seven seats. The rows are numbered one to eleven from front to back and the seats are labeled A to G from left to right as shown in Figure 3.4.

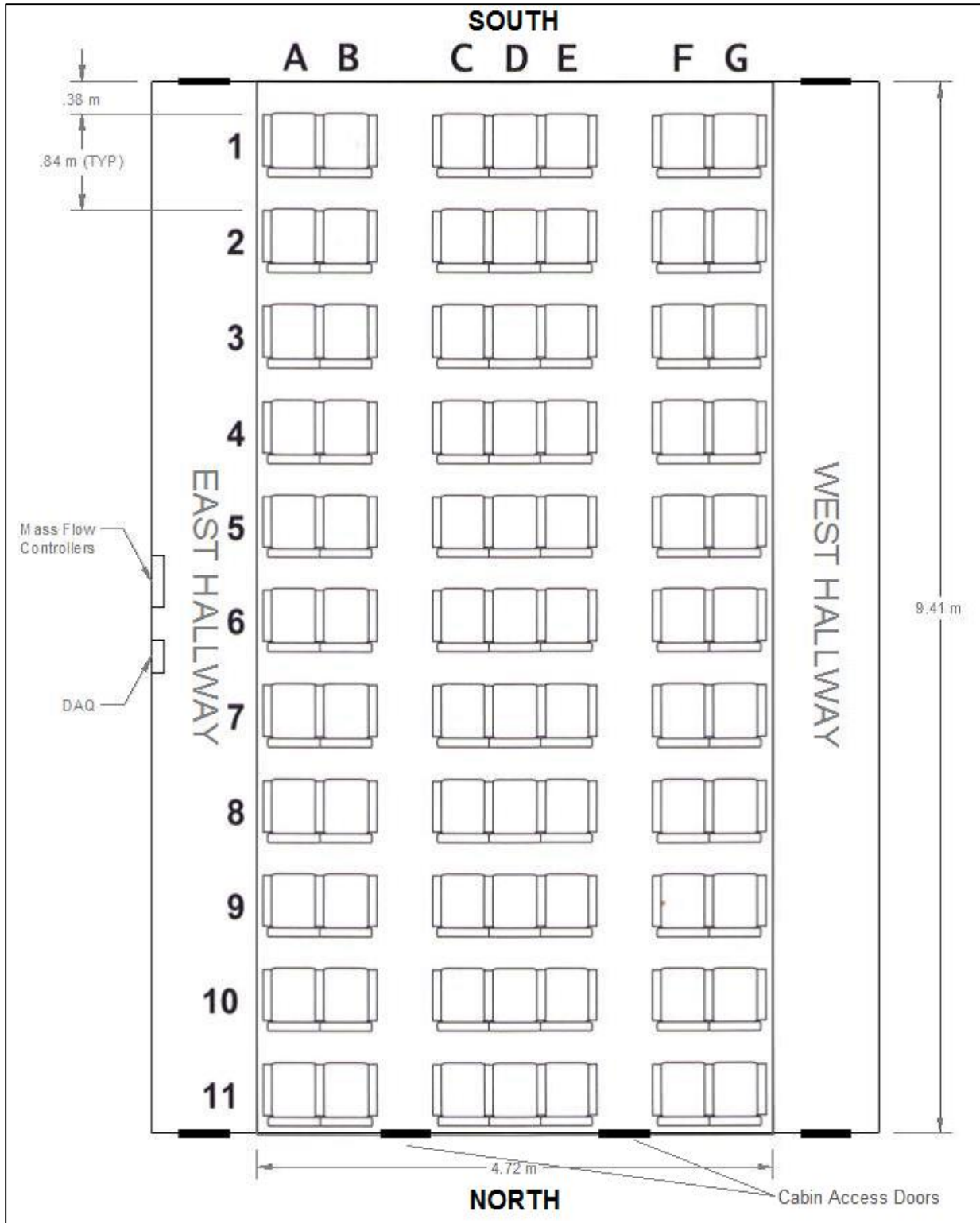


Figure 3.4 Boeing 767 Cabin Layout (Trupka, 2011)

Air enters the cabin through two linear diffusers located at the center ceiling of the cabin. After circulation, air exits the cabin through the ventilation gaps located at the cabin sidewalls near the floor. The ventilation gaps and the linear diffuser inside the Boeing 767 cabin mockup are shown in Figures 3.5 and 3.6 respectively.

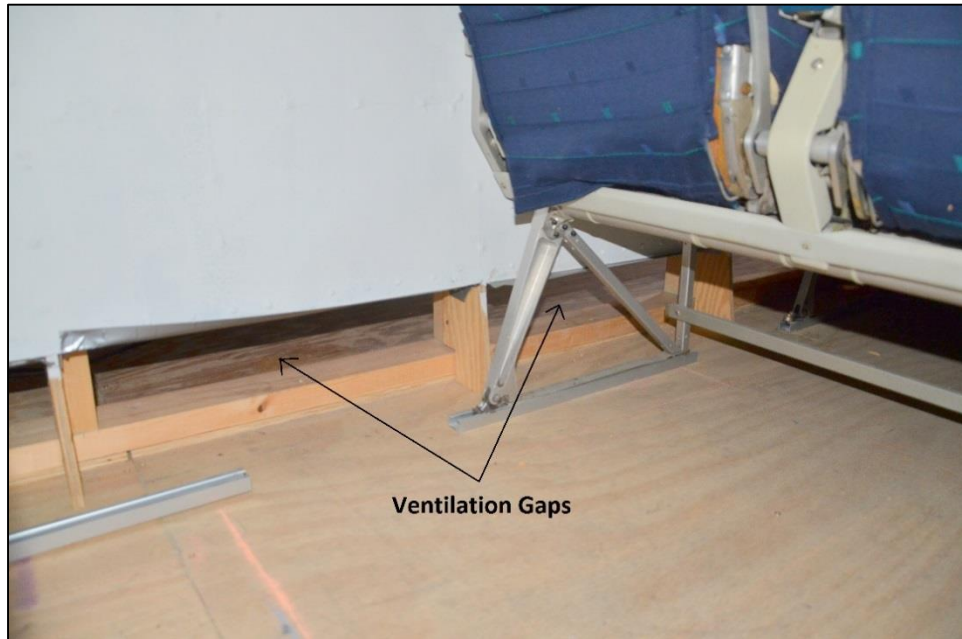


Figure 3.5 Ventilation Gaps Inside the Boeing 767 Cabin



Figure 3.6 Linear Diffuser Slots Inside the Boeing 767 Cabin

3.1.1.2 Seat Geometry

As mentioned earlier, the Boeing 767 cabin has a 2-3-2 seat configuration. The center-to-center distance between seats in consecutive rows is 0.84 m (2.75 ft). The two aisles separating the seats inside the cabin are 0.48 m (1.58 ft) wide. The seats are placed 0.38 m (1.25 ft) from the front wall of the cabin. Geometrical dimensions of the center and side seats placed inside the cabin are shown in Figures 3.7, 3.8 and 3.9. The above mentioned dimensions are representative of dimensions in a real Boeing 767 aircraft cabin.

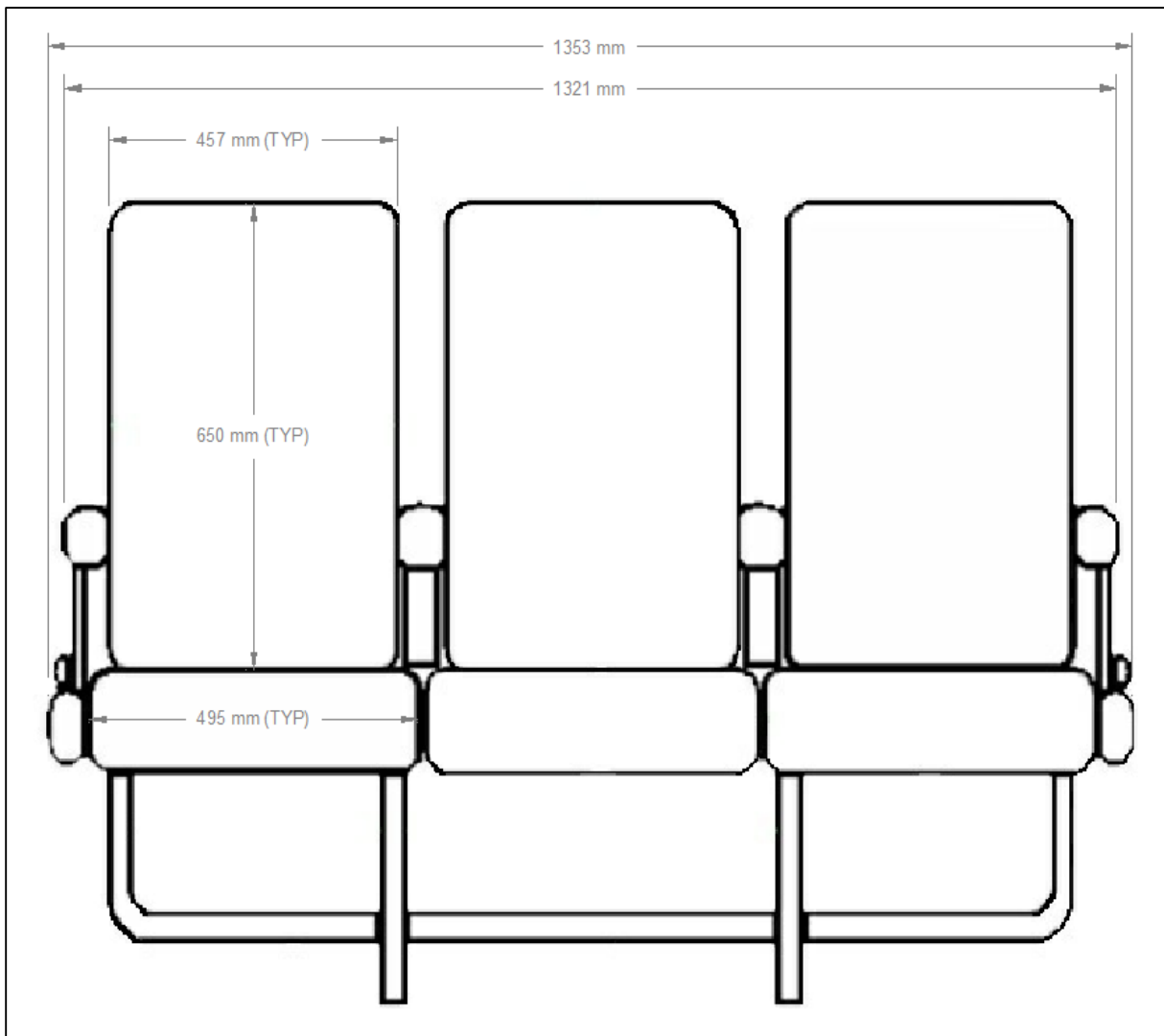


Figure 3.7 Boeing 767 Center Seat Dimensions (Trupka, 2011)

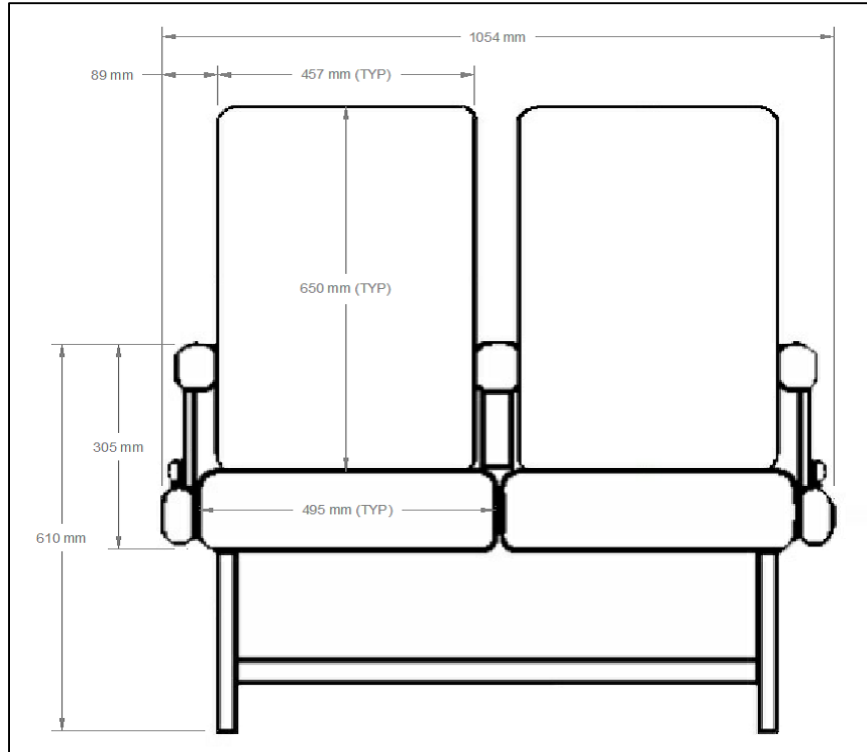


Figure 3.8 Boeing 767 Side Seat Dimensions (Trupka, 2011)



Figure 3.9 Side View Dimensions of the Seats (Trupka, 2011)

3.1.2 Boeing 737 Mockup Cabin

The Boeing 737 mockup cabin is a 5.6 m (18.3 ft) long, 3.6 m (11.8 ft) wide and 2.8 m (9.2 ft) high, fuselage section from an actual Boeing 737 aircraft as shown in Figure 3.10. The front and back ends of the cabin are sealed using plywood sheets and insulated from the inside using insulation boards. The back of the cabin that faces south has a door for access to the cabin space as can be seen in Figure 3.12. The front of the cabin contains the tracer gas sampling system and electrical boxes to supply power to the manikins.



Figure 3.10 Boeing 737 Mockup Cabin

3.1.2.1 Cabin Geometry

The inner cabin space is 4.83 m (15.85 ft) long and has a floor width of 2.84 m (9.33 ft). The cross-sectional cabin profile along with detailed dimension of the Boeing 737 mockup cabin is shown in Figure 3.11.

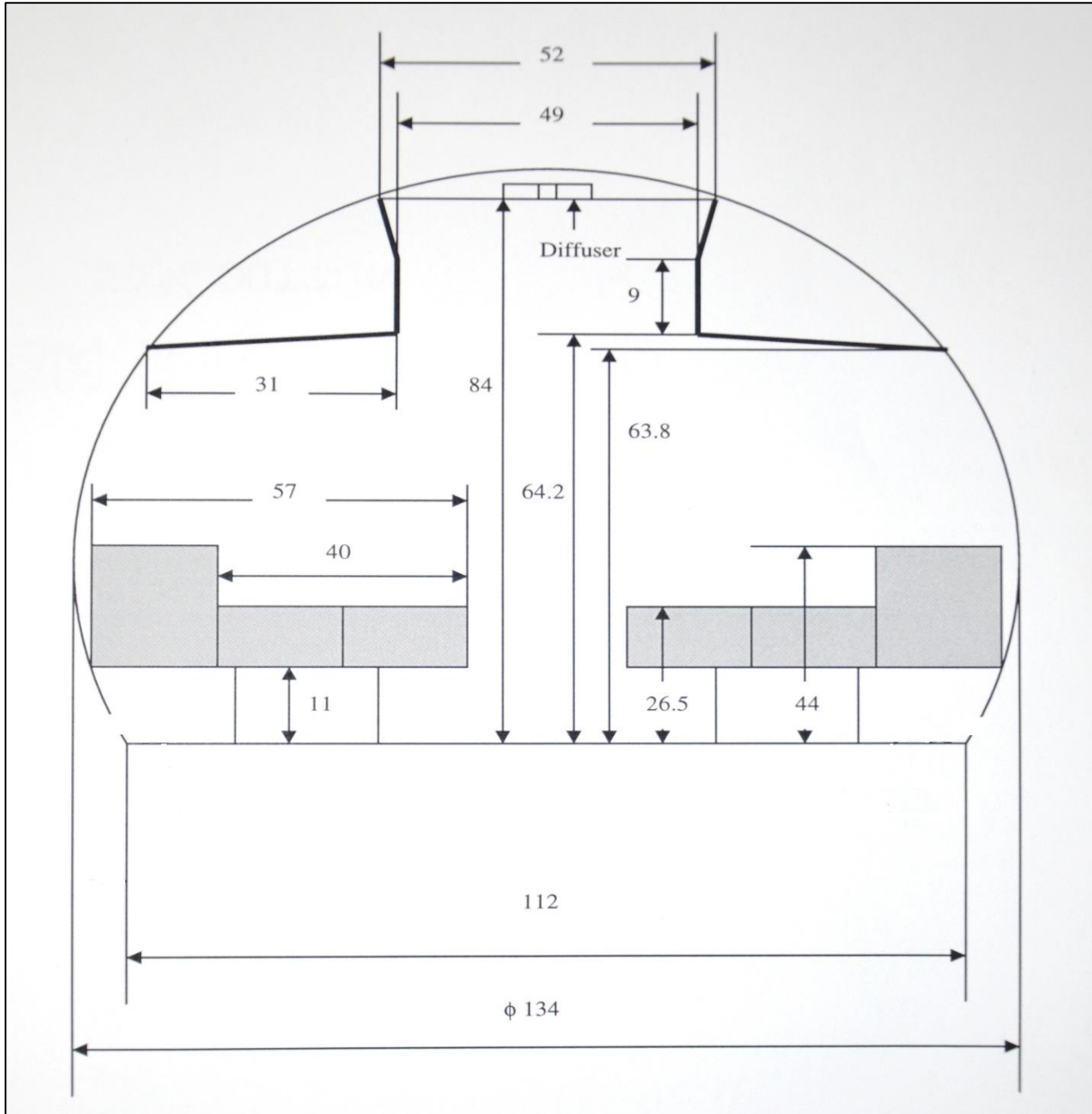


Figure 3.11 Boeing 737 Cabin Cross-Sectional View (Mo, 2012)

The Boeing 737 cabin has a 3-3 seat configuration. The mockup cabin contains five rows and six seats per row for a total of thirty seats. The rows are labeled one to five from front to back and the seats are labelled A to F from left to right as shown in Figure 3.12.

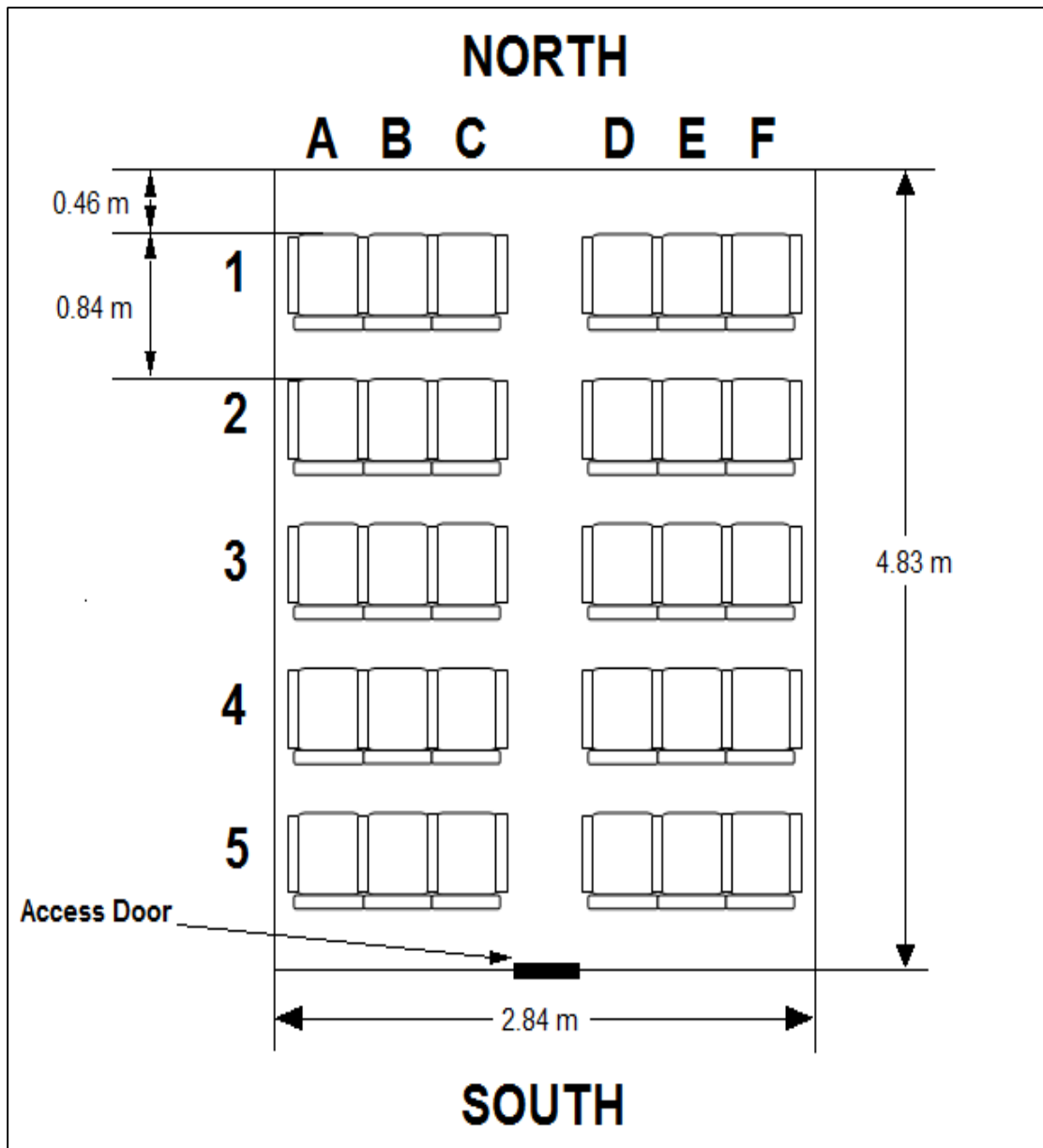


Figure 3.12 Boeing 737 Cabin Layout

Air enters the cabin through a diffuser installed in the ceiling at the center of the cabin as shown in Figure 3.13. The diffuser only covers 4.02 m (13.2 ft) of the cabin length with a gap of 0.41 m (1.33 ft) from both end walls of the cabin. The diffuser is made up of sections linked using connectors. Figure 3.13 shows the locations of these connectors. The connectors are responsible for breaking the flow along the length of the cabin as no air flows through them. Hence, connectors and their locations are important factors in establishing uniform airflow inside the cabin.

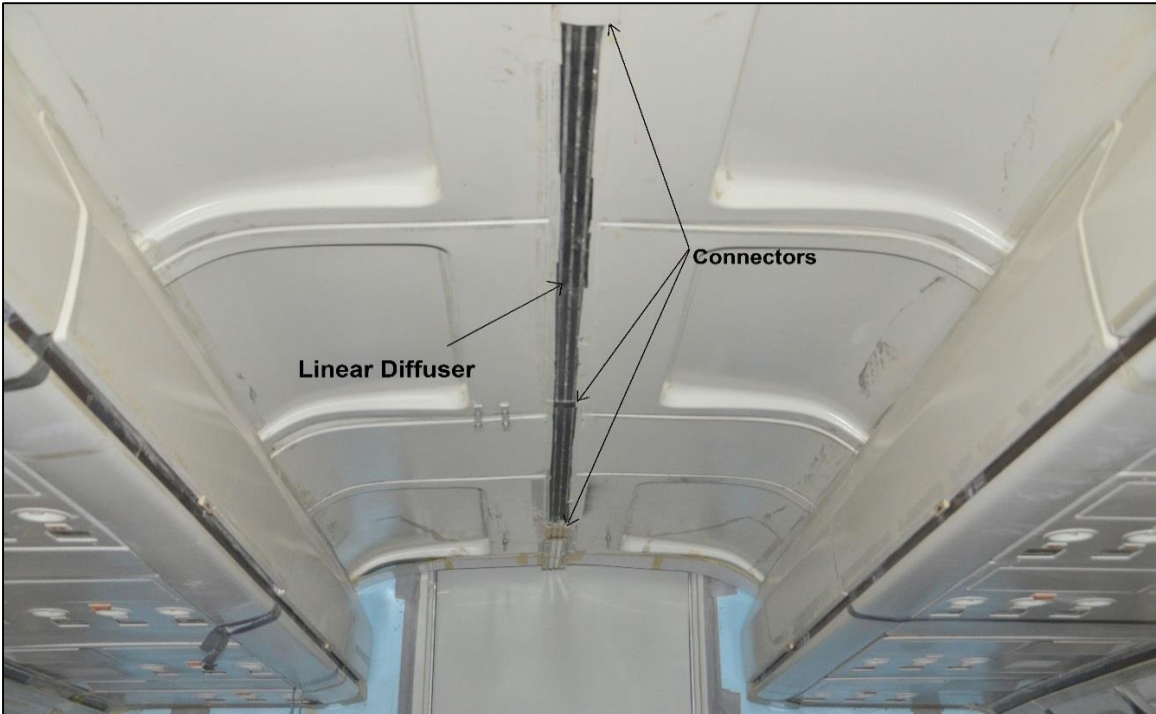


Figure 3.13 Linear Diffuser and Connectors Inside the Boeing 737 Cabin

After circulation, air exits the cabin through the exhaust grills located along the length of the cabin sidewalls near the floor. Air from the cabin is exhausted into the open space of the testing facility. The exhaust grills are shown in Figure 3.14.

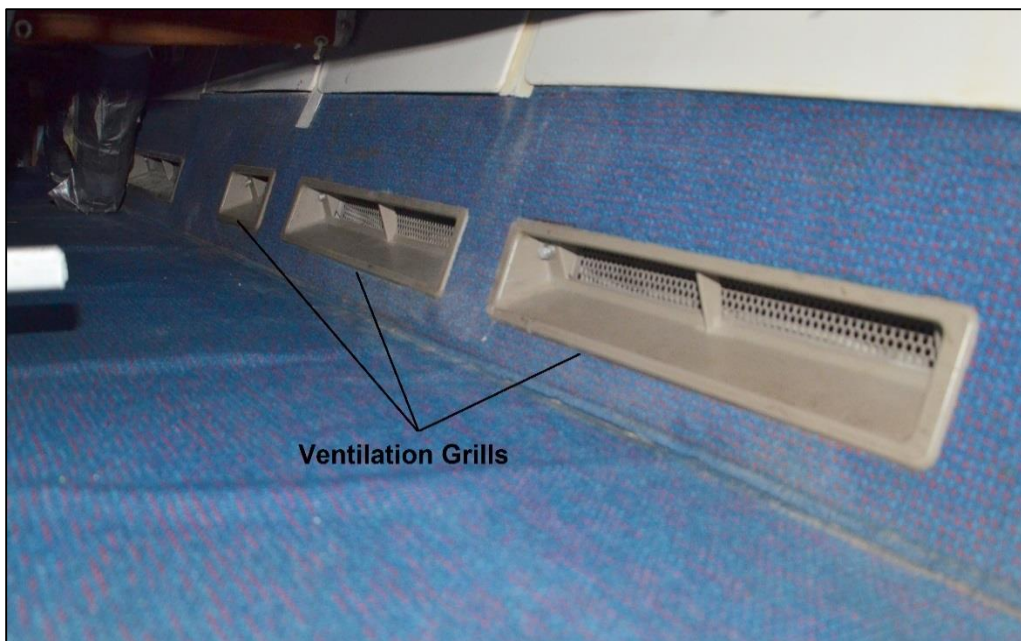


Figure 3.14 Ventilation Grills Inside the Boeing 737 Cabin

3.1.2.2 Seat Geometry

The seats are placed 0.46 m (1.5 ft) from the front wall and there is a gap of 0.46 m (1.5 ft) between the seats in the last row and the back wall. The aisle separating the seats on either sides of the cabin is 0.47 m (1.54 ft) wide. The spacing between seats in the consecutive rows is 0.84 m (2.75 ft) on centers. Geometrical dimensions of the seats placed inside the Boeing 737 cabin are shown in the Figures 3.15 and 3.16.

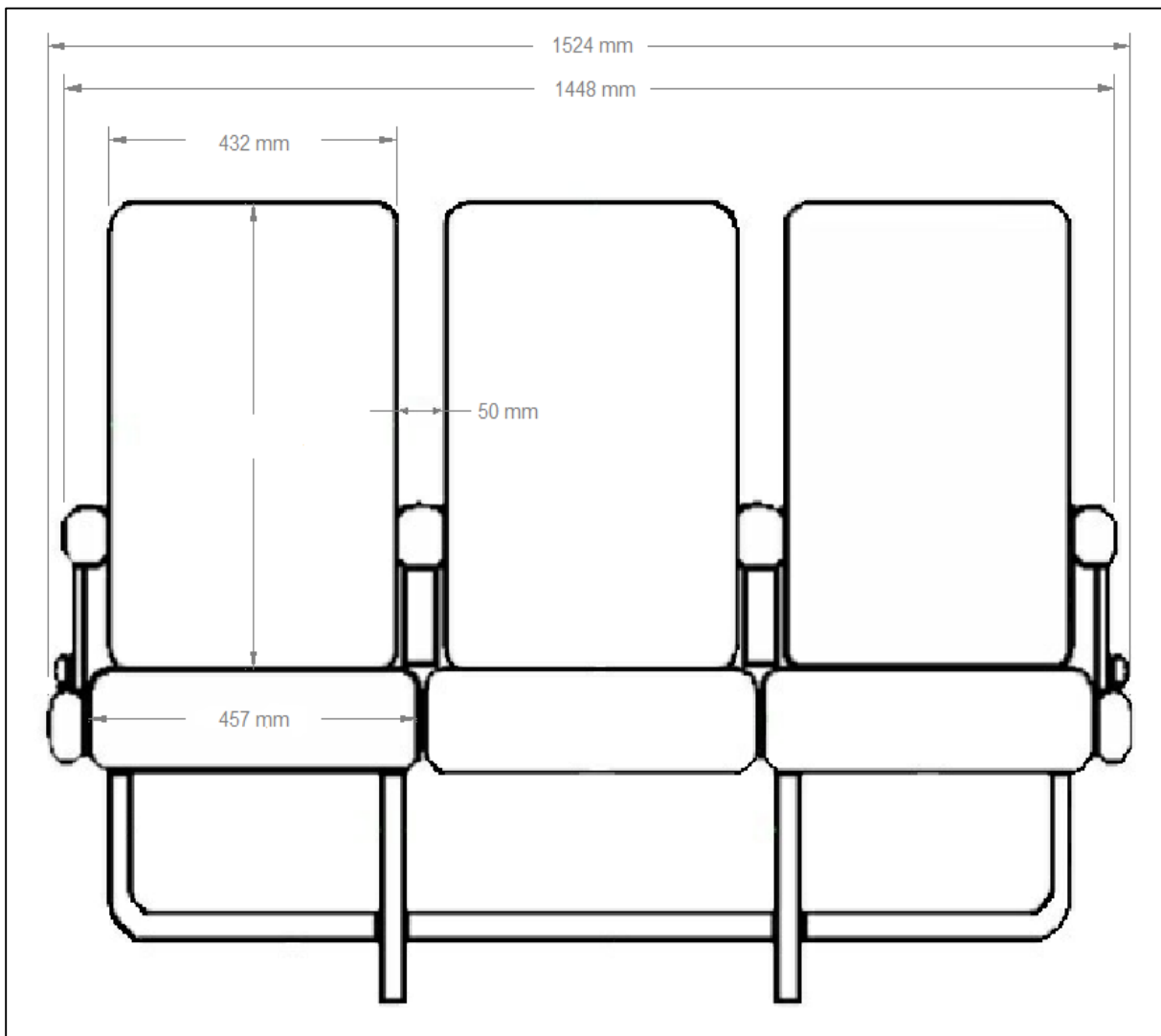


Figure 3.15 Dimensions of the Boeing 737 Cabin Triple Seats



Figure 3.16 Side View of the Triple Seats

3.1.3 Thermal Manikins

Experiments have been conducted to study the effects of occupant density and thermal load on the airflow inside the cabin. Madden (2015) concluded from his experimental analysis that occupant density has a considerable effect on the airflow and contaminant dispersion inside an aircraft cabin. For this study, heated manikins are used to simulate the heat load inside the cabin. The thermal manikins occupy all seats inside the mockup cabins. Figure 3.17 shows manikins occupying all seats inside the Boeing 767 mockup cabin. The body of the manikin is uniformly wrapped with heater wire, which is connected to a 115 V power outlet to generate about 102 W (348 BTU/hr) of heat. This number is based on the fact that an average comfortable sedentary person generates approximately 70 W (238 BTU/hr) of sensible heat (ASHRAE 2013). The extra power accounts for the heat generated from avionics and other electrical equipment such as personal laptops, in-flight entertainment system, etc. Two safety switches connected in series control power to the manikins to prevent damage by overheating. A thermostat located

inside the cabin controls the first switch. The power to the manikins will be cutoff if the temperature inside the cabin exceeds the set point of the thermostat. A pressure differential switch located in the air supply duct is connected in series with the thermostat switch. In case the airflow drops below a certain specified level, the manikins will receive no power.



Figure 3.17 Thermal Manikins Occupying All Seats Inside the Boeing 767 Mockup Cabin

3.2 Air Supply System

In order to mimic real aircraft cabin environment, the air supplied to the aircraft cabin mockups is controlled using a series of sensors and feedback controls on the air-handling unit. The Boeing 767 mockup cabin is supplied with 40 m³/min (1400 ft³/min) of air, while 17 m³/min (600 ft³/min) of air is supplied to the Boeing 737 cabin. Outside air passes through the dehumidifier unit, which maintains the relative humidity of the air below 15%. The dehumidified air is then passed through an air conditioner to bring it to a temperature of 15.6 °C (60 °F), which is then supplied to the cabins.

3.2.1 Ductwork

Rectangular duct connected at the south wall of the laboratory delivers outside air to the dehumidifier unit. Ductwork connects the dehumidification unit and the air conditioning unit to carry the dehumidified air to the conditioning system. Finally, ductwork from the conditioning system carries the conditioned air to the cabin supply duct, which supplies the conditioned air to the cabins through the diffusers. All the ductwork is insulated using fiberglass insulation sheets to ensure isothermal conditions. Figure 3.18 shows ductwork used to deliver air from outside to the Boeing 737 cabin.



Figure 3.18 Ductwork for the Boeing 737 Mockup Cabin

3.2.1.1 Boeing 767 Mockup Cabin Ductwork

A transition duct connects the duct section from the conditioning system to the actual Boeing 767 cabin supply duct. The cabin supply duct is 0.25 m (0.82 ft) in diameter and tapers along the length of the cabin. Air enters the cabin through two linear diffuser slots, which run along the ceiling of the cabin. The diffuser slots are connected to the cabin supply duct using 34 flexible tubes evenly spread along the length of the duct. The cabin supply duct also has connections to supply air to the gasper system. The gaspers are not used for the purpose of this study. Figure 3.19 shows the Boeing 767 cabin supply duct along with tube connection to a diffuser slot (Trupka, 2011).



Figure 3.19 Boeing 767 Cabin Supply Duct with Flexible Tubes Connected to Diffuser

3.2.1.2 Boeing 737 Mockup Cabin Ductwork

The duct section from the air conditioning system is connected to the Boeing 737 cabin supply duct using a transition duct. The cabin supply duct has an elliptical cross-section and tapers along the length of the cabin. The rear end of the duct is sealed using a plastic plate to ensure delivery of air to the cabin through the diffuser. Conditioned air from the air conditioning system enters the cabin supply duct, which runs along the center of the cabin above the ceiling. Linear diffuser connected to the bottom of the cabin supply duct supplies the air to the cabin mockup. Figure 3.20 shows the Boeing 737 cabin supply duct along with connection to the diffuser.



Figure 3.20 Boeing 737 Cabin Supply Duct with Connection to the Diffuser

3.2.2 Supply Air Conditioning System

The aircraft cabin mockups are supplied with 100% outside air, which is conditioned by the conditioning system. The main components of the air supply system are a supply fan, dehumidifier to remove moisture from the air, hot-water heater, commercial chiller and an electric heater used to fine-tune the air temperature. A schematic layout of the air conditioning system is shown in Figure 3.21 (Madden, 2015).

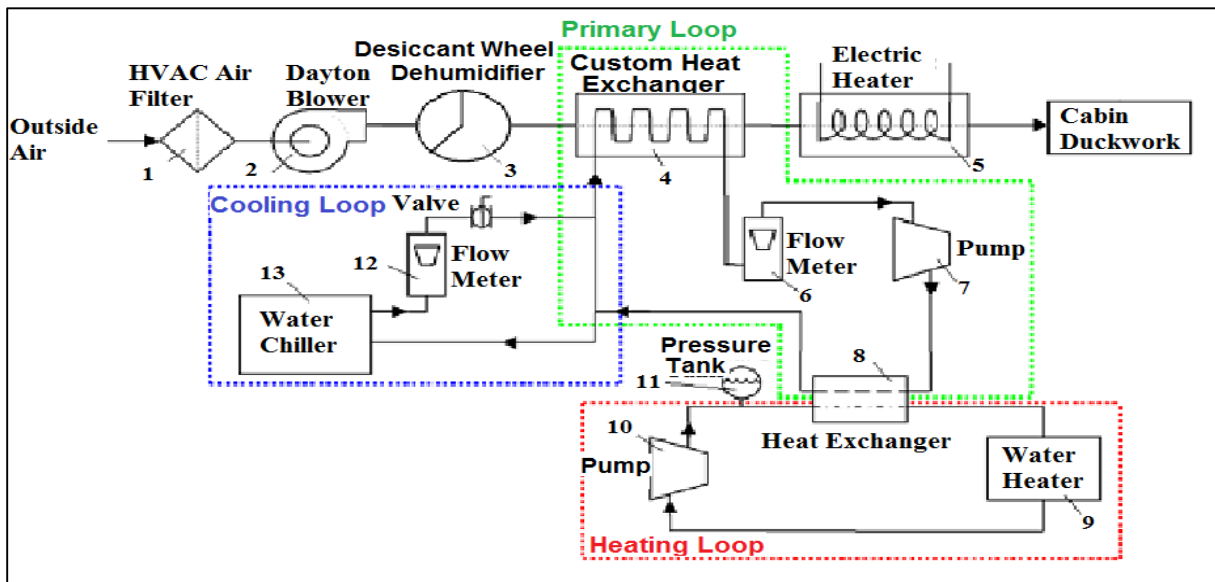


Figure 3.21 Schematic Flow Diagram of the Air Supply and Conditioning System

Different components of the conditioning system mentioned in Figure 3.21 are described in details as follows:

1. Air Filters
 - Glass Floss Z-line series
 - 2 parallel filters 24" × 24"
2. Blower/Supply Fan
 - Model # Yaskawa GPD315/V7 VFD
 - 12 1/4" Dayton Blower at 3 hp
3. Dehumidifier
 - Model # Munters ICA-0750-020
 - Desiccant dehumidifier type
 - Maximum Flow Rate: 1500 ft³/min
4. Heat Exchanger
 - Custom made: 24" × 24"
5. Electric Heater
 - Model # AccuTherm DLG-9-3
 - 220 V, 3 phase
6. Flow Meter
 - Model # Omega FL7204
 - Water Range: 40 GPH
7. Pump
 - Model # Marathon CQM 56C34D212OF P
8. Heat Exchanger
 - Model # Alfa Laval CB27-18H T06
9. Water Heater
 - Model # Rheem GT-199PVN-1
 - Temperature Range: 100° to 180° F
 - Gas Input Range: 19,000 to 199,900 btu/hr
 - 120 V, 60 Hz
10. Pump
 - Model # FHP C4T34DC35A

11. Pressure Tank

- Model # Dayton 4MY57
- Capacity: 6.5 gallons
- Precharge Pressure: 30 psi

12. Flow Meter

- Model # King 7205023133W
- Flow range: 1 to 200 GPM

13. Commercial Water Chiller

- Model # AccuChiller LQ2R15
- PV-B311 Condensing coils

As can be seen from Figure 3.21, the air supply system consists of three conditioning loops: primary loop, cooling loop and heating loop. The major components of the primary loop are two heat exchangers, a centrifugal pump and an electric heater. The primary loop is operated constantly in combination with either the heating or cooling loop to condition the air temperature to the desired set point of 15.6 °C (60 °F). The main goal of the heating or the cooling loop is to condition the air temperature to about 10 °C (50 °F). The heating loop consists of a natural gas water heater, a pressure tank, hot water heat exchanger and a pump. The heating loop is used only if the process air from the dehumidifier is below 10 °C (50 °F). The natural gas water heater is used to raise the air temperature to 10 °C (50 °F). The cooling loop consists of a commercial water chiller and a blending valve, which regulates the flow from the chiller. The cooling loop is used only if the temperature of the process air is above 10 °C (50 °F). The commercial chiller of the cooling loop is used to lower the air temperature to 10 °C (50 °F). After major temperature changes are provided by the cooling or heating loop, electric heater in the primary loop provides the fine-tuning of the air temperature to 15.6 °C (60 °F).

3.2.3 Control System

In order to achieve the desired cabin air quality with ease, all the components of the air handling and air conditioning system are controlled through a computer program written in National Instruments LabVIEW software. Figure 3.22 shows the screenshot of the program in LabVIEW used to control the air supply system. The program receives data from numerous sensors and control feedbacks through the Agilent 34970A and National Instruments FP-1000

data acquisition (DAQ) system. The output is controlled through a National Instruments FP-1000 with add-on modules PWM-520 and AO-210 for pulse width modulation and analog voltage output, respectively (Trupka, 2011). Key parameters controlled by the control system are the supply air temperature and airflow rate.

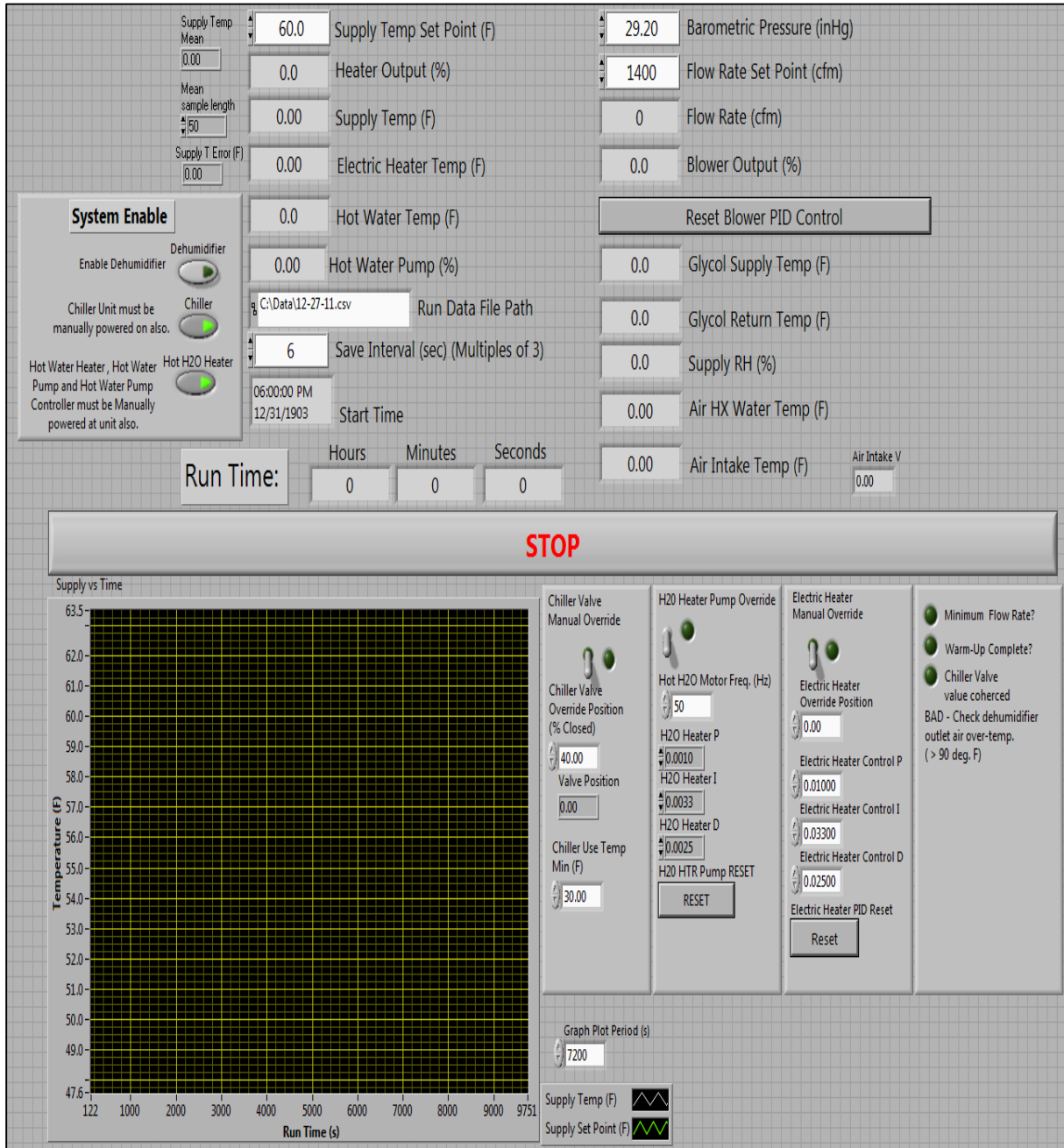


Figure 3.22 Graphical User Interface of the Supply Air Control System (Madden, 2015)

The flow rate of the supply air is measured in the duct section connecting the air conditioning system and the cabin supply duct. The DAQ system collects data from the flow measurement device and sends it to the computer program. The program then compares the measured flow rate with the set point to evaluate adjustments required to achieve the desired set point. Based on the evaluation, the DAQ system controls the variable frequency drive (VFD) controller that powers the blower motor. This process iterates until the desired set point is reached.

Temperature measurements are taken at seven different locations throughout the ductwork and the conditioning system. The temperature probes send data to the computer program through the National Instruments Field Point DAQ system. Table 3.1 gives the details of the temperature sensor locations and their feedback and control parameters (Madden, 2015).

Table 3.1 Temperature Probes Locations Along with Feedback and Control Parameters

No	Sensor Location	Feedback	Control
1	Dehumidifier Exit	Air Intake Temperature	-
2	Hot Water Temperature	Water Heater Exit	Mixing Valves
3	Supply Line to Heat Exchanger	Glycol Supply Temperature	Duct Heater
4	Return Line from Heat Exchanger	Glycol Return Temperature	Duct Heater
5	Hot Water Entrance to Plate Heat Exchanger	Heat Exchanger Temperature	-
6	Downstream of Electric Heater	Electric Heater Temperature	Heating Loop Pump VFD
7	Duct Section near Cabin Entrance	Cabin Supply Air Temperature	Duct Heater

The relative humidity is measured at the duct section near the cabin entrance. Although there is no set point assigned to the relative humidity, it is maintained below 15% by the dehumidifier unit.

The LabVIEW program allows the operator to control the set point for the supply air temperature and the flow rate. For the purpose of this study, the air temperature set point is always maintained at 15.6 °C (60 °F). The flow rate set point is varied depending on the mockup cabin used for experimentation.

3.3 Tracer Gas Supply and Measurement System

The same tracer gas supply and measurement system is used for all the testing done in this study with variations in the injection and sampling locations. Chapter 4 provides detailed explanation for the injection and sampling methods used for various testing scenarios.

Ventilation effectiveness studies are carried out using CO₂ as a tracer gas. While for experiments conducted to study contaminant dispersion inside an aircraft cabin, a mixture of CO₂ and He is used as a tracer gas.

3.3.1 Tracer Gas Supply System

Industrial grade CO₂ in 22.68 kg (50 lb) cylinders at a gauge pressure of 4 MPa (580 psi) and high purity He in type T cylinders at a gauge pressure of 16 MPa (2320 psi) are used to supply the tracer gas. The CO₂ and He flow rates are precisely metered through two separate mass flow controllers installed downstream of the gas cylinders. Clear vinyl tubes carry the gases from the cylinders to the mass flow controllers. As CO₂ gas and He gas in the cylinders are at a relatively high pressure for the vinyl lines, pressure regulators are installed on each cylinder to regulate the gases to 200 kPa (29 psi). For CO₂ an electric MKS 1559A-200L1-SV-S mass flow controller is used, while a pneumatic MKS 2179A00114CS mass flow controller is used for He. A MKS PR4000 power supply paired with a TS-232 interface unit controls the operations of the two mass flow controllers (Trupka, 2011). An air compressor located at the northwest corner of the cabin is also used to operate the pneumatic mass flow controller for He. From the mass flow controllers, the gases pass through two separate flow meters installed downstream. These flow meters verify the flow rates supplied by the mass flow controllers. Figure 3.23 shows the CO₂ and He mass flow controllers along with the flow meters. When CO₂ and He gas mixture is used as a tracer gas, the two gases after exiting the flow meters, are blended together in a simple brass tee fitting. A 12 mm (0.5 in) clear vinyl tube is then used to supply the tracer gas mixture to the locations of interest. For experiments where CO₂ alone is used as a tracer gas, the He gas supply system is not operated and tracer gas from the CO₂ flow meter is directly supplied to the desired location.

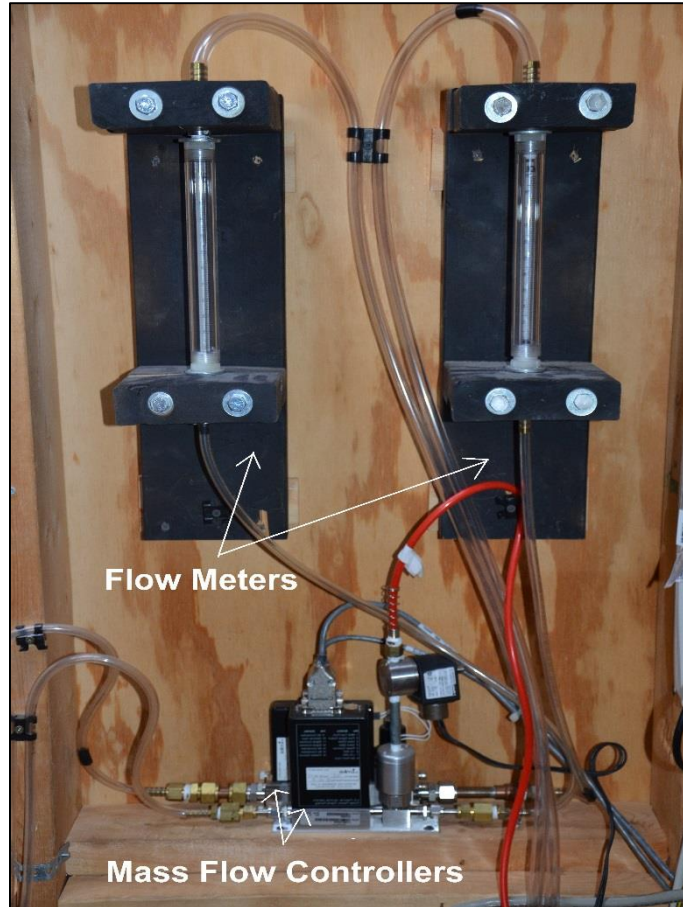


Figure 3.23 Mass Flow Controllers Along with the Two Flow Meters

3.3.2 Tracer Gas Measurement System

Four infrared CO₂ gas analyzers are used to measure CO₂ concentrations. In order to avoid moving CO₂ analyzers from seat to seat and to simplify the sampling process various sampling ports are used. A sampling port consists of a vinyl tube mounted on a wooden support. One end of the vinyl tube is connected to a CO₂ analyzer while the other end is mounted on a wooden support. A sampling port used to collect air samples at the breathing level of a seated passenger is showing in Figure 3.24. Various other sampling ports used for this research are discussed in details in Chapter 4. The vinyl tubes of the sampling ports draw air samples from various locations into the four infrared CO₂ sensors. The gas analyzers measure the CO₂ concentration and generate a voltage output, which is fed to the DAQ system. The DAQ system then transfers the data collected from the analyzers to the computer program controlling the tracer gas injection and sampling system. Three of the four sensors are WMA-4 model analyzers

from PP System Instruments. These analyzers are capable of measuring CO₂ concentration within the range of 0 to 2000 ppm. The fourth analyzer is custom made using an Edinburgh Instruments Gas Sampling Card and a 24 V supply with 60 Hz noise filters (Trupka, 2011). This analyzer measures the CO₂ concentration in the range of 0 to 3000 ppm. Figure 3.25 shows the WMA-4 analyzers mounted on the north wall of the Boeing 737 mockup cabin. The custom made analyzer is shown in Figure 3.26.

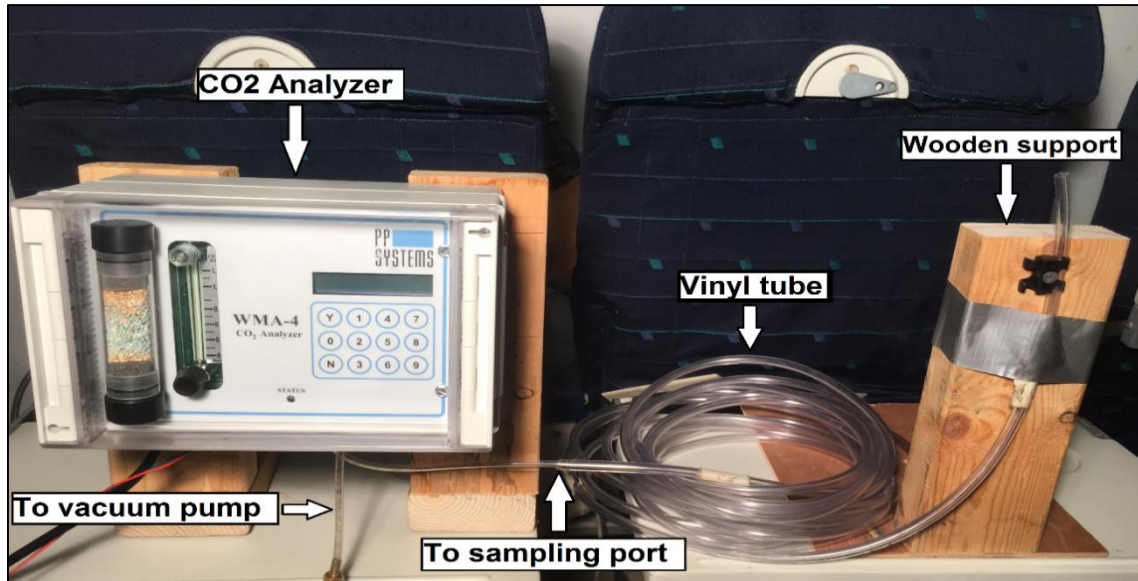


Figure 3.24 A Sampling Port Along With Tube Connections to a CO₂ Analyzer



Figure 3.25 WMA-4 Infrared CO₂ Gas Analyzers

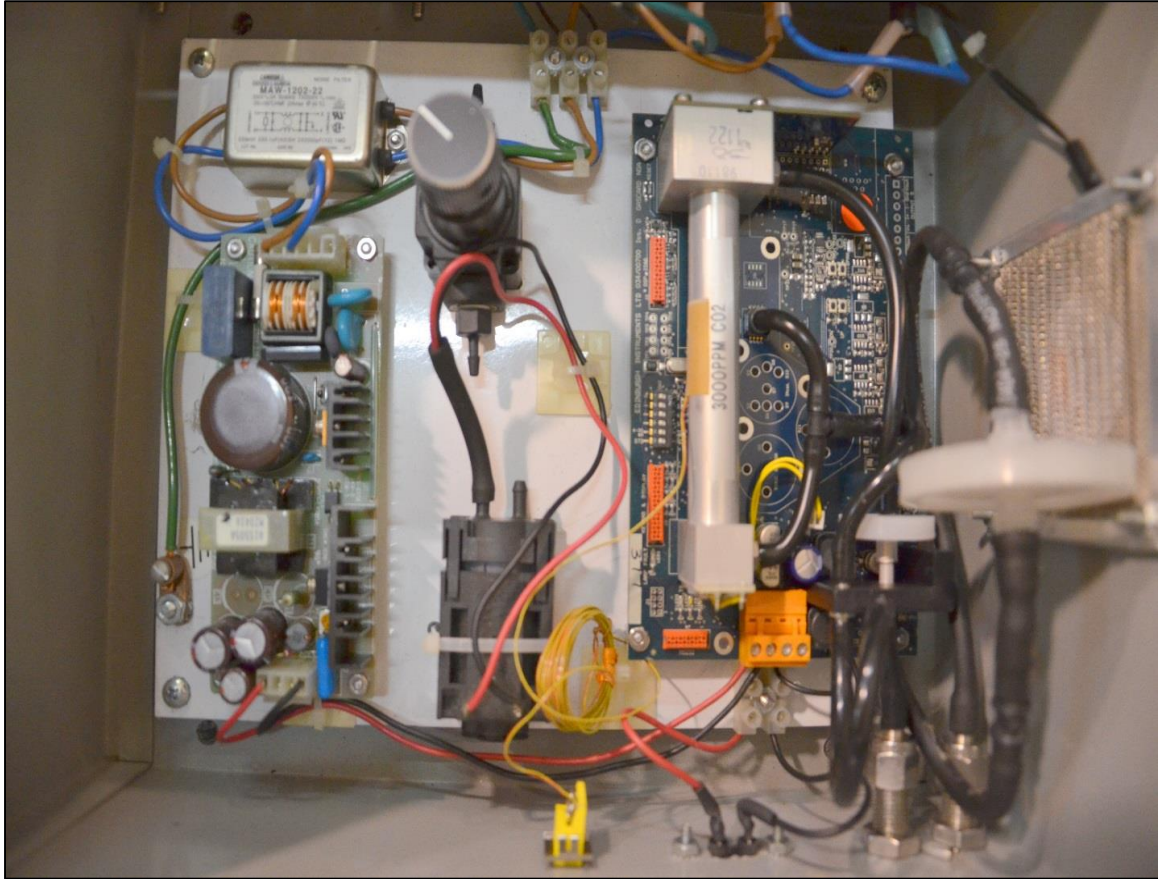


Figure 3.26 Interior View of the Custom Made CO₂ Gas Analyzer

As mentioned earlier, the analyzers draw air samples from desired locations through sampling tubes mounted on wooden supports. A single vacuum pump installed downstream of the analyzers is used to pull the air samples into the analyzers. Vinyl tubes connect the analyzers to the vacuum pump. Different lengths of sampling tubes and tubes connecting the pump and the analyzers results in a variation in the pressure drop. This variation in pressure drop results in variation in flow rates amongst the analyzers. Thus, in order to ensure the same sampling rate of 1 L/min (0.0353 ft³/min) for each analyzer, a balancing system is installed between the analyzers and the pump. The balancing system consists of three flow meters with flow adjustment knobs. Since there are only three flow meters and there are four analyzers, suction lines of equal length from two analyzers are merged using a brass tee fitting into a single suction line, which is then connected to one of the flow meters. This modification required the flow rate to be doubled in that particular suction line providing equal flow rates through the two analyzers. The balancing system is shown in the Figure 3.27.



Figure 3.27 The Flow Balancing System

3.3.3 Control System

In order to simplify control of the tracer gas supply and measurement system, various components of the systems are controlled by a computer interface using LabVIEW software. The computer collects data from the four CO₂ analyzers and numerous temperature sensors located throughout the cabins. An Agilent 34970A DAQ system is used to feed data into the computer program. The DAQ system along with the power supply for the mass flow controllers is shown in Figure 3.28.



Figure 3.28 DAQ System Along With the Power Supply

The LabVIEW program was written to be used with a sampling tree, but with some alterations to the input values, the program can also be used without the sampling tree. For the purpose of this testing the sampling tree is not used. Also, the program was initially written to read data from only three CO₂ analyzers, later the program was altered to accommodate an additional CO₂ sensor to cover more locations in one test. Shown in Figure 3.29 is the screenshot of the LabVIEW program used to control the tracer gas injection and measurement system.

The user interface allows the operator to control the CO₂ injection rate, He injection rate, the duration of testing and sampling interval. These values are altered depending on the experiments conducted. Data collected from various sensors is saved into a comma-separated values (.csv) file that can be easily accessed through Microsoft Excel. The user interface also displays the collected data in the form of graphical plots to allow visualization of data.

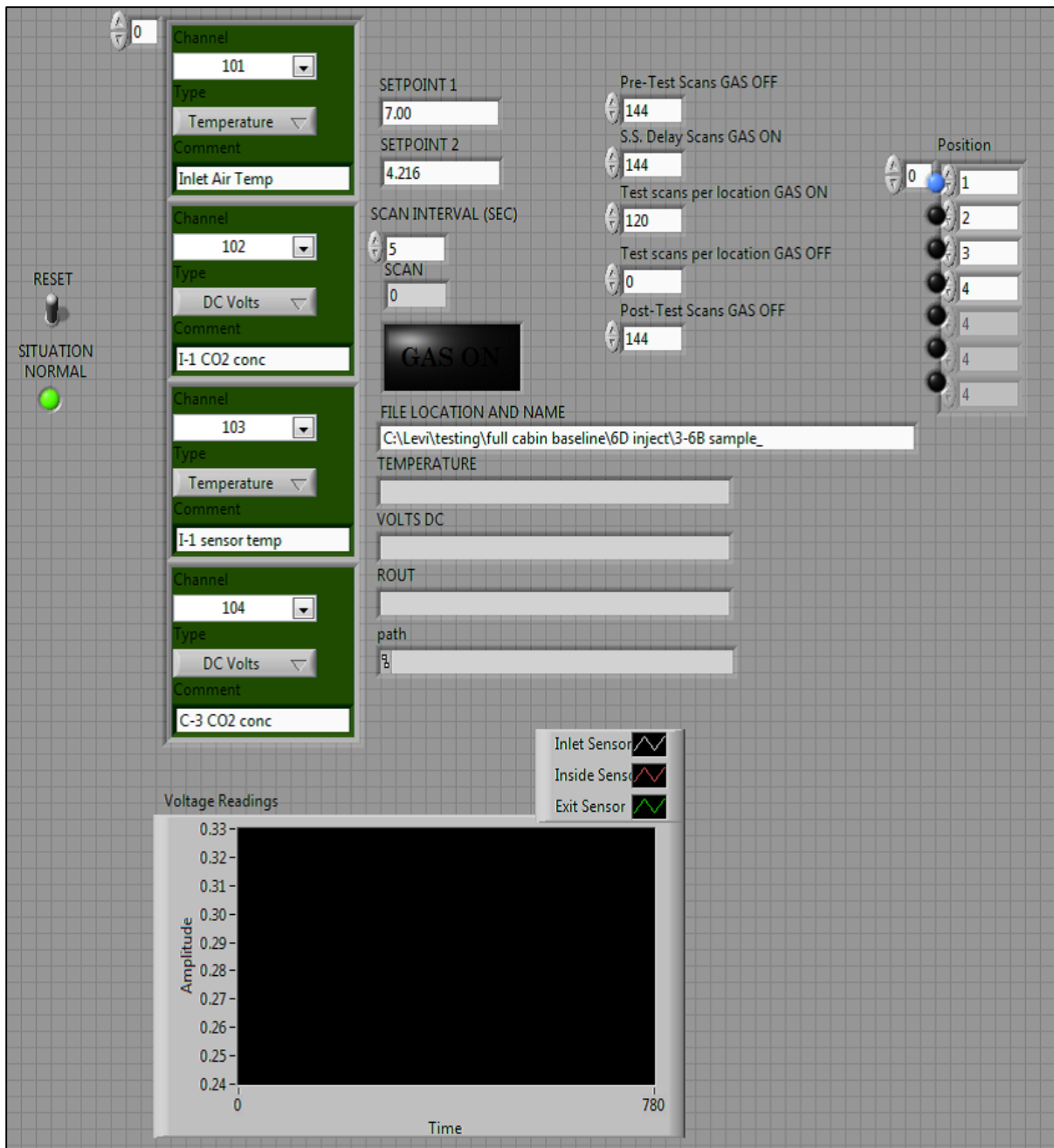


Figure 3.29 Screenshot of the LabVIEW Program (Madden, 2015)

Chapter 4 - Test Procedure

This research focuses on the experimental study of two important factors affecting the air quality and thus, the health of passengers inside an aircraft cabin. Ventilation effectiveness is one of the factors investigated. Dispersion of gaseous contaminants inside an aircraft cabin is another important issue of concern studied in this research. To ensure accuracy and reliability of measured data, experiments were conducted to determine the time response of the CO₂ analyzers, to check repeatability of the CO₂ analyzers and to determine effects of length of sampling tubes on measured data. This chapter provides detailed description of the testing procedures for various experiments conducted.

4.1 Ventilation Effectiveness Study

The first and second set of experiments conducted for the research reported in this thesis addressed ventilation effectiveness inside aircraft cabins. Experiments were conducted separately inside both the Boeing 767 and the Boeing 737 mockup cabins to evaluate the local effective ventilation rates (e_L) and ventilation effectiveness (E). The first set of experiments studied the effectiveness of the ventilation system inside a Boeing 767 mockup cabin. While, the second set of experiments was conducted to investigate ventilation effectiveness for various scenarios inside a Boeing 737 mockup cabin.

4.1.1 Tracer Gas Injection

As mentioned in earlier chapters, the study of ventilation effectiveness was accomplished using CO₂ as a tracer gas. Previous research done has found that it is difficult to achieve thorough mixing of tracer gas with point source injection. Thus, for all experiments conducted in the first and second set, tracer gas was directly injected into the supply air well upstream of the cabin supply diffusers. CO₂ from the mass flow controller was injected into the air supply duct through a vinyl tube. Injecting CO₂ directly into the supply air ensures thorough mixing of CO₂, eliminating the need to mix it with He to neutralize buoyancy effects. As the local effective ventilation rates were calculated using the tracer gas decay method, its values remain unaffected by the tracer gas injection rate. However, the CO₂ analyzers have a certain concentration measurement range. To maintain CO₂ concentrations inside the cabin within the measurable

range, an optimal injection rate needed to be selected. CO₂ was injected at a rate of 15 L/min (0.53 ft³/min) inside the Boeing 767 mockup cabin, while an injection rate of 7 L/min (0.247 ft³/min) was used for testing inside the Boeing 737 mockup cabin. Figure 4.1 shows the location of the vinyl tube used for injecting tracer gas into the air supply duct.



Figure 4.1 Tracer Gas Injection Location For Ventilation Effectiveness Study

4.1.2 Tracer Gas Measurement

For the Boeing 767 mockup cabin, the CO₂ concentration measurements were carried out at the breathing level of a seated adult passenger. In order to accomplish this, the sampling ports used were designed to collect air samples at a distance of 0.33 m (1.08 ft) in front of and level with the headrest. The sampling ports used for this set of experiments are shown in Figure 4.2. CO₂ concentration data were collected from all seventy-seven seats inside the cabin. Each measurement in this set was repeated three times to confirm repeatability of the results.



Figure 4.2 Sampling Ports Used for Testing at Breathing Level of Seated Adult Passengers

Ventilation effectiveness inside the Boeing 737 cabin was analyzed by conducting four series of experiments investigating different scenarios. The first series of experiments was conducted to study e_L rates at breathing height of seated adult passengers. The experiments for this series were conducted by sampling gas concentration at a distance of 0.33 m (1.08 ft) in front of and level with the headrest. Figure 4.2 shows the sampling ports used to achieve this. For this series of experiments all thirty seats inside the cabin were analyzed and measurement at each seat was repeated three times with variations in analyzer used at a particular seat location to ensure repeatability of the results.

Local effective ventilation rates at breathing level of seated infant passengers were evaluated in the second series. For this scenario, gas concentrations were sampled at a height of 0.76 m (2.5 ft) from the cabin floor and at a distance of 0.33 m (1.08 ft) from the seat back. The sampling system used for this set is as shown in Figure 4.3. In order to reduce the number of tests performed; twelve seat locations inside the cabin were investigated. Seat locations selected are spread uniformly throughout the cabin to give a clear idea about the ventilation effectiveness in various zones of the cabin. Figure 4.4 shows the seat locations selected for this scenario.



Figure 4.3 Sampling Ports Used for Testing at Breathing Level of Seated Infant Passengers

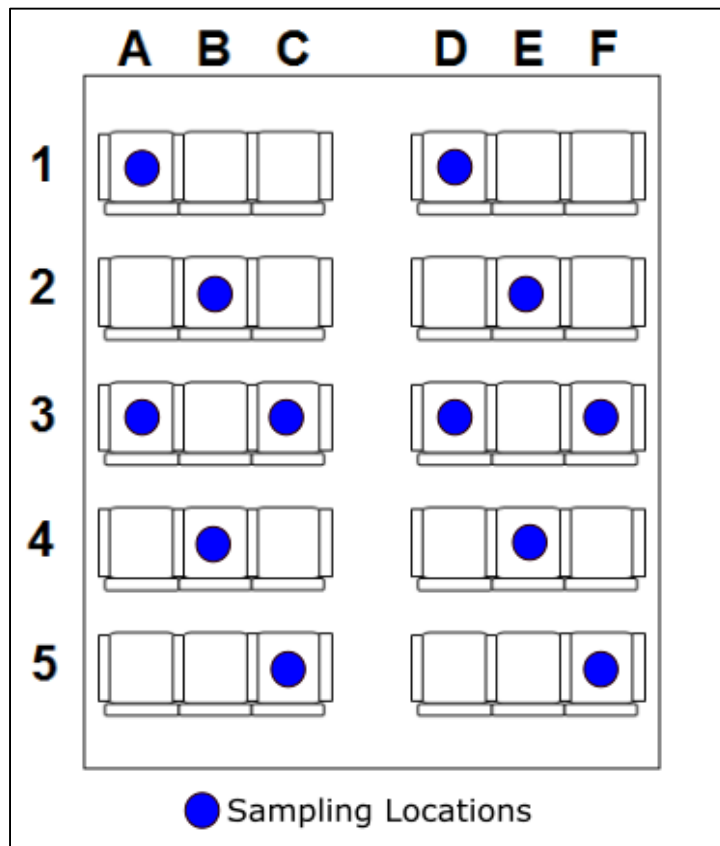


Figure 4.4 Measurement Locations for the Second and Third Series of Experiments

The third series of tests focused on evaluation of e_L rates at breathing level of adult passengers standing at seat locations. In the third series of experiments, air sampling was carried out at a height of 1.5 m (5 ft) from the cabin floor and at a distance of 0.33 m (1.08 ft) away from the seat back as shown in Figure 4.5. Seat locations selected for this set of experiments were same as the seat locations selected for the second series and are shown in Figure 4.4.



Figure 4.5 Sampling Ports Used for Testing at Breathing Level of Standing Passengers

The fourth series aimed at analyzing e_L rates at the breathing level of adult passengers at aisle locations. The experiments were conducted by sampling gas concentrations at the geometric center of each row and at a height of 1.5 m (5 ft) from the cabin floor. The sampling ports used for this series of experiments are similar to the ports used in series three experiments. Measurements were taken at the center of aisle of all the five rows as shown in Figure 4.6.

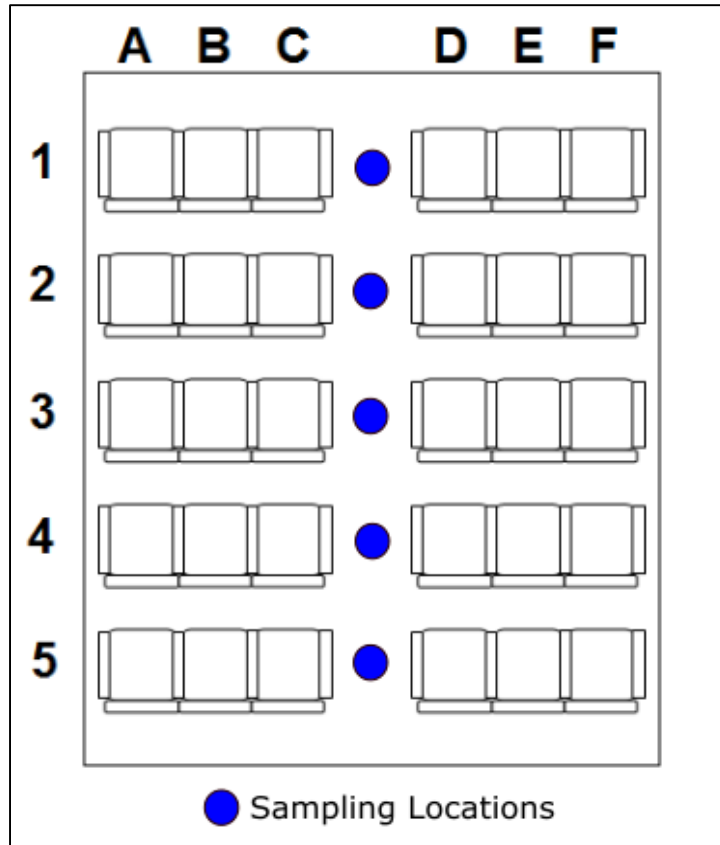


Figure 4.6 Measurement Locations for the Fourth Series of Experiments

To ensure repeatability of results from the second, third and fourth series of experiments, each test was repeated twice by varying the sensor used for measurement at a particular location.

4.1.3 Testing Procedure

Before collection of the experimental data, the air supply system was run for approximately 20 minutes to achieve the desired supply air temperature and flow rate. Movement of researchers inside the cabin can cause airflow disturbances, which can produce errors in measured data. In order to avoid recording any such disturbance, each experiment began by allowing the cabin to stabilize for 10 minutes. Tracer gas was then injected to allow the CO₂ concentration inside the cabin to reach steady state condition. Tracer gas injection was then stopped with continued ventilation to allow decay of CO₂ concentration inside the cabin. The transient data for CO₂ concentration decay were collected at various measurement locations. This test design was followed for all ventilation effectiveness experiments conducted in both mockup cabins.

In order to determine the duration of each experiment it was essential to obtain the time required to bring the cabin to steady state CO₂ concentration with injection of tracer gas in cabin supply air. In addition, as the data from the transient CO₂ concentration decay were used to evaluate the local ventilation effectiveness values, it was important to find the time required by the cabin to return to ambient CO₂ concentrations. Experiments were conducted separately in both cabins to evaluate the steady state time durations. For the Boeing 767 cabin, the experiment started by injecting CO₂ inside the cabin for 15 minutes. The injection was then stopped with ventilation continued for another 15 minutes. Throughout the test duration, CO₂ concentration data were collected from various seats inside the cabin. Steady state test results from seats B, D and F in row 6 inside the Boeing 767 mockup cabin are shown in Figure 4.7. As can be seen from this figure it took approximately 12 minutes for the cabin to reach steady state CO₂ concentrations and approximately 12 minutes to return to ambient CO₂ concentration levels.

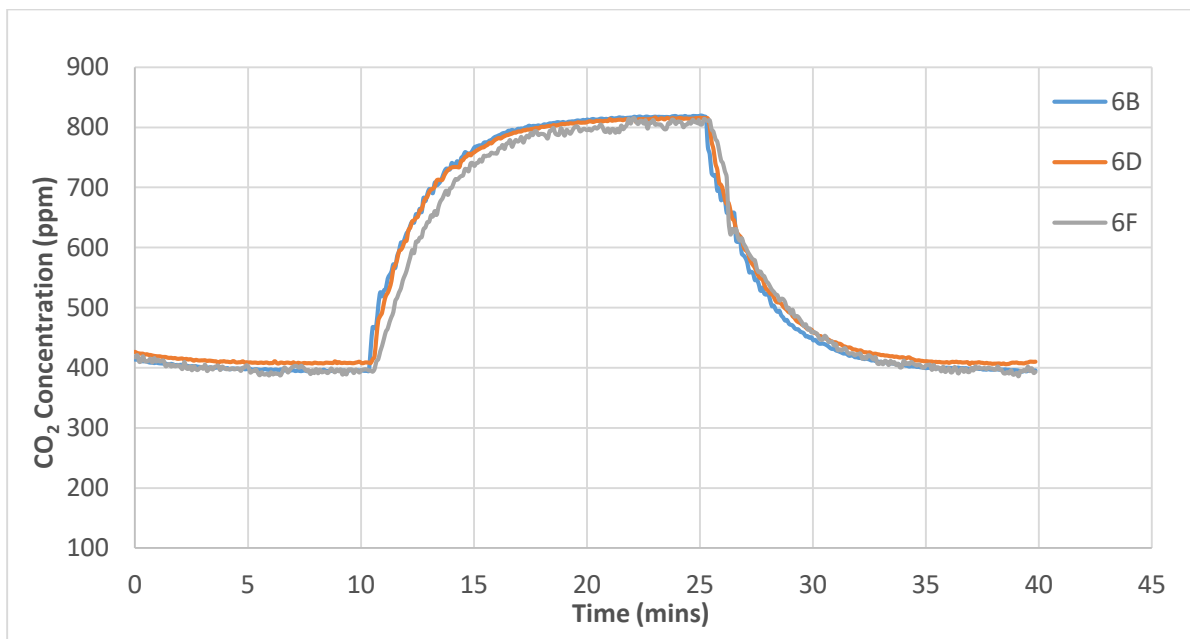


Figure 4.7 Steady State Test Results for Boeing 767 Mockup Cabin

Experiments following a similar procedure were conducted inside the Boeing 737 mockup cabin to determine the steady state time durations. The steady state results from test conducted at seats 1F, 3D and 5A inside the Boeing 737 mockup cabin are as shown in Figure 4.8. As can be seen from Figure 4.8 the CO₂ concentration reached steady state conditions

approximately 12 minutes after the start of injection and it took approximately 12 minutes for the CO₂ concentrations inside the cabin to return to ambient levels.

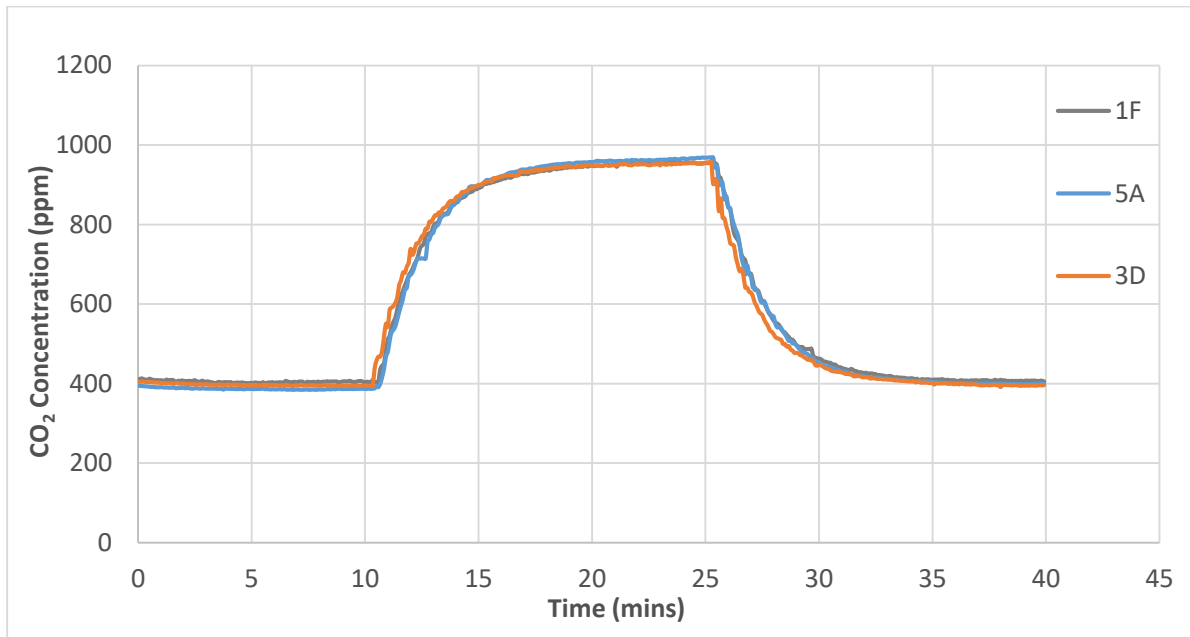


Figure 4.8 Steady State Test Results for Boeing 737 Mockup Cabin

Table 4.1 provides details of the experimental procedure for ventilation effectiveness studies inside the Boeing 767 and the Boeing 737 mockup cabins.

Table 4.1 Test Procedure for Ventilation Effectiveness Testing

Phase	Tracer Gas Injection Status	No. of Scans	Scan Interval (secs)	Time Duration (mins)	Notes
Pre-Test Scans	OFF	120	5	10	To allow the cabin to stabilize from disturbances
S.S. Delay Scans	ON	180	5	15	To allow the CO ₂ concentration to reach steady state conditions
Post-Test Scans	OFF	180	5	15	To collect transient CO ₂ concentration decay data for evaluation of e _L and E _L .

4.1.4 Data Analysis Method

The CO₂ sensors analyzed the gas concentration from various locations and generated a voltage output. This data from the CO₂ analyzers was saved by the LabVIEW program in a

comma separated values (.csv) file which can be accessed using Microsoft Excel. The collected CO₂ concentration data were analyzed to evaluate the ventilation effectiveness. The tracer gas decay method was used to calculate the e_L rates and E_L values. Using a locally perfectly mixed model and applying mass balance of tracer gas inside the cabin gives Equation 4.1, where ‘ e_L ’ is the local effective ventilation rate, ‘ C_p ’ and ‘ C_{inlet} ’ are CO₂ concentrations at the measuring point and inlet to the cabin respectively.

$$e_L = (\dot{Q}/V)_{local} = \frac{dC_p/dt}{C_p - C_{inlet}} \quad (4.1)$$

The E_L values were then calculated by simply dividing the corresponding e_L rate by the ratio of the cabin volume and the total supply airflow rate. The local ventilation effectiveness values are calculated using Equation 4.2, where ‘ E_L ’ is the local ventilation effectiveness, ‘ \dot{Q} ’ is the supply air flow rate, ‘ V ’ is the volume. The ventilation effectiveness of the entire cabin is calculated by taking the mean of all the E_L values.

$$E_L = \frac{(\dot{Q}/V)_{local}}{(\dot{Q}/V)_{cabin}} = \frac{e_L}{(\dot{Q}/V)_{cabin}} \quad (4.2)$$

As can be seen from Equation 4.1, the tracer gas decay technique uses relative CO₂ concentrations to evaluate the e_L rates. This approach eliminates the need for precise calibration of the CO₂ analyzers for this study.

To avoid the influence of noise in CO₂ concentration data on the ventilation effectiveness values, a transient average of CO₂ concentration data from each analyzer was calculated. A nine count rolling average of CO₂ data at a particular time was calculated by taking average of the four preceding and four following concentration values along with the current concentration. The transient averaging provided smoothed CO₂ concentration values, which were then used in Equation 4.1 to calculate the e_L rates. Figure 4.9 shows plots of the raw CO₂ concentration data and the corresponding smoothed data from one of the experiments conducted.

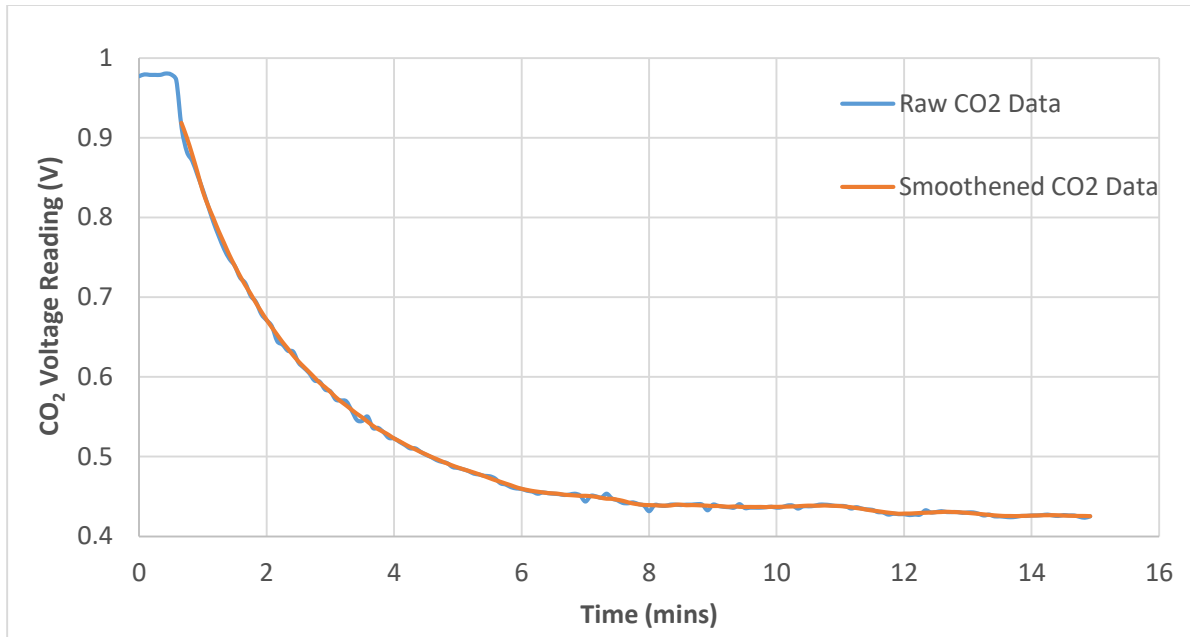


Figure 4.9 Comparison Between Raw and Smoothened CO₂ Concentration Data

4.2 Dispersion of Tracer Gas Study

Dispersion of gaseous contaminants inside an aircraft cabin was examined for two different scenarios in the third and fourth set of experiments. The third set focused on the dispersion of gaseous contaminants while the ventilation air was being supplied at a normal rate. The main objective of the fourth set of experiments was to study the dispersion of gaseous contaminants inside an aircraft cabin in the absence of ventilation air. Experiments to investigate these two scenarios were conducted inside the Boeing 737 mockup cabin.

4.2.1 Testing with Ventilation Air

The main objective of the third set of experiments was to study contaminant transport inside an aircraft cabin. For the entire flight duration, the aircraft cabin is supplied with fresh air to provide ventilation. To mimic cabin conditions during a typical flight, this study of transport of gaseous contaminants was carried out with the supply of ventilation air.

4.2.1.1 Tracer Gas Injection

For the purpose of this study, a gas mixture mainly consisting of CO₂ was used as a tracer gas. Because CO₂ is denser than air, there is a need to neutralize the buoyancy to achieve

thorough mixing with the cabin air. Helium (He) was used as a neutralizing gas to increase the buoyancy of CO₂ to that of cabin air. The mixing ratio of He and CO₂ in the tracer gas mixture was calculated using the ideal gas principles. As the cabin supply air contains traces of CO₂, an injection rate needed to be selected to accurately measure the CO₂ concentration from tracer gas injection inside the aircraft cabin. Three injection rates of 3 L/min (0.106 ft³/min), 5 L/min (0.177 ft³/min) and 7 L/min (0.247 ft³/min) were analyzed to determine the optimal CO₂ injection rate. It was found from analysis that a CO₂ injection rate of 5 L/min (0.177 ft³/min) was optimal to get accurate measurements inside the cabin without wasting too much of CO₂. The He gas injection rate corresponding to the CO₂ injection rate was calculated to be 3.01 L/min (0.106 ft³/min) giving a total injection rate of 8.01 L/min (0.283 ft³/min). As mentioned in Chapter 3, CO₂ and He gas were mixed downstream of the flow meter before injection at locations inside the cabin. An injection apparatus consisting of a copper tube of inner diameter 25.4 mm (1 in.) was used to inject the tracer gas mixture at various locations inside the cabin. The injection apparatus was designed to inject tracer gas at a height of 1.17 m (3.84 ft) from the cabin floor. Figure 4.10 shows the apparatus used for injection of tracer gas inside the cabin.



Figure 4.10 Tracer Gas Injection Apparatus for Tracer Gas Dispersion Study

In order to reduce the time of experimentation without compromising on quality of research, only a few selected injection locations were tested. Five injection locations were selected to cover multiple sections of the cabin. Tracer gas was injected at the center of the aisle at rows 1, 3 and 5 and at seats 2B and 4E. Only one injection location was tested at a time. Figure 4.11 shows the injection locations selected for the purpose of this study

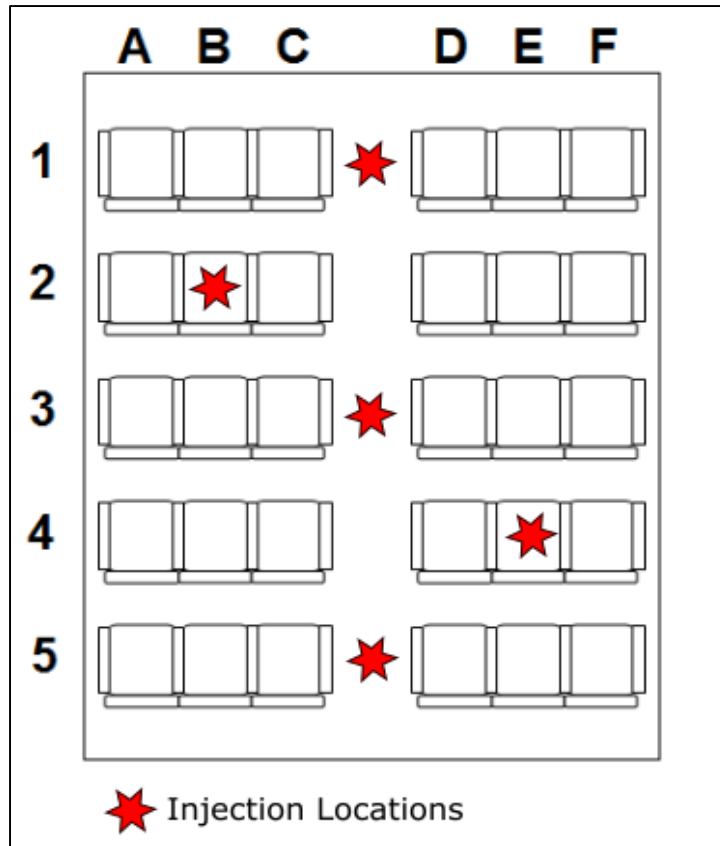


Figure 4.11 Tracer Gas Injection Locations for Dispersion Study With Ventilation Air

4.2.1.2 Tracer Gas Measurement

For each injection location, various sampling locations were selected to help clearly describe the dispersion phenomenon inside the cabin. For injection at aisle locations, seats of column A, C, D and F in alternate rows starting with row 1 were sampled. For injection at seats 2B and 4E, all seats in column B and E along with all seats in rows 2 and 4 except for the respective injection locations were sampled. The sampling locations for various injection locations are shown in Figure 4.12. Measurements at all sampling locations for each injection locations were repeated twice to ensure repeatability of results.

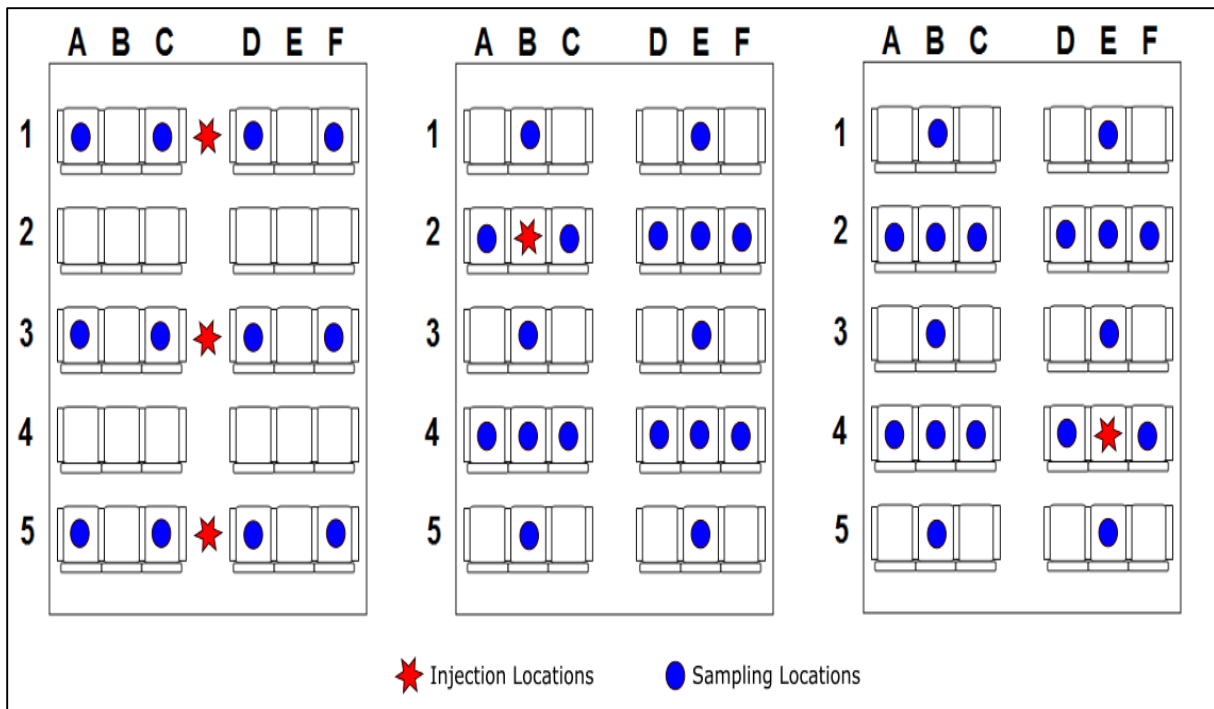


Figure 4.12 Sampling Locations for Various Injection Locations

4.2.1.3 Testing Procedure

Similar to the testing procedure for ventilation effectiveness studies, each test in this set of experiments began by allowing the cabin to stabilize for 10 minutes. Tracer gas mixture was then injected at various locations as described in section 4.2.1.1 to allow the CO₂ concentration inside the cabin to reach steady state condition. Steady state CO₂ concentration was then measured at various sampling locations as described in section 4.2.1.2. After the sampling process was completed, the injection was stopped with continued ventilation to allow the cabin to reach ambient CO₂ concentration levels.

In order to determine the time durations for various processes of each experiment, it was essential to determine the time required for the CO₂ concentration inside the cabin to reach steady state conditions with injection at a point source. To determine the time durations, tracer gas was injected at seat 2B for a period of 30 minutes. The tracer gas injection was then stopped with continued supply of ventilation air and the experiment was continued for 30 more minutes. For the entire experiment duration, CO₂ concentrations were measured at seats 1F, 3D and 5F inside the cabin. Results from this experiment to study steady state time duration is shown in Figure 4.13. The results revealed that it took approximately 12 minutes for the cabin to reach

steady state CO₂ concentration and that 12 minutes was enough time to allow the CO₂ concentration in the cabin to reach ambient levels. It can also be seen that 10 minutes of measurement period is sufficient to give reliable CO₂ concentration data.

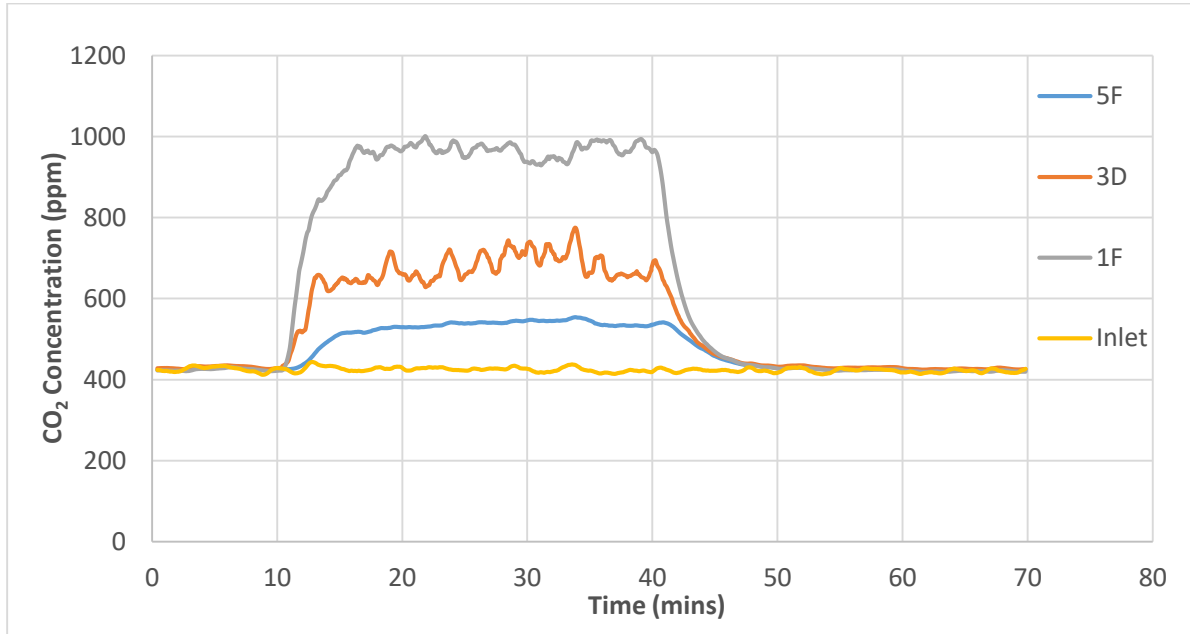


Figure 4.13 Steady State Results for Point Source Injection

Table 4.2 summarizes the details of the procedure for experiments to study gaseous contaminants dispersion with ventilation air.

Table 4.2 Test Procedure for Tracer Gas Dispersion Study with Ventilation Air

Phase	Tracer Gas Injection Status	Ventilation Air Supply Status	No. of Scans	Scan Interval (sec)	Time Duration (mins)	Notes
Pre-Test Scans	OFF	ON	120	5	10	To allow the cabin to stabilize from disturbances
S.S. Delay Scans	ON	ON	180	5	15	To allow the CO ₂ concentration to reach steady state conditions
S.S. Delay Scans	ON	ON	120	5	10	To collect steady state CO ₂ concentration data.
Post-Test Scans	OFF	ON	180	5	15	To allow cabin to reach ambient CO ₂ concentration levels.

4.2.1.4 Data Analysis Method

The data collected by the CO₂ analyzers are in the form of voltage readings. In order to draw meaningful conclusions from the data, it needs to be manipulated to the proper units. The CO₂ analyzers were calibrated on a regularly basis to convert the voltage readings to ppm of CO₂. Three cylinders of calibration gas with concentrations of 500 ppm, 1000 ppm and 2000 ppm of CO₂ were used for calibration. The same sampling system as mentioned in Chapter 3 was used to draw calibration gas into the analyzers. To prevent damage to the analyzers, a pressure regulator is connected to the gas cylinder to reduce the pressure of the sampled gas. In addition, a water manometer apparatus is installed in the sampling line between the analyzer and the gas cylinder as shown in Figure 4.14. The manometer was used to verify positive pressure on the analyzer suction line, to protect the analyzers from over pressure and to avoid entrance of atmospheric air into the sampling line to avoid any interference with the calibration process.

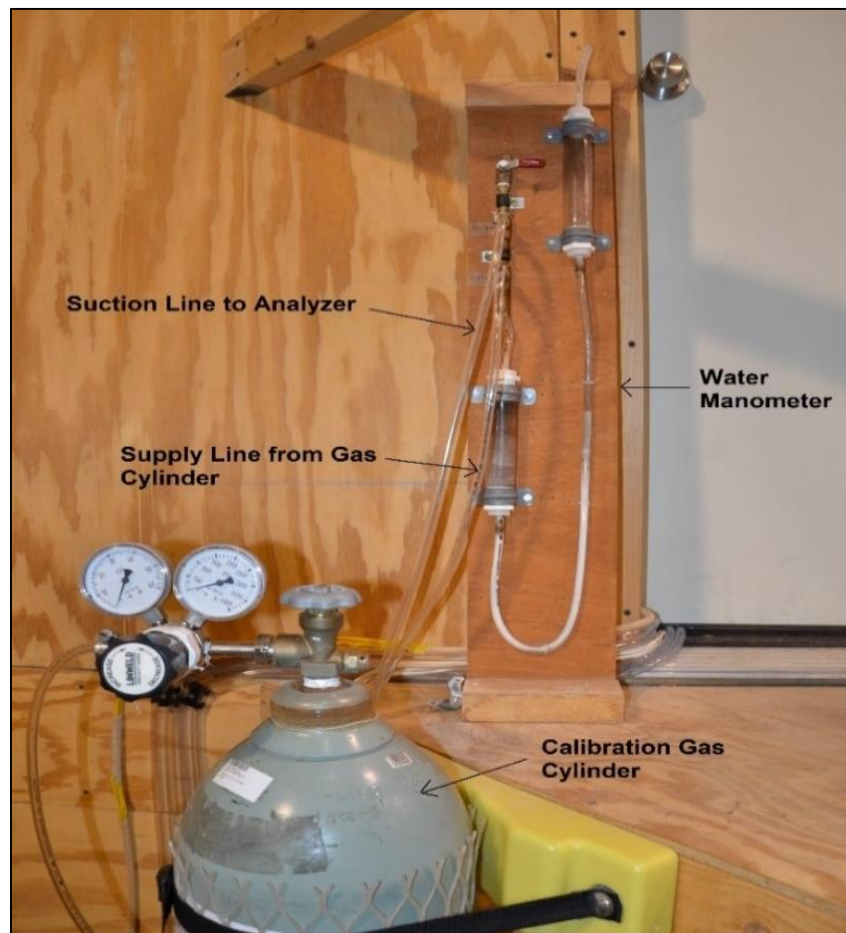


Figure 4.14 Setup for Calibration Process

Each analyzer sampled each of the three calibration gases separately for 10 minutes. The average voltage readings measured by each analyzer for the three calibration gases were plotted against the corresponding concentrations to give a linear equation relating the two properties. This equation was then used to convert the voltage readings from experiments to ppm of CO₂. Figure 4.15 shows the plot from one of the calibration process.

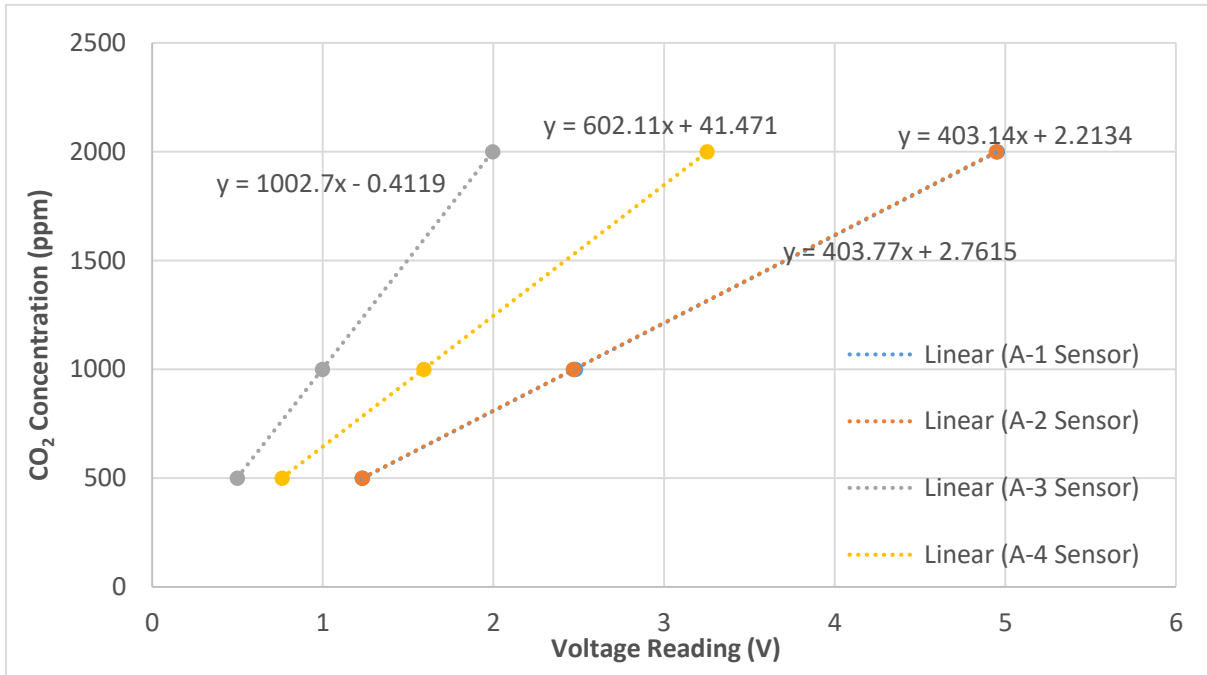


Figure 4.15 Results from One of the Calibrations

It is a known fact that CO₂ concentration in the atmosphere varies throughout the day. As 100 % outside air is supplied to the cabin and CO₂ is used as a tracer gas, it is essential to account for these variations to get accurate results. Normalization of the CO₂ concentration is carried out to account for the variations in ambient CO₂ concentrations. Equation 4.3 is used to calculate the normalized CO₂ count (**N**), where ‘C_p’ and ‘C_i’ are the CO₂ concentrations at the sampling point and supply air, respectively, and ‘V_{supply}’ and ‘V_{CO2}’ are the supply air flow rate and CO₂ injection rate respectively. This normalization also allows results with different injection rates to be compared and thus, the normalized value should be the same regardless of injection rate.

$$N = \frac{C_p - C_i}{\dot{V}_{CO_2} / \dot{V}_{supply}} \quad (4.3)$$

As described by Trupka (2011), to reduce the effects of the noise generated by the sudden variations in ambient CO₂ concentration levels a transient average of the inlet/supply air CO₂ concentration was used. The transient average for the supply air CO₂ concentrations was calculated using a thirty-one count moving average. The CO₂ concentration at a particular time was calculated by taking an average of the preceding thirty concentration values along with the current value. With a scan interval of 5 seconds, the transient average concentration at a particular time was an average of 2.5 minutes of data preceding the current value. Thus, this particular averaging method required disregarding of the first 2.5 minutes of the CO₂ concentration data. Figure 4.16 compares the CO₂ concentration data before and after application of the transient moving average method.

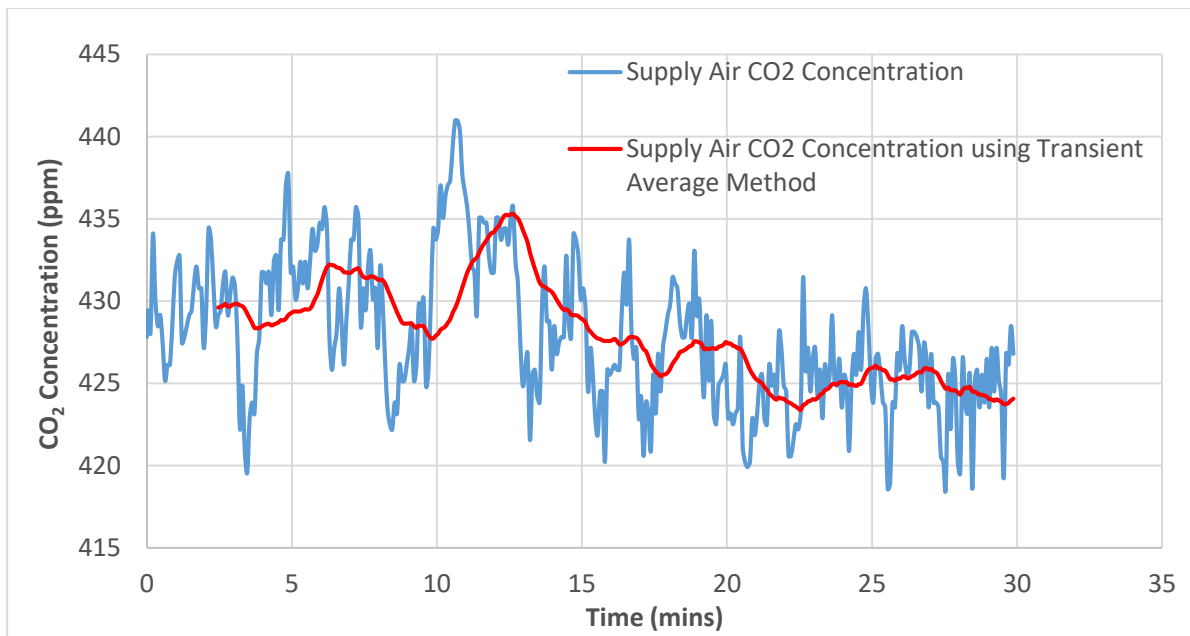


Figure 4.16 Comparison of Supply Air CO₂ Concentration Data

4.2.2 Testing with No Ventilation Air

There are situations when the aircraft cabin is not supplied with ventilation air. For example, no ventilation air would be supplied to the cabin in case of malfunction of the ventilation system. During de-icing operations, the air supply system may be shut down for a certain period. In addition, the ventilation system is sometimes turned off for a certain time period while an aircraft is parked at the gates. Thus, the objective of the fourth set of experiments was to study gaseous contaminant dispersion in the absence of ventilation air.

4.2.2.1 Tracer Gas Injection

Similar to the tests conducted for set three, a mixture of CO₂ and He was used as a tracer gas for this study. The injection apparatus used was also similar to the apparatus used for study with supply of ventilation air. In the absence of ventilation air, the CO₂ concentration increases significantly within a short period of time as there is no ventilation to remove the injected CO₂ from the cabin. As mentioned earlier, the gas analyzers have a certain range for measurement of CO₂ concentration. It was important to identify an optimal injection rate in order to get accurate CO₂ concentration measurements inside the cabin. Three injection rates of 2 L/min (0.071 ft³/min), 3 L/min (0.106 ft³/min) and 5 L/min (0.177 ft³/min) were analyzed. It was found that 2 L/min (0.071 ft³/min) is an optimal injection rate to measure considerable CO₂ concentrations without exceeding the measurement range of the analyzers. To study dispersion of tracer gas with no ventilation air, three injection locations were selected throughout the cabin. The seats 2B and 4E along with center location of aisle of row 3 were selected for injection of tracer gas. The injection locations selected for this study are shown in Figure 4.17.

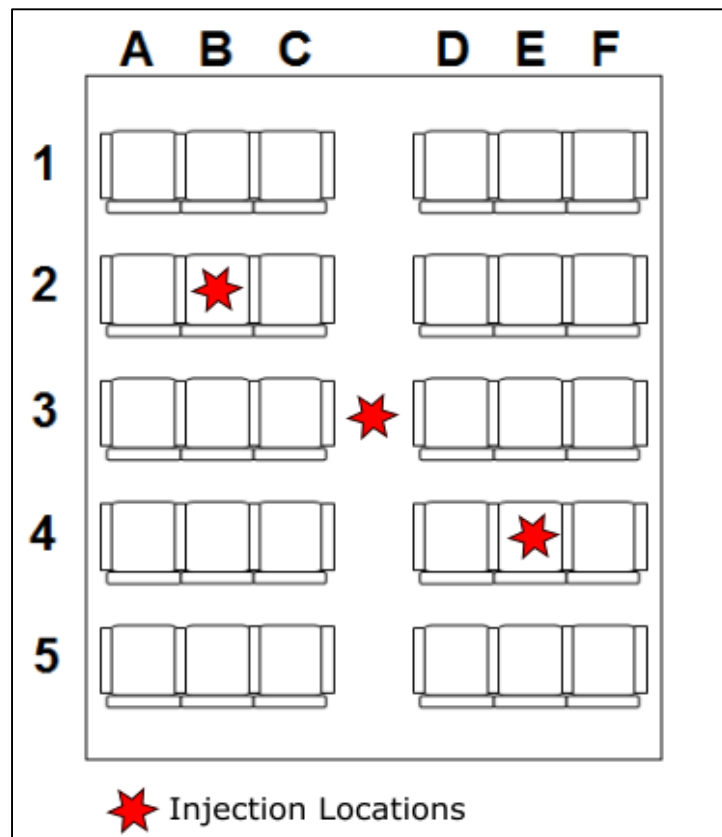


Figure 4.17 Tracer Gas Injection Locations for Dispersion Study with No Ventilation Air

4.2.2.2 Tracer Gas Measurement

In order to reduce the time of experimentation, only selected locations for each injection locations were tested. The sampling seat locations for a particular injection location for this set of experiments were similar to the seats sampled in set three for the corresponding injection location. For each injection location shown in Figure 4.17, the corresponding sampling seats are shown in Figures 4.12.

4.2.2.3 Testing Procedure

In the absence of ventilation air, movement of air inside the cabin is caused due to natural circulation, which is greatly influenced by the temperature difference between various zones of the cabin. Thus, for the study of contaminant dispersion with no ventilation air, it is essential to bring the cabin to steady state thermal conditions. The experiments conducted in this set began by supplying the cabin with conditioned air at 15.6 °C (60 °F) to bring the cabin to a state of thermal equilibrium. Tracer gas was then injected to bring the cabin to steady state CO₂ concentrations. After steady state condition was achieved, the ventilation air supply was stopped with continued tracer gas injection. The transient CO₂ concentrations with no ventilation were then measured at various sampling locations.

To evaluate the duration of each test, it was necessary to determine the time required by the cabin to attain thermal equilibrium and steady state CO₂ concentration. The experiment to determine these durations began by supplying the cabin with ventilation air at a temperature of 15.6 °C (60 °F) for a period of 3 hours and 30 minutes. Tracer gas was then injected with continued supply of ventilation air for 30 minutes to allow the CO₂ concentration inside the cabin to reach steady state concentration. Then the ventilation supply was cut off with continued CO₂ injection. The experiment was then run for another 2 hours in the absence of ventilation. Fourteen temperature sensors spread uniformly throughout the cabin were used to measure the cabin temperature and analyzers were placed at seats 1B, 3E and 5F. Figure 4.18 shows the average cabin temperature for the entire testing duration and Figure 4.19 shows the CO₂ concentration data throughout the testing period. As can be seen from Figure 4.18, the cabin took approximately 3 hours to achieve thermal equilibrium. In addition, it is to be noted that after the ventilation supply was cut off, the thermal manikins heated the cabin for approximately 90 minutes until the maximum allowable cabin temperature was reached. At this point, the thermal

switch disconnected the power to the manikins and the CO₂ supply was stopped manually allowing the cabin to cool down and reach ambient CO₂ concentration levels.

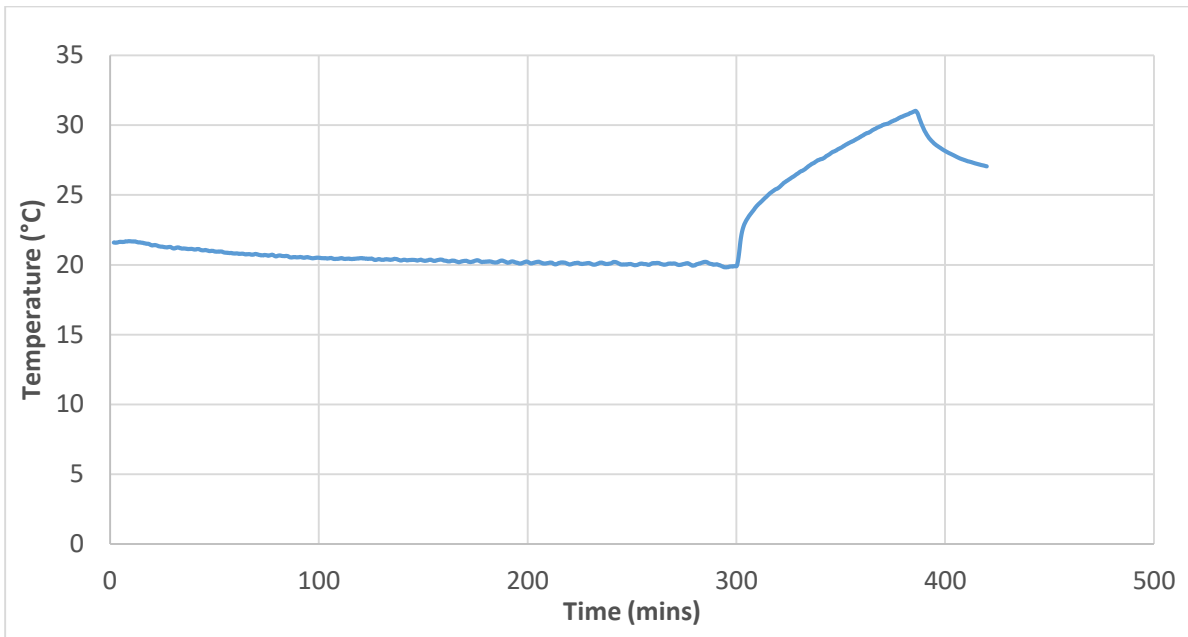


Figure 4.18 Result for Thermal Equilibrium Testing

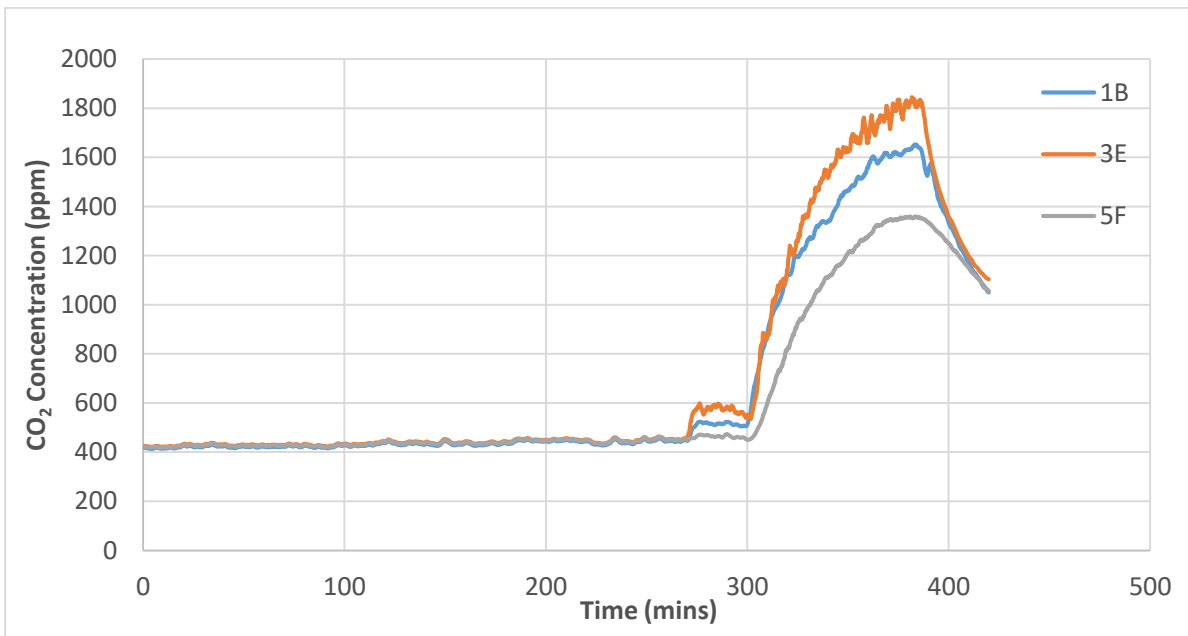


Figure 4.19 CO₂ Concentration Data

Based on the results shown in Figure 4.18 and 4.19 the experimental procedure for contaminant dispersion with no ventilation testing was constructed and is detailed in Table 4.3.

Table 4.3 Test Procedure for Tracer Gas Dispersion Study with No Ventilation Air

Phase	Tracer Gas Injection Status	Ventilation Air Supply Status	No. of Scans	Scan Interval (sec)	Time Duration (mins)	Notes
Pre-Test Scans	OFF	ON	2160	5	180	To allow the cabin to reach thermal equilibrium condition
S.S. Delay Scans	ON	ON	360	5	30	To allow the CO ₂ concentration to reach Steady State Conditions
S.S. Delay Scans	ON	OFF	360	5	30	To collect transient CO ₂ concentration data with no ventilation air.

4.2.2.4 Data Analysis Method

CO₂ concentrations recorded by analyzers in the form of voltage readings were converted to ppm of CO₂ utilizing the same calibration procedure as described in section 4.2.1.4 of this chapter.

In the absence of ventilation air, tracer gas injection causes the CO₂ concentration to increase rapidly with time, as there is no ventilation to flush out CO₂ from inside the cabin. Thus, for study with no ventilation air, the normalization equation needed to be modified to be a function of time as well. For this study the CO₂ concentration is normalized using Equation 4.4 (Madden, 2015), where ‘C_p’ is the CO₂ concentration at the sampling point, ‘C_{start}’ is the CO₂ concentration when the ventilation is stopped, ‘T’ is the time since the elimination of ventilation, ‘ \dot{V}_{CO_2} ’ is the CO₂ injection rate and ‘V_{cabin}’ is the cabin volume.

$$N = \frac{C_p - C_{start}}{\dot{V}_{CO_2} \times T / V_{cabin}} \quad (4.4)$$

4.3 Repeatability of CO₂ Analyzers

In order to understand the significance of the variations found in ventilation effectiveness studies, it was important to check the repeatability of each analyzer used. To analyze the repeatability of the CO₂ sensors, a number of experiments were conducted inside the Boeing 767 mockup cabin. The test procedure used for each experiment is similar to the procedure used for the study of ventilation effectiveness. The analysis began by placing sampling ports of CO₂ analyzers at particular convenient locations. Six consecutive experiments were performed with placement of a particular analyzer at a fixed location to evaluate the local effective ventilation rates at the selected locations. The data from each analyzer for each of the six cases were compared to determine the repeatability of analyzers.

4.4 Effect of Transient Response

As mentioned earlier, in order to simplify the sampling procedure, sampling lines consisting of approximately 7.92 m (26 ft) long vinyl tubes are used. Thus, it is essential to evaluate the effects of time delay caused by the length of the sampling tubes. Experiments were performed inside the Boeing 767 mockup cabin to study these effects. Two experiments were conducted with variations in the lengths of the sampling tubes to evaluate the local effective ventilation rates inside the Boeing 767 cabin. For the purpose of comparison, the same sampling locations were selected for both the experiments conducted. In order to avoid moving the CO₂ sensors to far off locations, seats closer to the power source for the analyzers were selected. Based on this criterion the seats 5B, 4D, 3A and 4C were chosen as sampling locations. The first experiment was conducted using 0.36 m (14 in.) long vinyl tubes connected to each of the analyzers and the second experiment was conducted by placing the analyzers at the seat locations without any tubes. The experimental procedure for this set of experiments was similar to the procedure for ventilation effectiveness study. The local effective ventilation rates were evaluated for the two cases at the selected seat locations. These results were then compared with the results from experiments conducted with 7.92 m (26 ft) long vinyl tubes for the same seats.

4.5 Time Response of CO₂ Analyzers

Time response of a CO₂ analyzer is defined as the time required by the analyzer to record steady state CO₂ concentration after being subjected to a step change in the CO₂ concentration. As the transient CO₂ concentration data is analyzed to evaluate the ventilation effectiveness values, it is important to study the time response of the analyzers used. High time response of an analyzer is undesirable as it can cause errors in measurement. Thus, experiments were performed inside the Boeing 767 cabin mockup to evaluate the time response of each analyzer used for experimentation. The tests began by placing sampling ports of three CO₂ sensors outside the cabin exposed to atmospheric condition, while sampling port of the fourth analyzer was placed inside the cabin to record CO₂ concentrations inside the cabin. Tracer gas was then injected allowing the cabin to reach steady state CO₂ concentration. After a certain period of time, the sampling ports outside the cabin were simultaneously inserted inside the cabin through the ventilation gaps. This provided the analyzers with the step change in CO₂ concentration required to evaluate the time response of the analyzers. This experiment was conducted three times with variations in the analyzer measuring CO₂ concentration inside the cabin to ensure assessment of all four analyzers.

Chapter 5 - Results and Discussions

This chapter presents important findings from the experiments conducted for various studies reported in this thesis. The following sections provide the results along with discussions for the study of ventilation effectiveness, examination of tracer gas dispersion with ventilation air and with no ventilation air.

5.1 Ventilation Effectiveness

This section presents the results from ventilation effectiveness studies carried out inside the Boeing 767 and the Boeing 737 cabin mockups. The experiments for ventilation effectiveness studies were conducted following the testing procedure mentioned in Chapter 4 of this thesis. Equation 4.1 and 4.2 were used to calculate the e_L rates and E_L values at various locations inside the cabins. It is important to note that, in most aircraft, the supply air is composed of part recirculated air and part outside air. Based on the mixed supply air scenario the ventilation effectiveness can be defined as either the effectiveness with which supply air is distributed to a given space or the effectiveness with which outside air is distributed to a given space. The ventilation effectiveness values determined in this research are from measurements with supply air being 100 % outside air. Therefore, the ventilation effectiveness values presented in this thesis are representative of the supply air ventilation effectiveness. With a given recirculation fraction, the experimentally determined supply air ventilation effectiveness values can be converted to outside air ventilation effectiveness values using the equations derived by Jones (2016). Detailed explanation and derivation of the conversion equations are provided in Appendix C of this thesis.

5.1.1 Ventilation Effectiveness Study inside the Boeing 767 Cabin

As tracer gas was directly injected into the supply air well upstream of the diffusers, even after the interruption of CO₂ injection, certain amount of time was required to flush the existing CO₂ from inside the supply duct. In addition, as the decay process progresses the CO₂ concentration inside the cabin approaches ambient levels giving erratic values for local effective ventilation rates. This necessitates the need to identify an optimal time from the 15 minutes of decay period for which the data would be analyzed. A plot of local effective ventilation rates

against the decay time for a typical ventilation effectiveness experiment is shown in Figure 5.1. Due to the length constraint for this report, only selected plots are presented. Similar plots for other experiments are provided in the Electronic Appendix attached with this thesis. The plot shown in Figure 5.1 along with other plots provided in the Electronic Appendix revealed that the local effective ventilation rates remain more or less constant between the period from 2 minutes to 5 minutes. Thus, to avoid end-effects the values between this period were averaged to evaluate the e_L rates at various sampling locations.

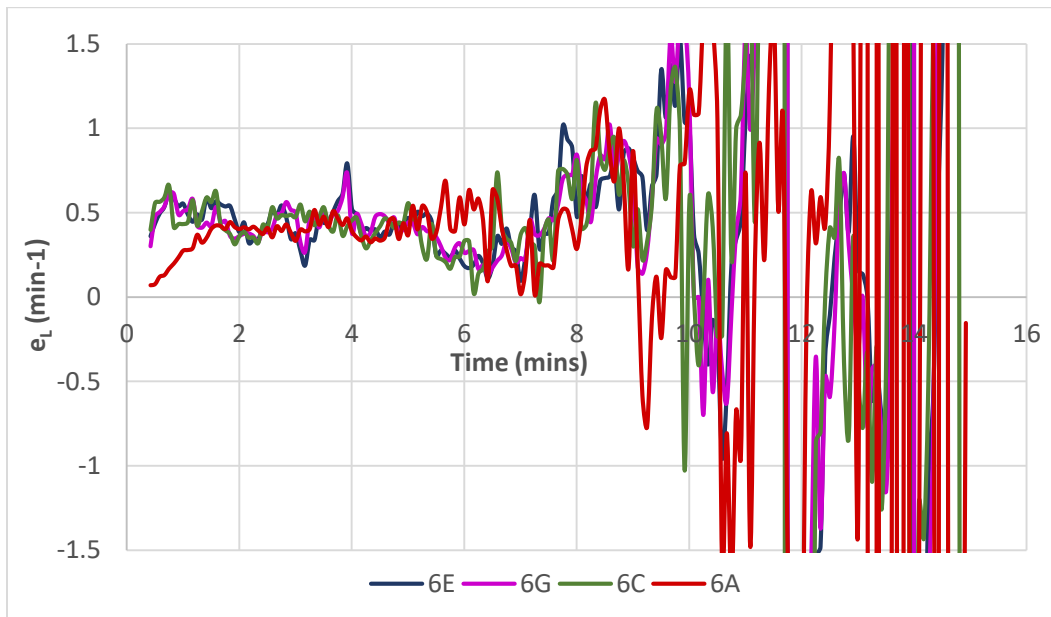


Figure 5.1 Result for Optimal Time Period Analysis

The average e_L rates for the two repeats of experiments are summarized in Table 5.1. As can be clearly seen from the table there is only slight variations in the e_L rates from seat location-to-seat location throughout the cabin. The e_L rates ranged from 0.39 min^{-1} to 0.47 min^{-1} . The standard deviation for all values in Table 5.1 was found to be 0.015 min^{-1} . The e_L rates from Table 5.1 indicate that the ventilation system of this particular aircraft cabin uniformly replaces air from all seat locations inside the cabin. Figure 5.2 shows the uniformity of e_L rates from seat location-to-seat location inside the cabin mockup.

Table 5.1 Average e_L Rates for Entire Cabin (min⁻¹)

	A	B	C	D	E	F	G
Row 1	0.41	0.43	0.43	0.42	0.43	0.44	0.45
Row 2	0.45	0.44	0.44	0.45	0.45	0.47	0.42
Row 3	0.43	0.42	0.43	0.43	0.42	0.43	0.41
Row 4	0.44	0.44	0.43	0.47	0.44	0.43	0.42
Row 5	0.41	0.43	0.42	0.44	0.42	0.44	0.42
Row 6	0.42	0.45	0.41	0.44	0.42	0.40	0.42
Row 7	0.42	0.43	0.40	0.44	0.44	0.43	0.43
Row 8	0.41	0.41	0.40	0.43	0.42	0.42	0.40
Row 9	0.42	0.42	0.40	0.44	0.41	0.43	0.42
Row 10	0.44	0.42	0.40	0.42	0.41	0.43	0.43
Row 11	0.44	0.40	0.41	0.39	0.43	0.40	0.42

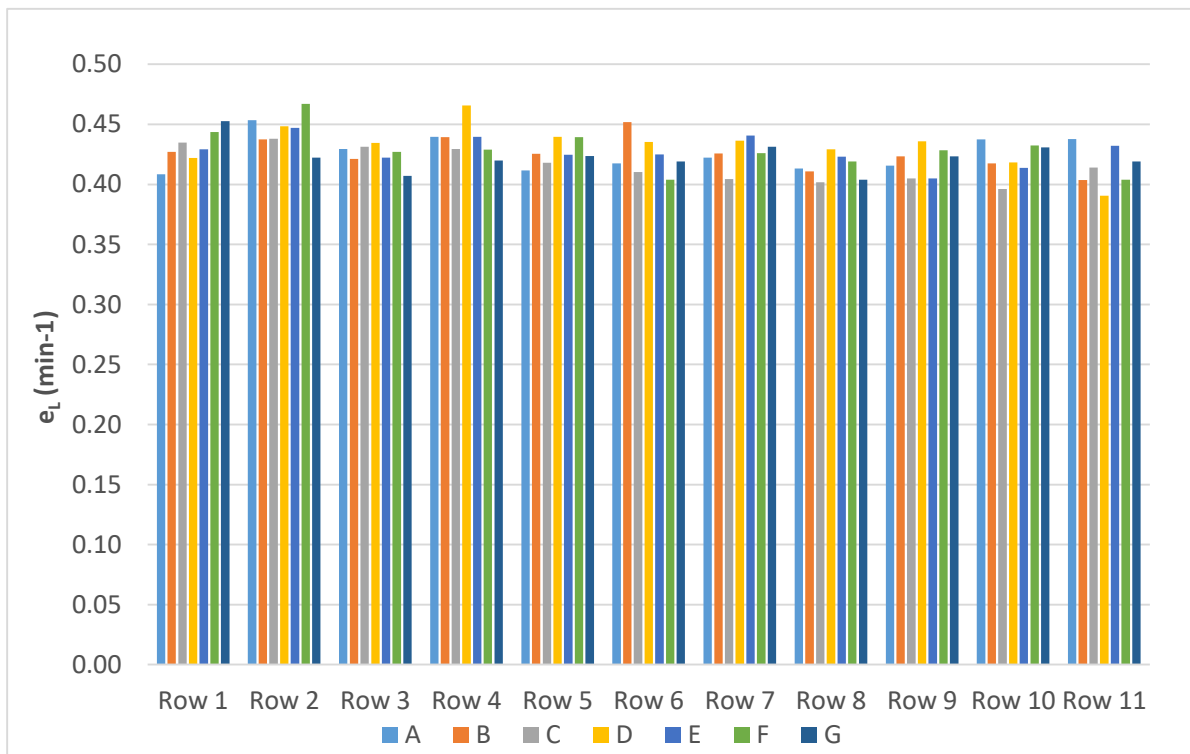


Figure 5.2 Seat-to-Seat Variation of e_L Rates

After the e_L rates were evaluated, the E_L values were calculated by simply dividing the corresponding e_L rate by the ratio of supply airflow rate and the volume of the cabin. The volume

of the Boeing 767 mockup cabin was calculated using the mathematical equations of the cabin profile given by Lebbin (2006). The total volume of the empty cabin was calculated to be 91 m³ (3210 ft³). However, the volume of the seats and manikins inside the cabin needed to be subtracted from the total cabin volume before it could be used to calculate the **E_L** values. The total volume of all seventy-seven seats and manikins inside the cabin was found to be approximately 11.61 m³ (410 ft³) giving a net cabin volume of 79.29 m³ (2800 ft³). As the volume of the cabin remains fixed and the air supply rate was maintained constant for all experiments, the ratio of these two quantities is a constant value. Therefore, the **E_L** values are directly proportional to the corresponding **e_L** rates. Table 5.2 shows the results for the **E_L** values for all seats inside the cabin. Table 5.2 values show that the variations in the **E_L** values are the same as that observed in Table 5.1. The **E_L** values ranged from 0.78 to 0.93. The standard deviations for **E_L** values from the entire cabin was found to be 0.030. The average of all the **E_L** values or the ventilation effectiveness of the entire cabin was calculated to be 0.85. Figure 5.3 plots the variation of the local ventilation effectiveness values throughout the cabin. As can be seen from Figure 5.3, the values are consistently uniform throughout the cabin.

Table 5.2 Average **E_L Values for Entire Cabin**

	A	B	C	D	E	F	G
Row 1	0.82	0.85	0.87	0.84	0.86	0.89	0.91
Row 2	0.91	0.87	0.88	0.90	0.89	0.93	0.84
Row 3	0.86	0.84	0.86	0.87	0.84	0.85	0.81
Row 4	0.88	0.88	0.86	0.93	0.88	0.86	0.84
Row 5	0.82	0.85	0.84	0.88	0.85	0.88	0.85
Row 6	0.83	0.90	0.82	0.87	0.85	0.81	0.84
Row 7	0.84	0.85	0.81	0.87	0.88	0.85	0.86
Row 8	0.83	0.82	0.80	0.86	0.85	0.84	0.81
Row 9	0.83	0.85	0.81	0.87	0.81	0.86	0.85
Row 10	0.87	0.84	0.79	0.84	0.83	0.87	0.86
Row 11	0.88	0.81	0.83	0.78	0.86	0.81	0.84

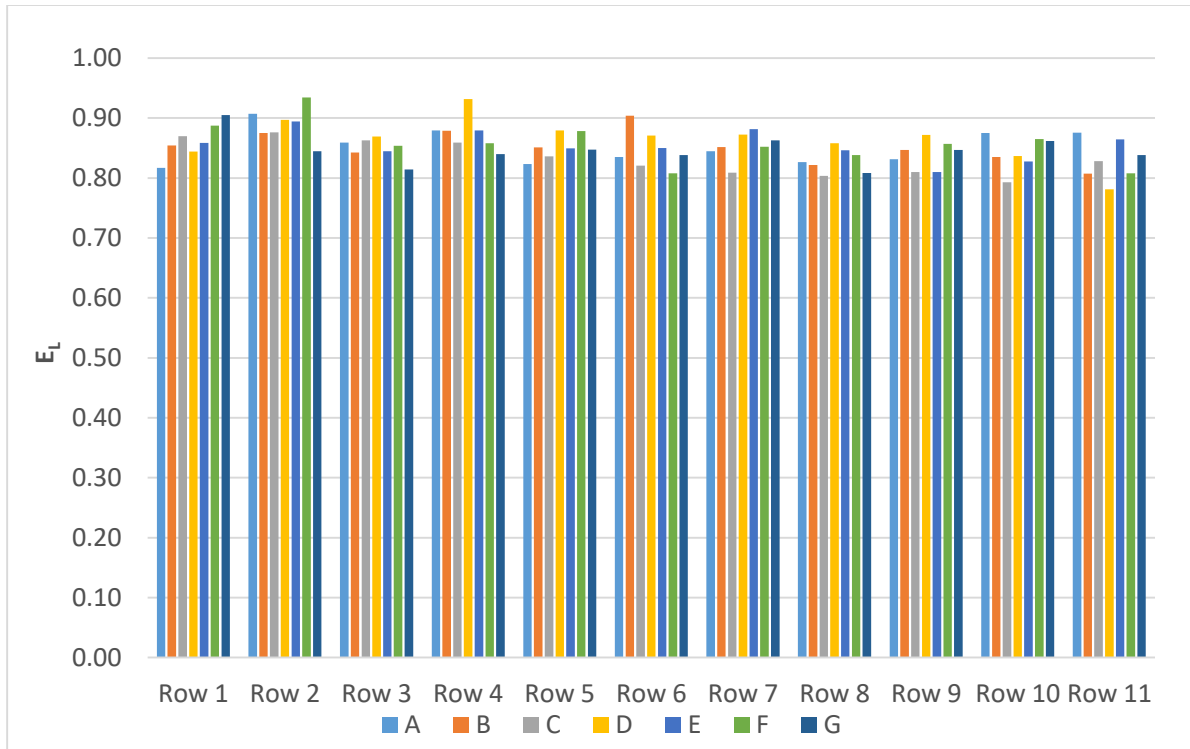


Figure 5.3 Seat-to-Seat Variation of E_L Values

Although the variations in ventilation effectiveness values from seat location-to-seat location are slight, it was important to study the significance of these variations. To investigate this, the mean value of ventilation effectiveness for each repetition was calculated and compared for the two repeats as shown in Table 5.3. As can be seen from the table, there are only slight variations in mean values of the two repeats indicating consistency in the results from the two repeats. In addition, for each repeat, the variation of the mean from each sampled seat was calculated and compared between the two repeats to observe any correlation between the replications. The results for comparison between the two sets are shown in Figure 5.4. As can be seen from Figure 5.4, the variations are highly random with no clear correlations between the E_L values from the two replications. Therefore, it is concluded that, for this particular aircraft cabin type, air is uniformly and efficiently ventilated for all seats inside the cabin.

Table 5.3 Comparison of Experimental Repeats for Boeing 767 Mockup Cabin

	Mean Value
Repeat 1	0.86
Repeat 2	0.85

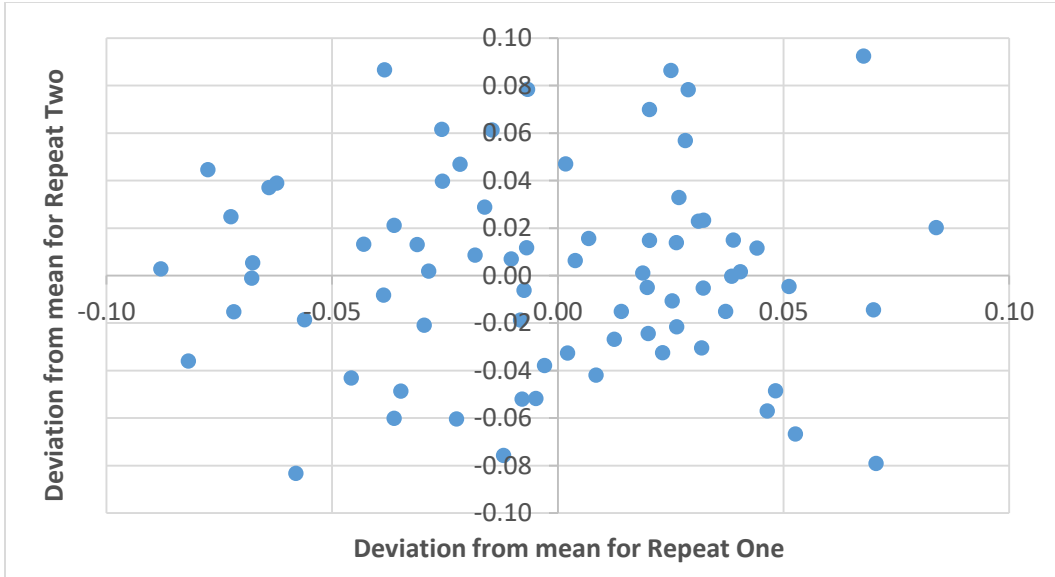


Figure 5.4 Comparison Plot of Variation of e_L Rates from Mean for Set One Repeats

5.1.2 Ventilation Effectiveness Study inside the Boeing 737 Cabin

For reasons mentioned in section 5.1.1 of this chapter, an optimal time period is determined to calculate e_L rates inside the Boeing 737 mockup cabin. Figure 5.5 plots the e_L rates against the decay time from an experiment analyzing seats 1A, 1B and 1C. Again, the plots from other experiments conducted are provided in the Electronic Appendix. As can be seen from the plot the time period 2 minutes to 5 minutes is optimal to evaluate the e_L rates.

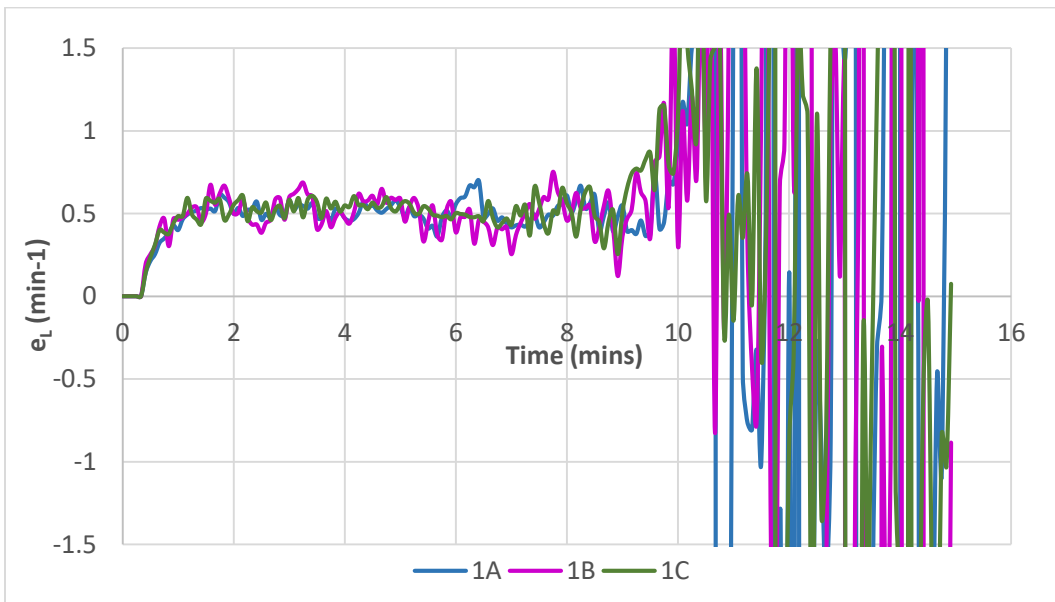


Figure 5.5 Result for Optimal Time Period Analysis

To calculate E_L values, it was necessary to determine the cabin volume. The volume of the empty Boeing 737 cabin was calculated using major dimensions of the cabin and was found to be 31.15 m^3 (1100 ft^3). The total volume of all thirty manikins and seats inside the cabin was calculated to be approximately 4.42 m^3 (156 ft^3) giving a net cabin volume of 26.73 m^3 (944 ft^3).

Four series of experiments were performed inside the Boeing 737 cabin to evaluate ventilation effectiveness at various locations and heights inside the cabin. The first series of experiments evaluates the e_L rates at breathing level of seated adult passengers. The results for the e_L rates for the first series of experiments are shown in Table 5.4 and Figure 5.6. In addition, the E_L values for this series are shown in Table 5.5 and Figure 5.7. Each value in both the tables is an average of data from three repeats. As can be seen from Table 5.4 the e_L rates for this series of experiments ranged from 0.49 min^{-1} to 0.54 min^{-1} , with a standard deviation of 0.014 min^{-1} . Table 5.5 shows that the E_L values ranged from 0.77 to 0.85, with a standard deviation of 0.022.

Table 5.4 Average e_L Rates for First Series of Experiments (min^{-1})

	A	B	C	D	E	F
Row 1	0.52	0.53	0.54	0.52	0.52	0.52
Row 2	0.49	0.51	0.52	0.51	0.50	0.49
Row 3	0.49	0.49	0.50	0.52	0.51	0.51
Row 4	0.49	0.49	0.49	0.51	0.52	0.50
Row 5	0.51	0.50	0.50	0.52	0.50	0.51

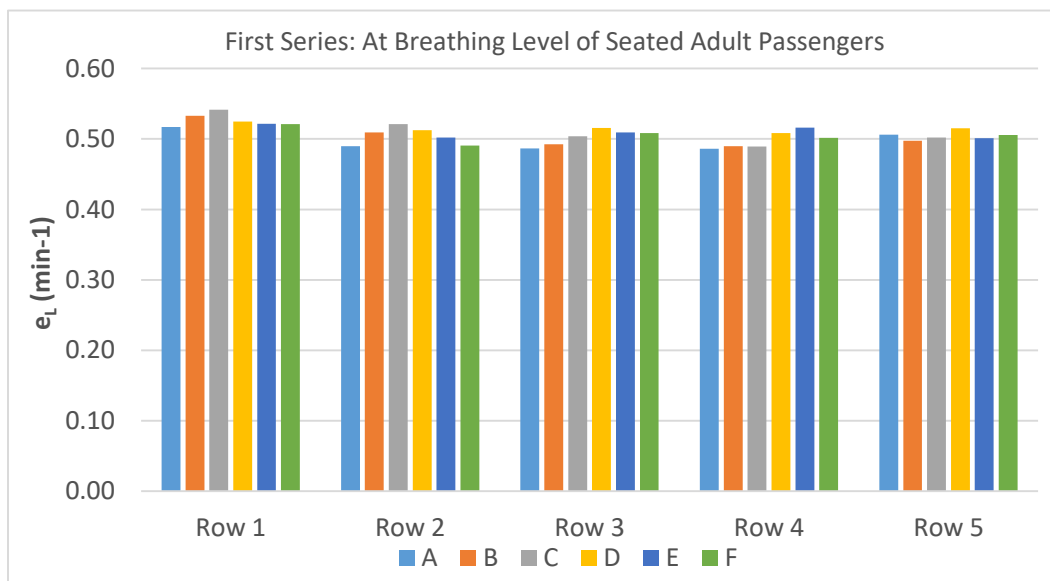


Figure 5.6 Location-to-Location Variation of e_L Rates

Table 5.5 Average E_L Values for First Series of Experiments

	A	B	C	D	E	F
Row 1	0.81	0.84	0.85	0.83	0.82	0.82
Row 2	0.77	0.80	0.82	0.81	0.79	0.77
Row 3	0.77	0.78	0.79	0.81	0.80	0.80
Row 4	0.77	0.77	0.77	0.80	0.81	0.79
Row 5	0.80	0.78	0.79	0.81	0.79	0.80

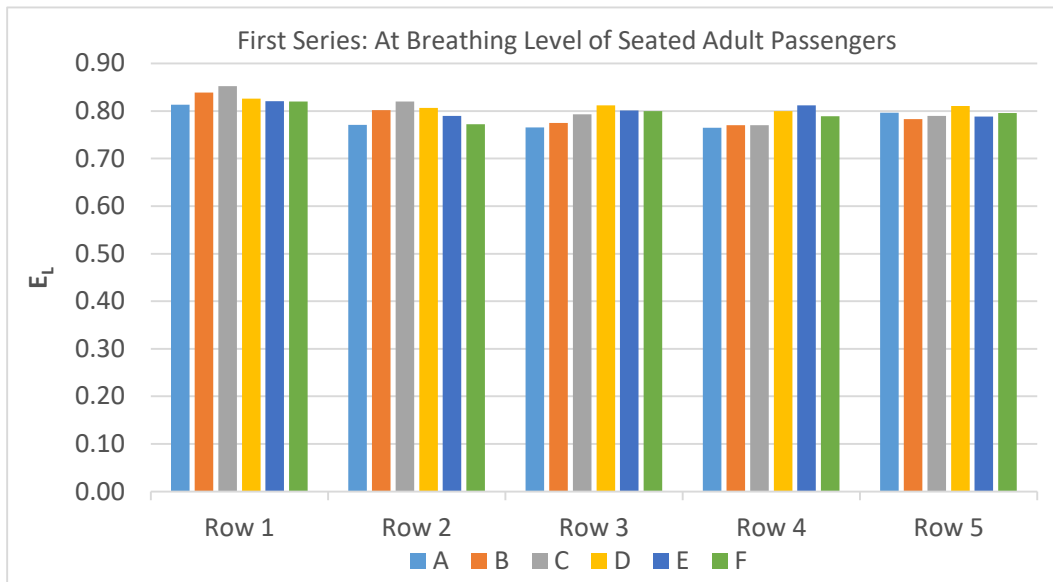


Figure 5.7 Location-to-Location Variation of E_L Values

The second series of experiments are performed to evaluate ventilation effectiveness at breathing level of seated infant passengers. The average results from two repeats for the local effective ventilation rates for the second series of experiments are shown in Table 5.6 and Figure 5.8. In addition, the average local ventilation effectiveness values for the second series are shown in Table 5.7 and Figure 5.9. Table 5.6 reveals that e_L rates for this series of experiments ranged from 0.48 min^{-1} to 0.52 min^{-1} , with a standard deviation of 0.012 min^{-1} for all the values. As can be seen from Table 5.7, the E_L values ranged from 0.75 to 0.82, with a standard deviation of 0.019 for all values.

Table 5.6 Average e_L Rates for Second Series of Experiments (min^{-1})

	A	B	C	D	E	F
Row 1	0.52			0.52		
Row 2		0.50			0.50	
Row 3	0.50		0.48	0.50		0.50
Row 4		0.50			0.49	
Row 5			0.50			0.49

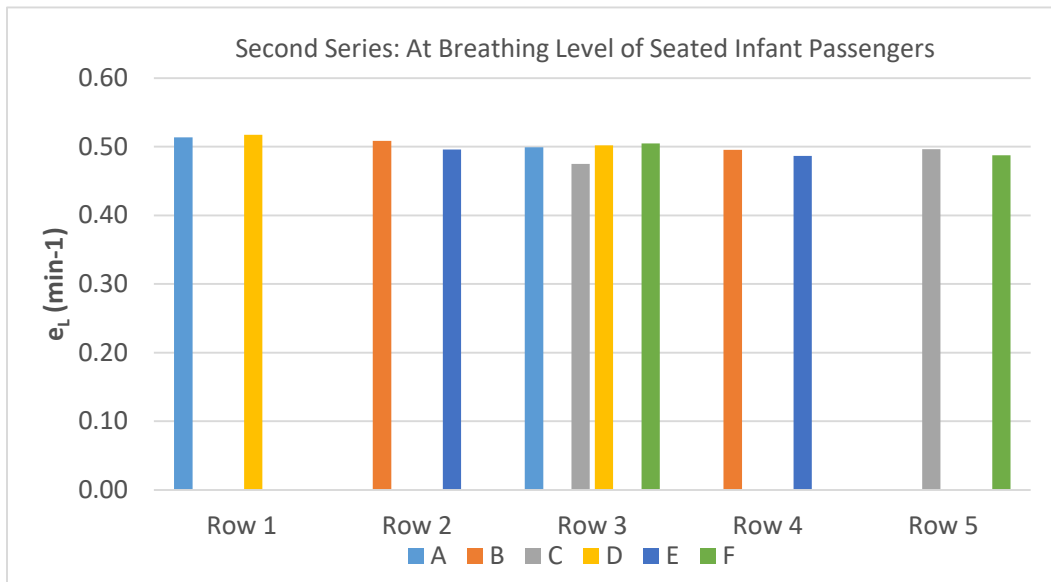


Figure 5.8 Location-to-Location Variation of e_L Rates

Table 5.7 Average E_L Values for Second Series of Experiments

	A	B	C	D	E	F
Row 1	0.82			0.81		
Row 2		0.79			0.78	
Row 3	0.79		0.75	0.79		0.79
Row 4		0.78			0.77	
Row 5			0.78			0.77

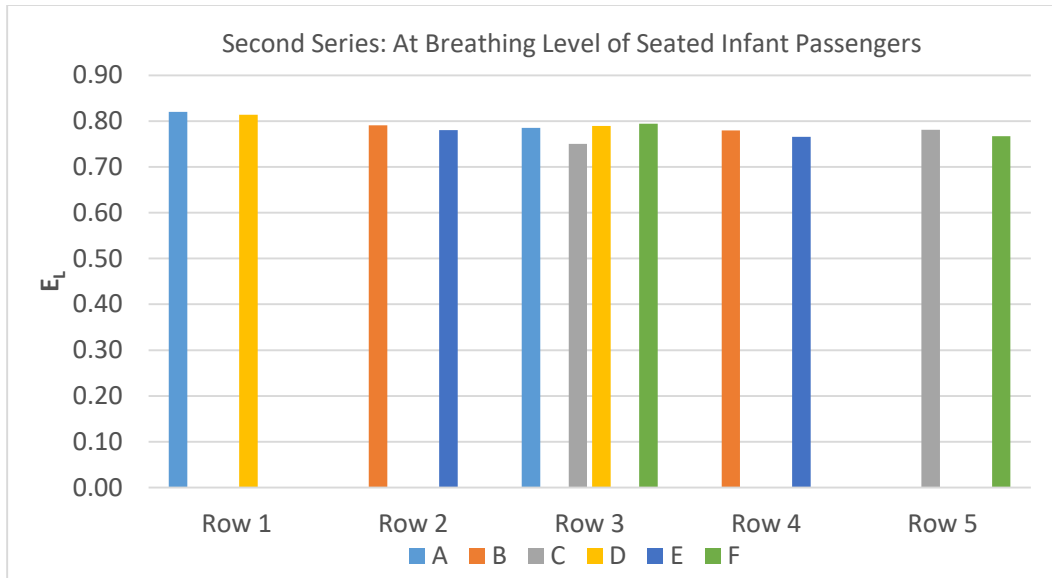


Figure 5.9 Location-to-Location Variation of E_L Values

The third series of experiments focuses on ventilation effectiveness at breathing level of adult passengers standing at seat locations. The results for the local effective ventilation rates for the third series of experiments are shown in Table 5.8 and Figure 5.10. The average local ventilation effectiveness values for the third series are shown in Table 5.9 and Figure 5.11. Each value in the given tables is an average of data from two repeats. As can be seen from Table 5.8, e_L rates for this series ranged from 0.50 min^{-1} to 0.52 min^{-1} , with a standard deviation of 0.0074 min^{-1} for all the values. Table 5.9 shows that the E_L values ranged from 0.78 to 0.83, with a standard deviation of 0.012 for all values.

Table 5.8 Average e_L Rates for Third Series of Experiments (min^{-1})

	A	B	C	D	E	F
Row 1	0.52			0.51		
Row 2		0.51			0.50	
Row 3	0.50		0.50	0.52		0.50
Row 4		0.50			0.51	
Row 5			0.51			0.51

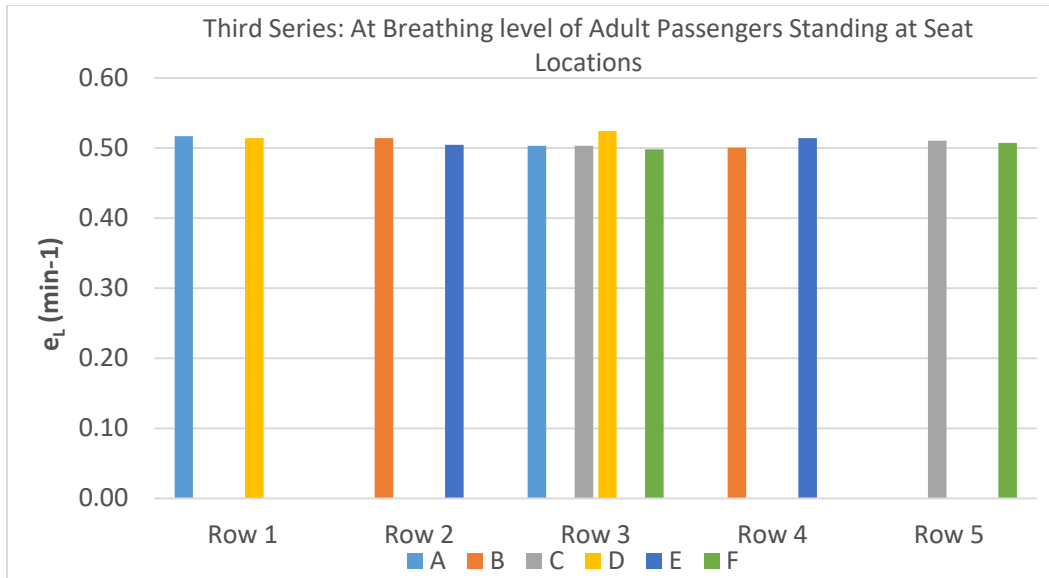


Figure 5.10 Location-to-Location Variation of e_L Rates

Table 5.9 Average E_L Values for Third Series of Experiments

	A	B	C	D	E	F
Row 1	0.81			0.81		
Row 2		0.81			0.79	
Row 3	0.79		0.79	0.83		0.78
Row 4		0.79			0.81	
Row 5			0.80			0.80

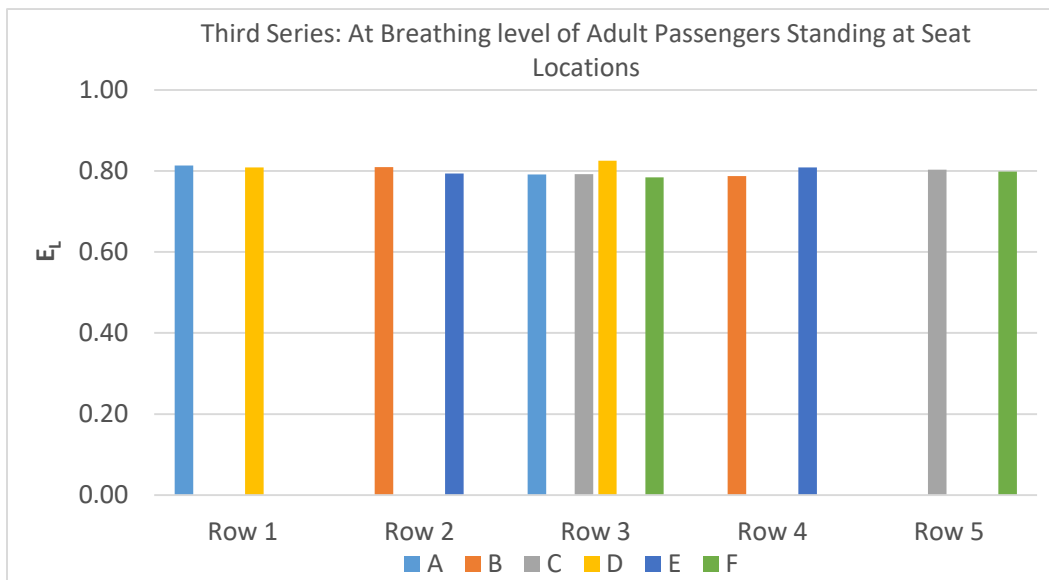


Figure 5.11 Location-to-Location Variation of E_L Values

Ventilation effectiveness at breathing level of adult passengers standing at aisle locations was determined in the fourth series of experiments. The results for the local effective ventilation rates for the fourth series of experiments are shown in Table 5.10 and Figure 5.12. In addition, the average local ventilation effectiveness values for this series are shown in Table 5.11 and Figure 5.13. Each value in both the tables is an average of data from two repeats. As can be seen from Table 5.10, e_L rates for this series of experiments ranged from 0.48 min^{-1} to 0.52 min^{-1} , with a standard deviation of 0.011 for all the values. Table 5.11 reveals that the E_L values ranged from 0.76 to 0.81, with a standard deviation of 0.017 for all values.

Table 5.10 Average e_L Rates for Fourth Series of Experiments (min^{-1})

Row 1	Row 2	Row 3	Row 4	Row 5
0.50	0.50	0.52	0.50	0.48

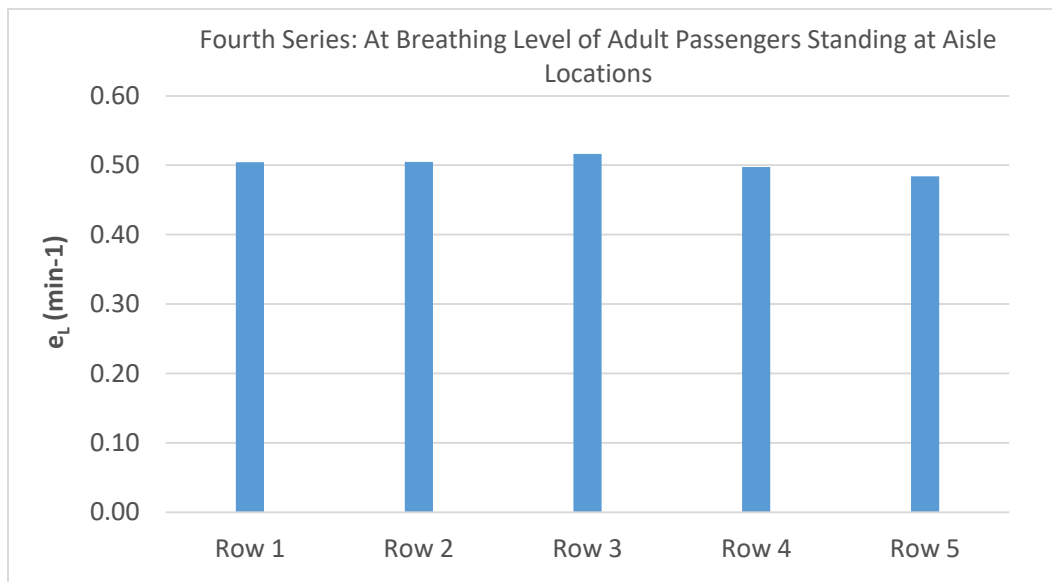


Figure 5.12 Location-to-Location Variation of e_L Rates

Table 5.11 Average E_L Values for Fourth Series of Experiments

Row 1	Row 2	Row 3	Row 4	Row 5
0.79	0.79	0.81	0.78	0.76

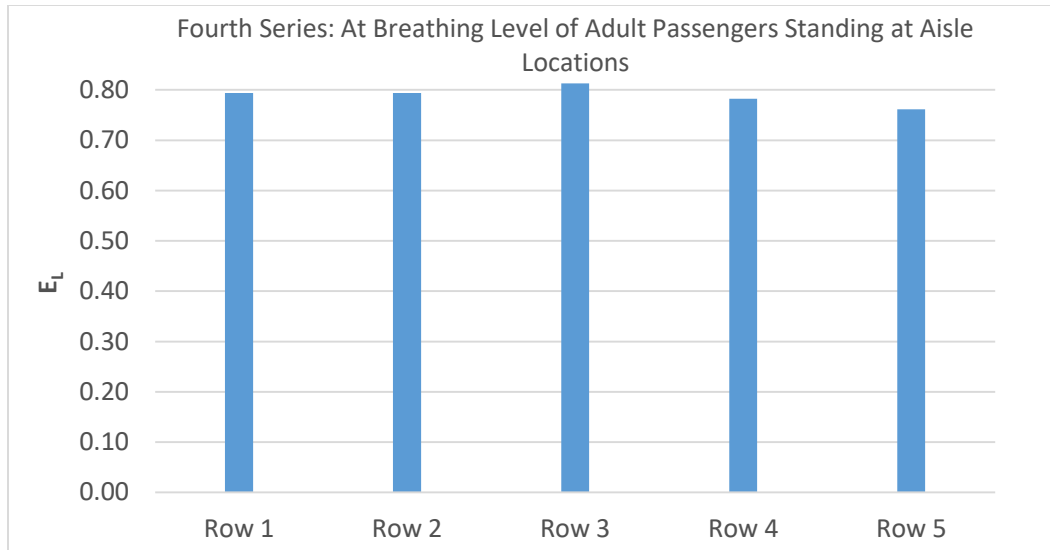


Figure 5.13 Location-to-Location Variation of E_L Values

Investigation similar to the one carried out for the Boeing 767 cabin results were done to analyze the significance of variations in the ventilation effectiveness values. For each series of experiments, the mean value of ventilation effectiveness for each repetition was calculated and compared as shown in Table 5.12. It is clear from Table 5.12 values, that there are only slight variations in the mean values of various replications for each series. This shows consistency in results from various repetitions for each series. In addition, for every series, the variation of ventilation effectiveness value at each seat from the mean is calculated and compared between replications of that particular series to observe any correlations between these replications. For example, the results for comparison between the first replication and second replication of series one are shown in Figure 5.14. As can be clearly seen from Figure 5.14, the variations are highly random with no clear correlation between the E_L values from the two replications. This trend is noticed in all series of experiments conducted and the plots can be found in the Electronic Appendix. This indicates that the differences in the E_L values are likely due to experimental variability rather than variations in E_L values by location.

Table 5.12 Comparison of Experimental Repeats for Boeing 737 Mockup

	Series 1 Mean Values	Series 2 Mean Values	Series 3 Mean Values	Series 4 Mean Values
Repeat 1	0.80	0.79	0.79	0.78
Repeat 2	0.79	0.78	0.81	0.80
Repeat 3	0.80	-	-	-

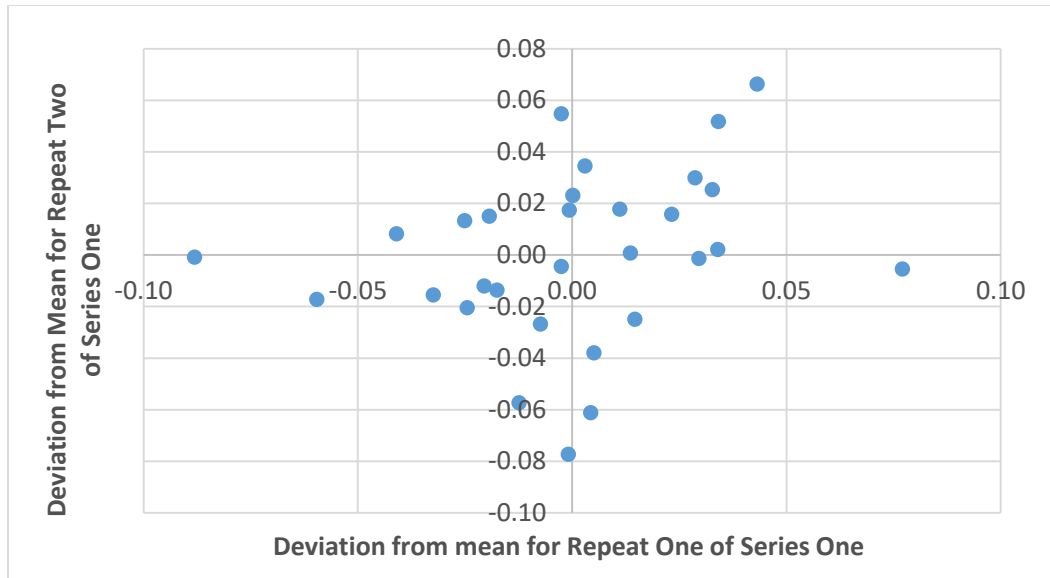


Figure 5.14 Comparison Plot of Variation of EL Values from Mean for Series One Repeats

Thus, it is clear from Tables 5.4 to 5.12 and Figures 5.6 to 5.14, that ventilation effectiveness is uniform throughout the cabin. The variations in the local effective ventilation rates and the local ventilation effectiveness values for various locations and heights inside the cabin are not very large. In addition, these variations are likely due to experimental variability. The results from ventilation effectiveness study inside the Boeing 737 cabin reveals that air is efficiently supplied to the entire cabin irrespective of the seat locations or heights inside the cabin. In other words, contaminants are uniformly and efficiently removed from the entire cabin.

5.2 Dispersion of Tracer Gas with Ventilation Air

The dispersion of tracer gas study is carried out by injecting tracer gas mixture at various locations inside the cabin. The aisle locations of rows 1, 3 and 5 along with seat locations 2B and 4E are used as injection locations to clearly understand the dispersion phenomenon. Experiments are conducted following the test procedure mentioned in Chapter 4 of this thesis. For each injection location, the normalized CO₂ count is calculated at various sampling locations using Equation 4.3.

Results from tracer gas dispersion study with injection at centerline of aisle at row 1 are presented in Table 5.13. As can be seen from Table 5.13, CO₂ counts at seats in row of injection i.e. row 1 are higher than CO₂ counts at most seats in rows away from the source. As shown in Figure 5.15, for a given seat column the CO₂ count decreased moving away from the source row

in the longitudinal direction. For example, 1D that is adjacent to the injection location had a CO₂ count of 1.62, while seats 3D and 5D in the same column had CO₂ counts of 1.10 and 0.54 respectively. This shows that the risk of exposure to gaseous contaminants decreases moving away from the source along the longitudinal direction. As can be observed from Figure 5.16, the CO₂ counts at most seats within a row are symmetrical about the centerline of the cabin to some extent. This can be expected given that the injection occurred at the centerline of the cabin. However, it is close to impossible to have perfect symmetry about the centerline, as it is difficult to achieve symmetrical air supply to the two halves of the cabin; also, the high level of turbulence in airflow makes it asymmetrical.

Table 5.13 Average Normalized CO₂ Count for Injection at Centerline of Aisle at Row 1

	A	B	C	D	E	F
Row 1	1.58		1.57	1.62		1.58
Row 2						
Row 3	0.99		1.75	1.10		0.87
Row 4						
Row 5	0.53		0.47	0.54		0.50

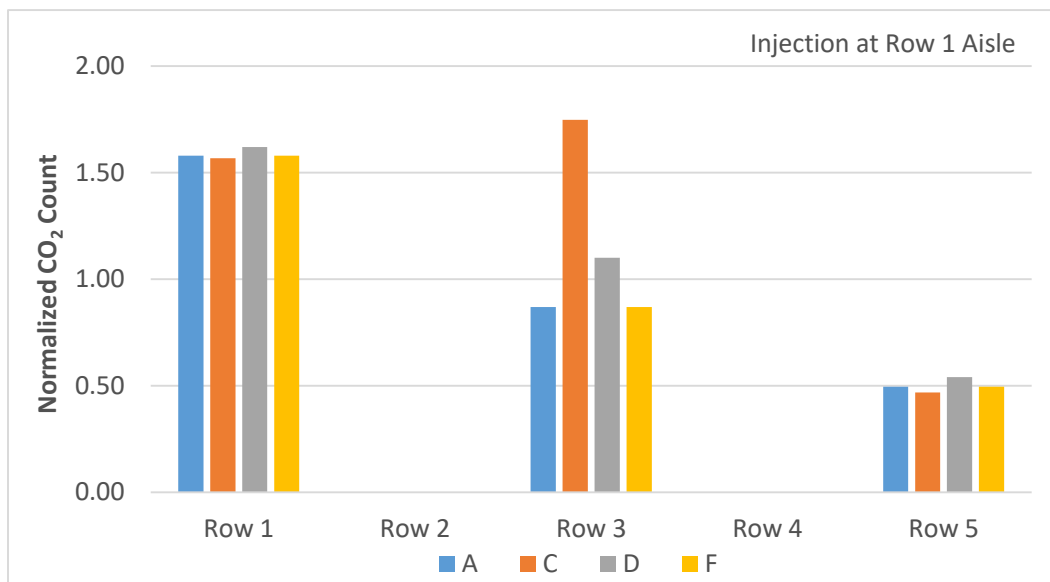


Figure 5.15 Longitudinal Dispersion of Tracer Gas

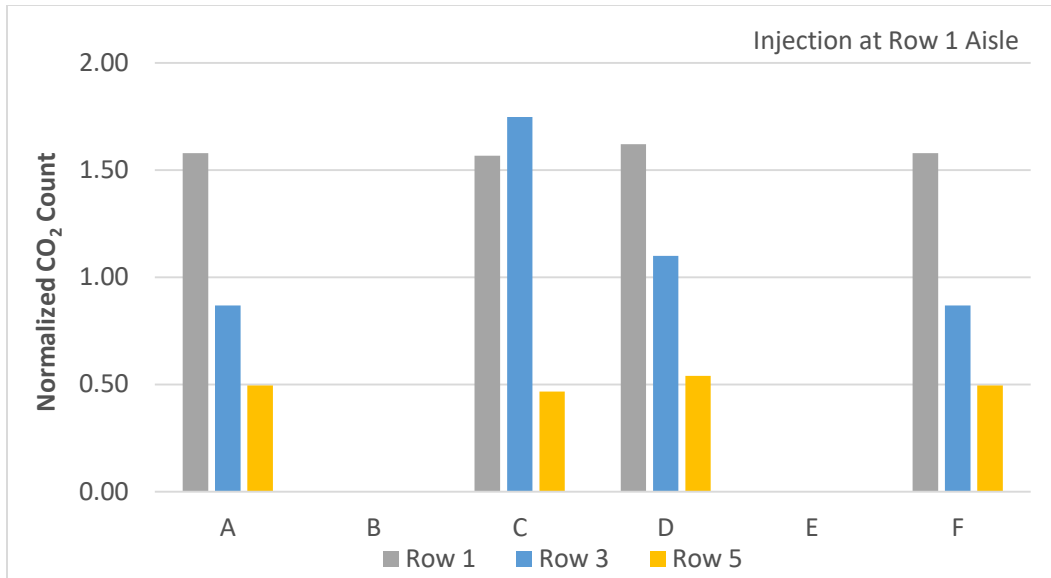


Figure 5.16 Lateral Dispersion of Tracer Gas

The results for average steady state CO₂ counts for various sampling locations with injection at centerline of aisle at row 1 are shown in Figures 5.17 to 5.20. Due to the constraint on the length of the report, plots for steady state CO₂ counts for injection at centerline of aisle at rows 3 and 5 are included in the Electronic Appendix attached with this thesis.

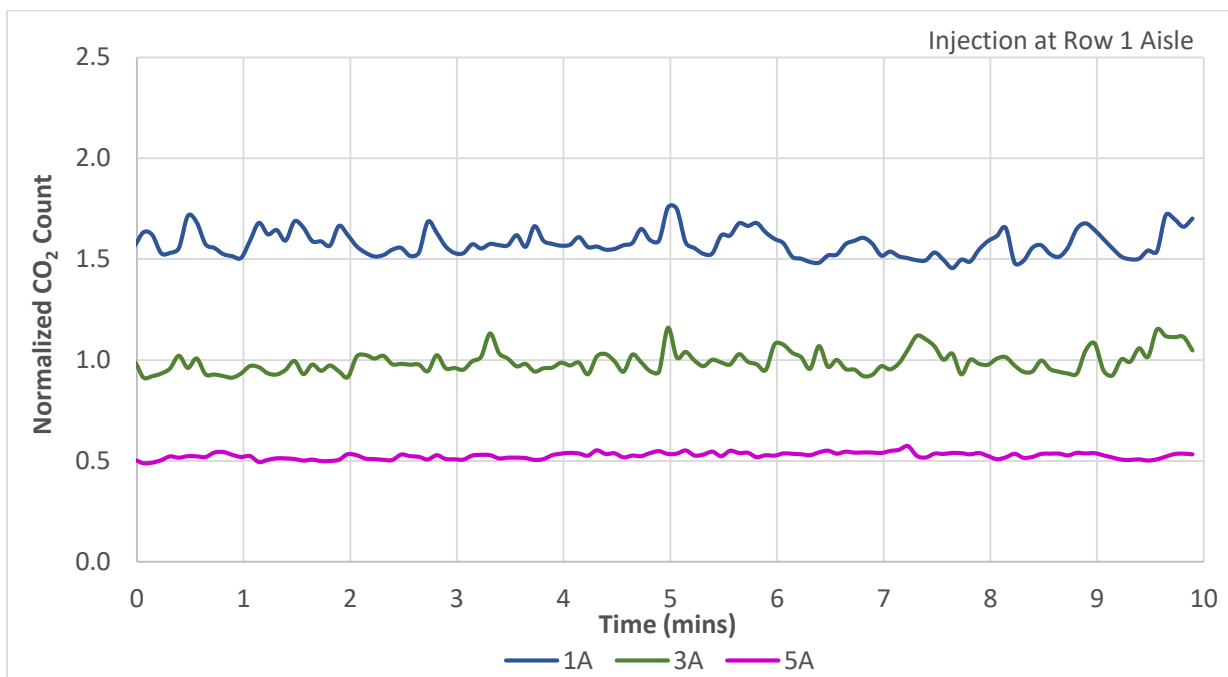


Figure 5.17 Average Normalized CO₂ Counts for Seats 1A, 3A and 5A

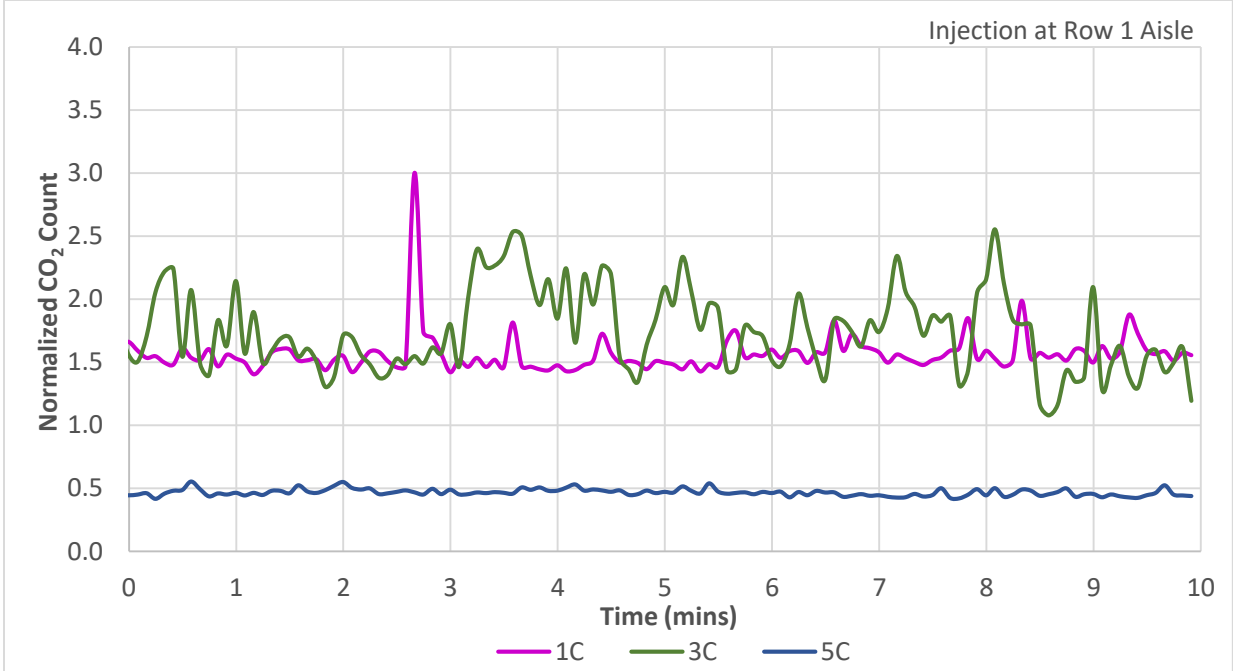


Figure 5.18 Average Normalized CO₂ Counts for Seats 1C, 3C and 5C

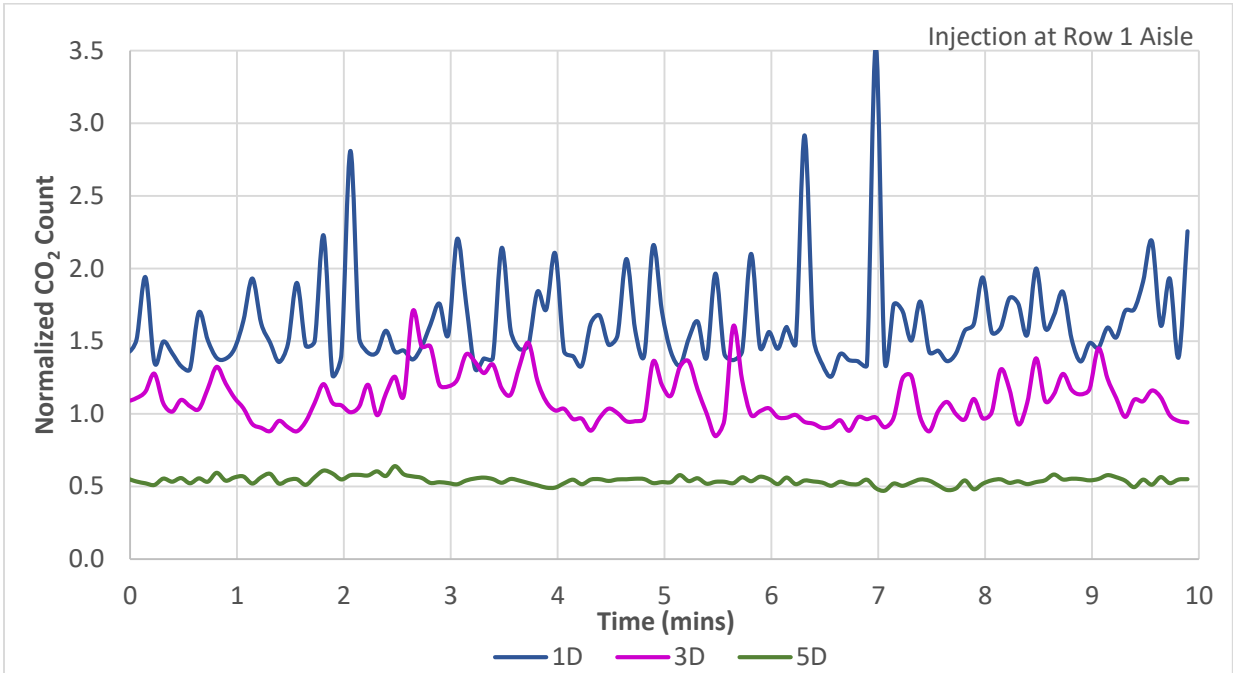


Figure 5.19 Average Normalized CO₂ Counts for Seats 1D, 3D and 5D

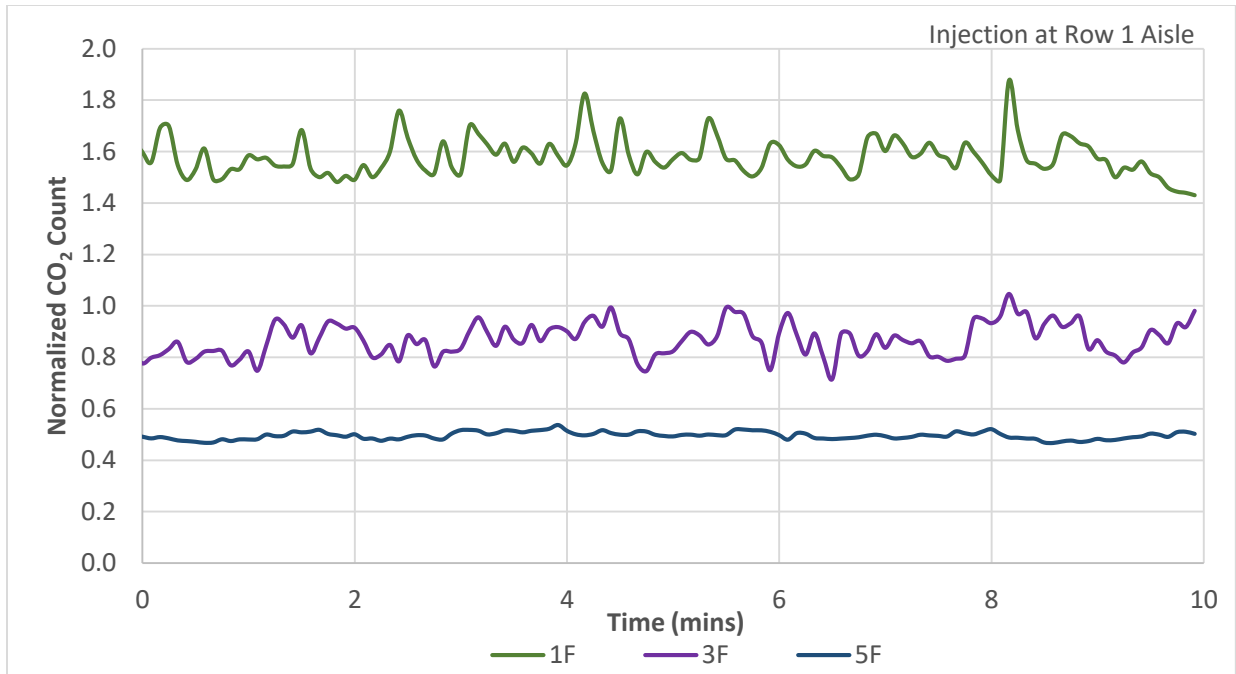


Figure 5.20 Average Normalized CO₂ Counts for Seats 1F, 3F and 5F

The results for dispersion study with injection at centerline of aisle at row 3 are summarized in Table 5.14. As expected, the seats in the row of injection recorded relatively higher CO₂ concentrations than seats in rows away from the source. As shown in Figure 5.21 the normalized CO₂ counts at seats in row 1 ranged from 0.89 to 0.97, which are close to the CO₂ counts recorded at seats in the injection row. In addition, the normalized CO₂ counts at row 5 seats ranged from 0.41 to 0.46, which is less than fifty percent of the values found in injection row seats. This shows that, at least for this particular injection location, the tracer gas has a tendency to flow more towards the front of the cabin than to the rear. As can be seen from Figure 5.22 the somewhat symmetrical distribution of tracer gas about the centerline of the cabin is observed with injection at row 3 aisle location as well.

Table 5.14 Average Normalized CO₂ Count for Injection at Centerline of Aisle at Row 3

	A	B	C	D	E	F
Row 1	0.97		0.96	0.89		0.89
Row 2						
Row 3	1.04		1.28	0.94		0.95
Row 4						
Row 5	0.42		0.41	0.46		0.45

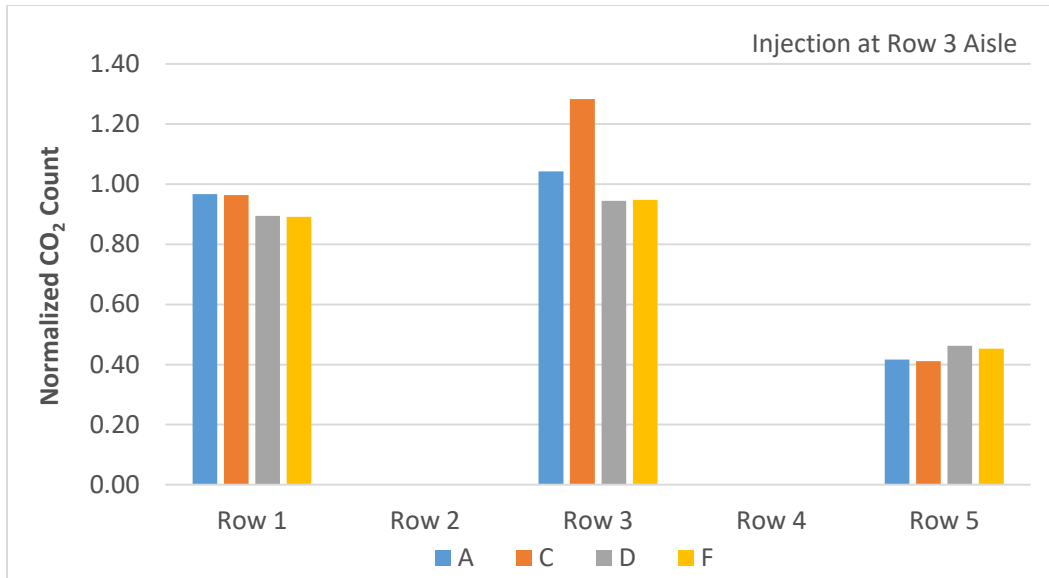


Figure 5.21 Longitudinal Dispersion of Tracer Gas

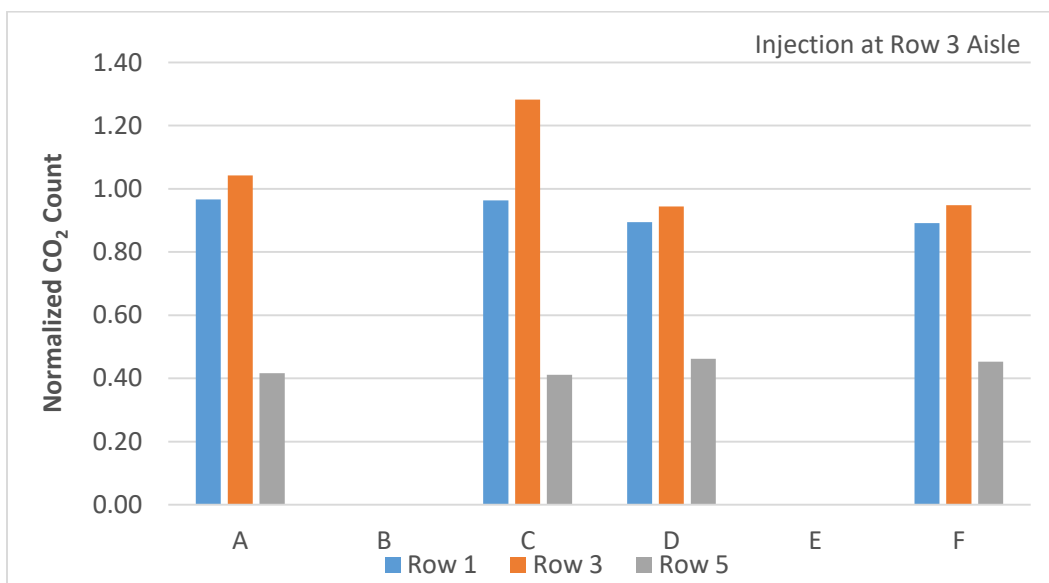


Figure 5.22 Lateral Dispersion of Tracer Gas

The average normalized CO₂ counts at various sampling locations for injection at centerline of aisle at row 5 are summarized in Table 5.15. The results from Table 5.15 reveal that most of the CO₂ injected is dispersed in the row of injection. Figure 5.23 plots the longitudinal dispersion of tracer gas inside the cabin. It is evident from Figure 5.23 that the CO₂ concentration decreases significantly moving away from the source along the longitudinal direction. For example, for column C seats, the CO₂ concentration decreased from 1.40 at 5C, which is right

next to the injection location to 0.19 at 1C, which is towards the front end of the cabin. As can be seen from Figure 5.24, within a particular row the spread of tracer gas is roughly symmetrical between the right and left halves of the cabin.

Table 5.15 Average Normalized CO₂ Count for Injection at Centerline of Aisle at Row 5

	A	B	C	D	E	F
Row 1	0.18		0.19	0.17		0.27
Row 2						
Row 3	0.54		0.35	0.42		0.79
Row 4						
Row 5	1.31		1.40	1.30		1.41

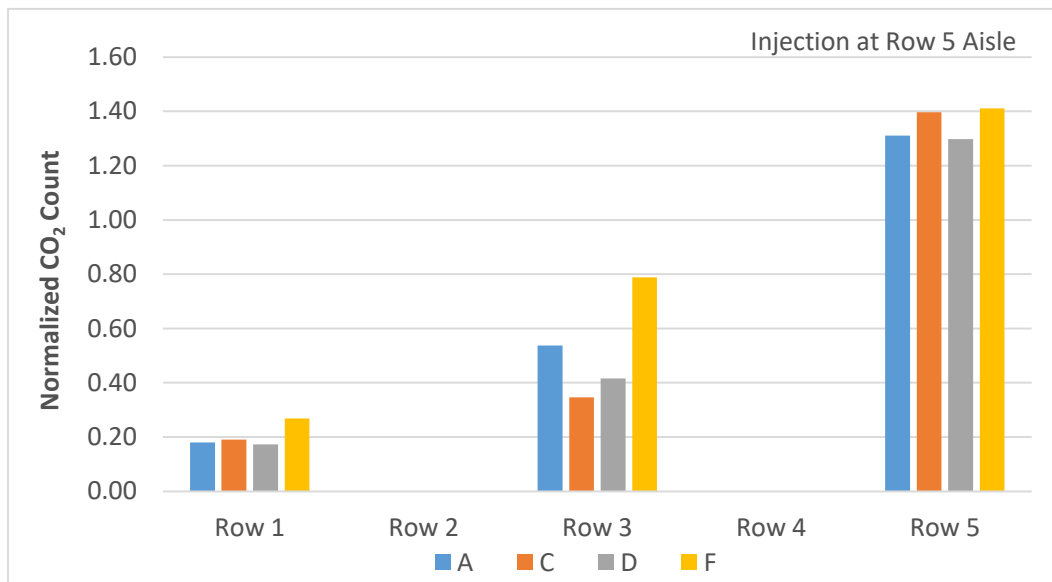


Figure 5.23 Longitudinal Dispersion of Tracer Gas

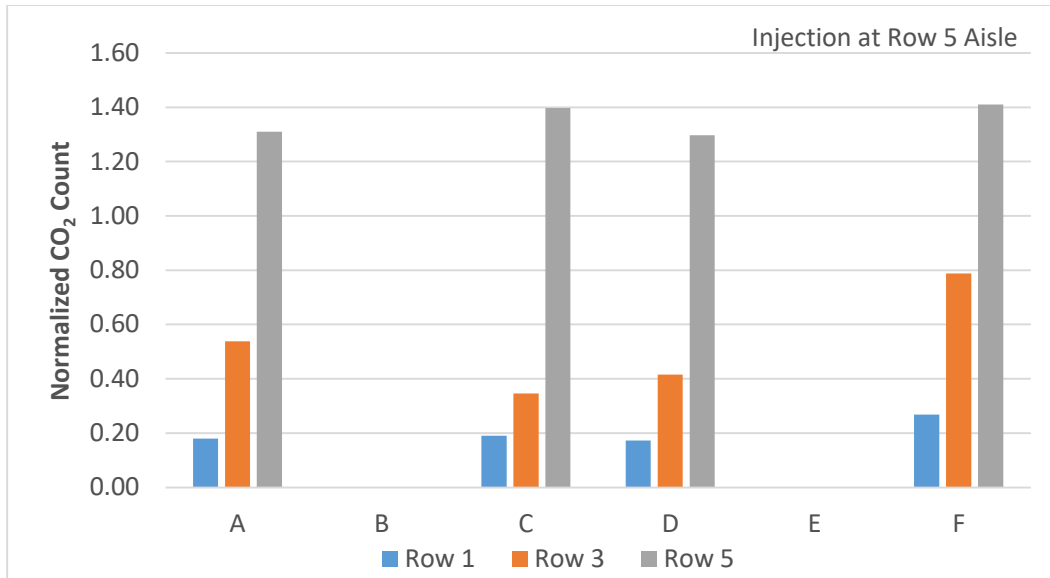


Figure 5.24 Lateral Dispersion of Tracer Gas

For injection at 2B, the average normalized CO₂ count for various sampling locations are given in Table 5.16. As can be seen from this table, the highest CO₂ count of 2.42 was recorded at seat 2C which is closest to the source, while the lowest CO₂ count was 0.37 at seat 5E, which is furthest away from the source. Figures 5.25 and 5.26 show tracer gas dispersion in the lateral and longitudinal directions respectively. Figure 5.25 indicates that seats in row of injection i.e. row 2 consistently recorded higher CO₂ counts than seats in row away from the source i.e. row 4. This along with CO₂ counts at various seats in rows away from row 2 indicate that risk of exposure to gaseous contaminants is lower in rows away from the source. It is also observed that within the row of injection, the CO₂ count decreased moving away from the source. The highest CO₂ count of 2.42 was recorded at seat 2C, which is adjacent to the source, while 2F, which is furthest away from the source, recorded a CO₂ count of 1.06, which is less than fifty percent of the value at 2C. Figure 5.25 also reveals that the CO₂ count at all seats in row 4, which is away from the source row are roughly uniform. This could be a result of dilution of tracer gas by ventilation air along its path to these seats. It is clear from Figure 5.26 that in column B and column E the CO₂ count drastically decreases moving away from the source indicating reduced risk of exposure to gaseous contaminants moving away from the source along the longitudinal direction. Table 5.16 results show that although the flow is intended to be primarily in the lateral direction, substantial dispersion occurs in the longitudinal direction as well.

Table 5.16 Average Normalized CO₂ Count for Injection at 2B

	A	B	C	D	E	F
Row 1		1.78			1.92	
Row 2	1.19	Injection	2.42	1.68	1.46	1.06
Row 3		0.95			0.91	
Row 4	0.79	0.78	0.75	0.83	0.70	0.78
Row 5		0.43			0.37	

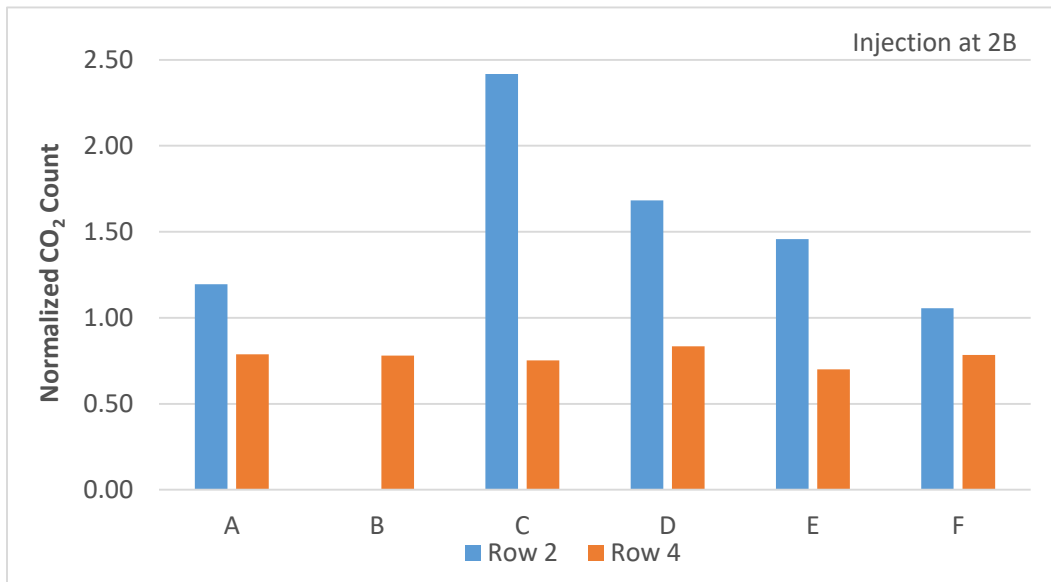


Figure 5.25 Lateral Dispersion of Tracer Gas

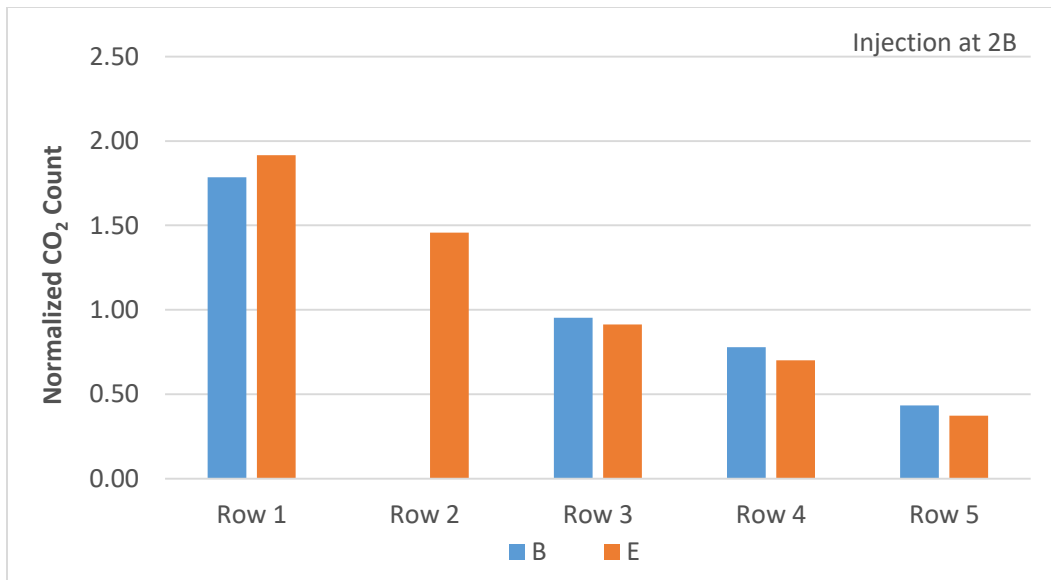


Figure 5.26 Longitudinal Dispersion of Tracer Gas

The results for average steady state CO₂ counts for various sampling locations with injection at 2B are shown in Figures 5.27 to 5.32. Again, due to the limit on the length of this thesis, the plots for injection location 4E are provided in the Electronic Appendix.

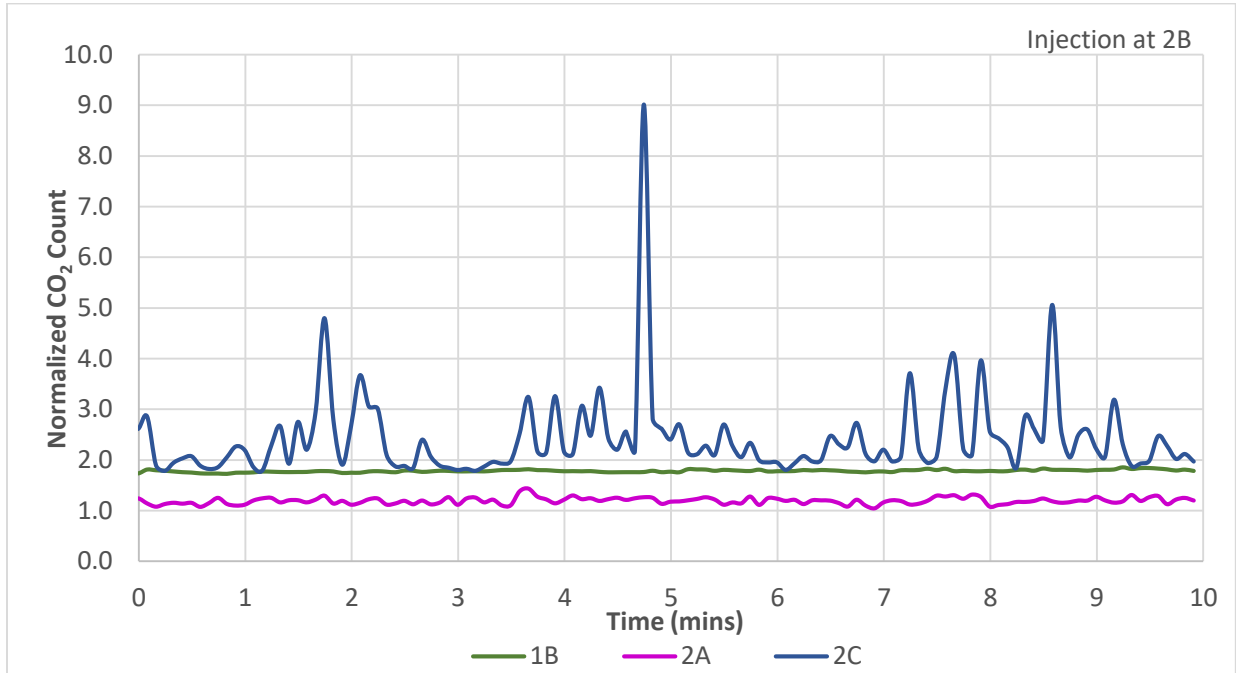


Figure 5.27 Average Normalized CO₂ Counts for Seats 1B, 2A and 2C

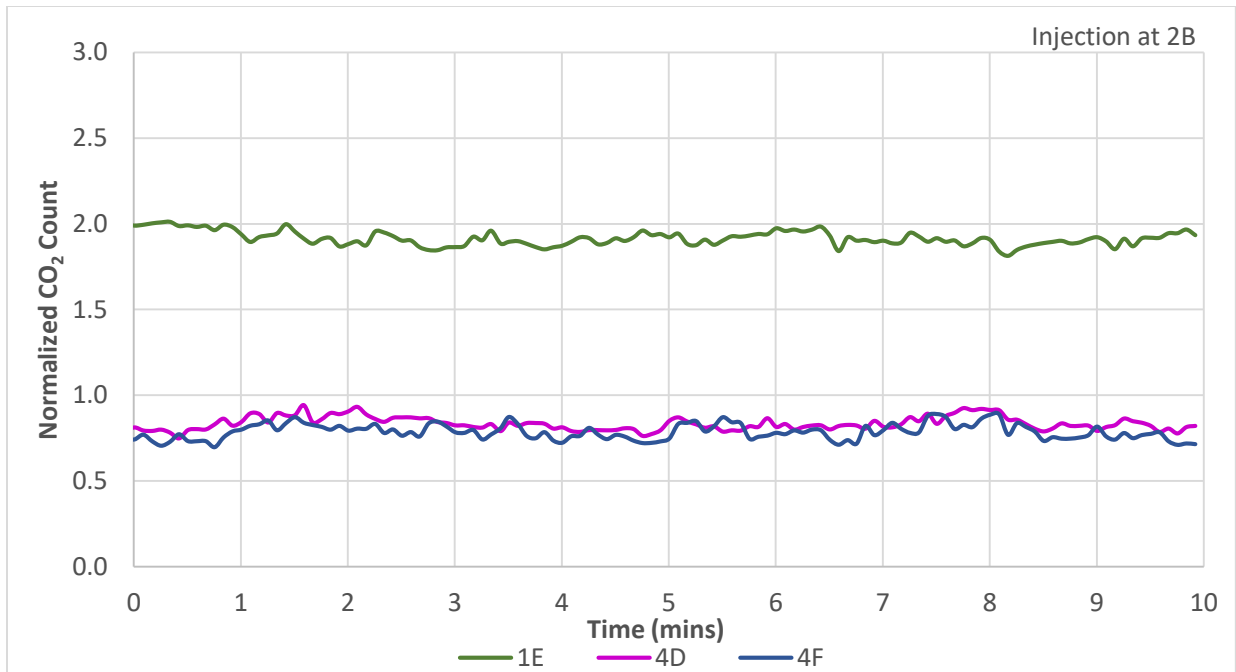


Figure 5.28 Average Normalized CO₂ Counts for Seats 1E, 4D and 4F

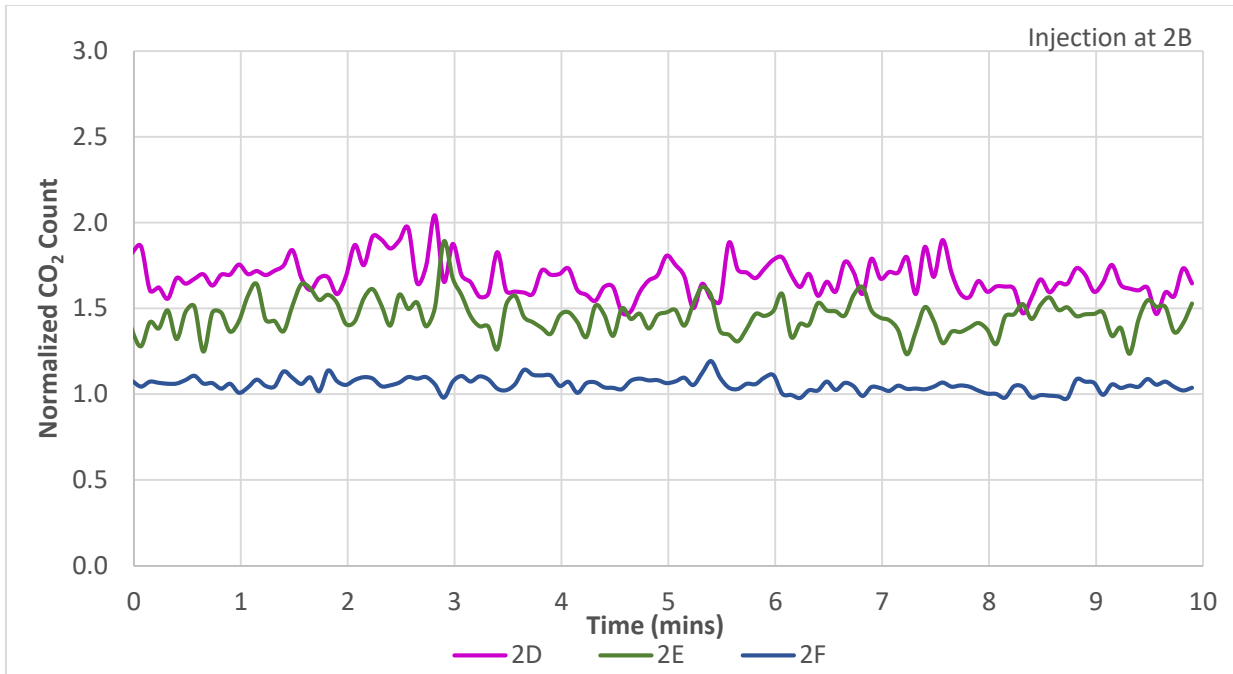


Figure 5.29 Average Normalized CO₂ Counts for Seats 2D, 2E and 2F

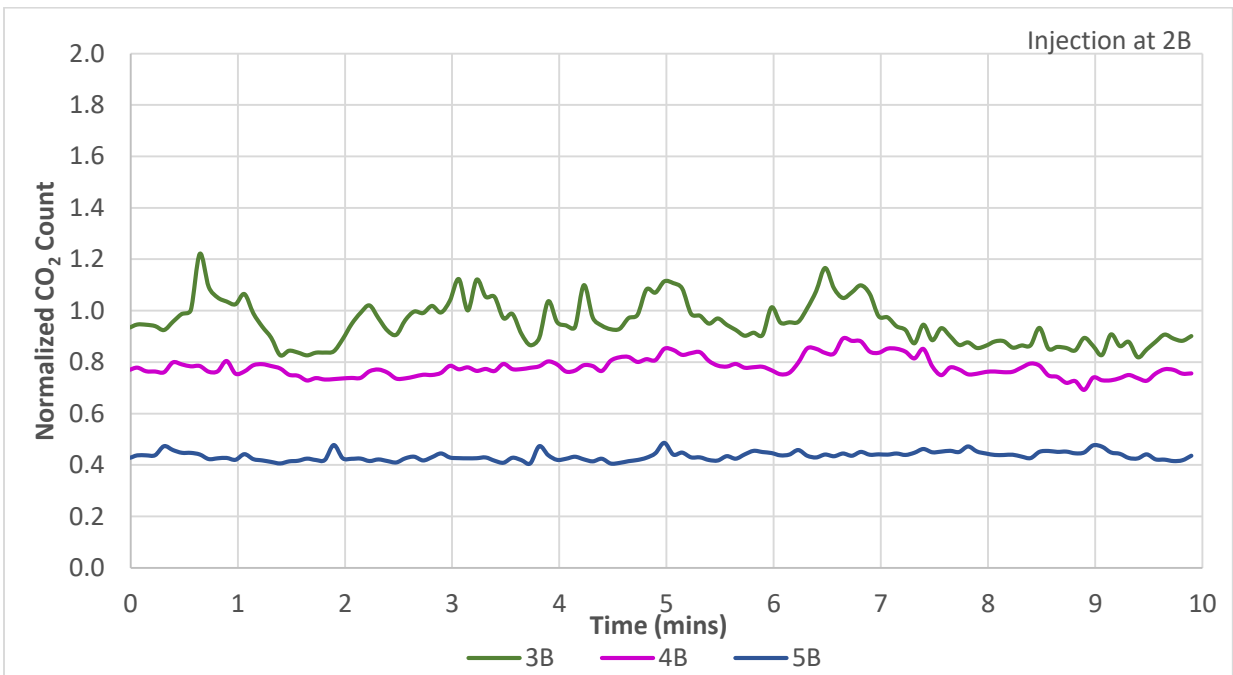


Figure 5.30 Average Normalized CO₂ Counts for Seats 3B, 4B and 5B

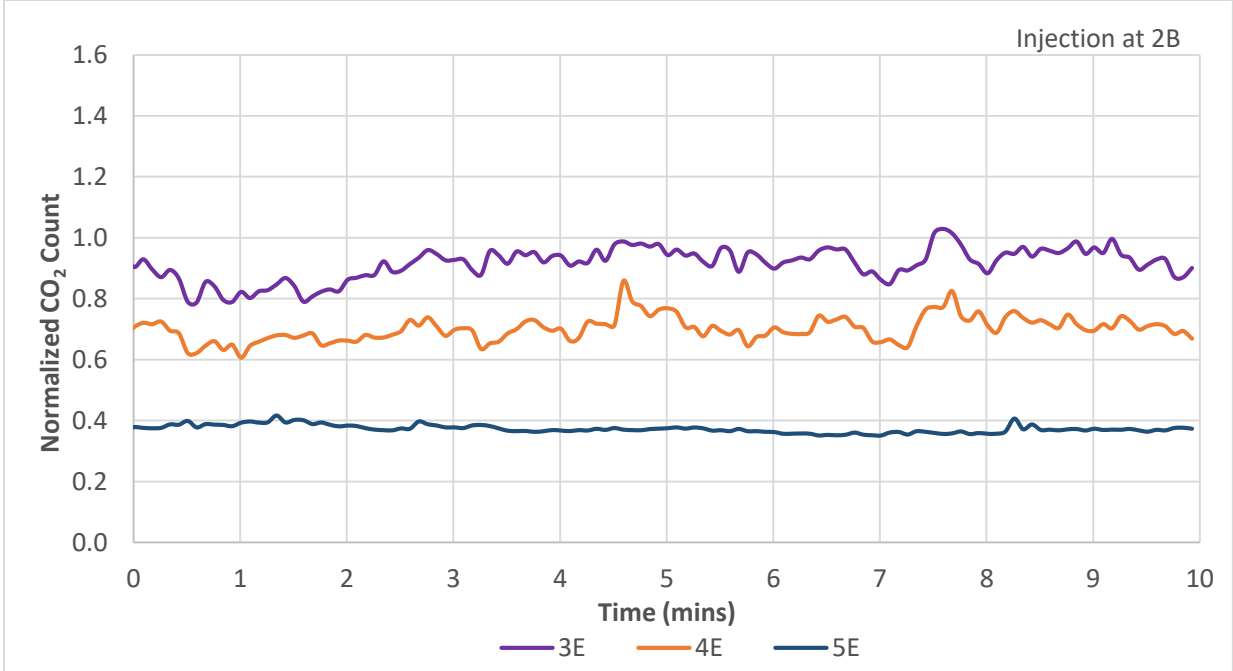


Figure 5.31 Average Normalized CO₂ Counts for Seats 3E, 4E and 5E

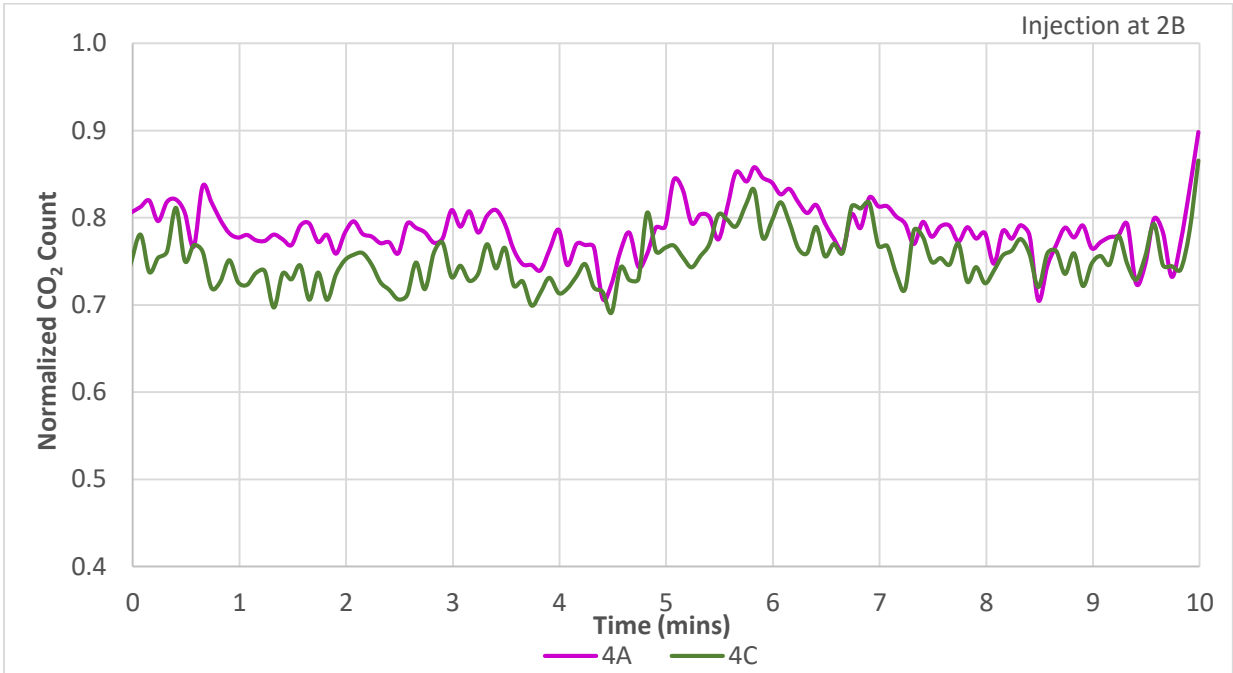


Figure 5.32 Average Normalized CO₂ Counts for Seats 4A and 4C

Table 5.17 demonstrates the average results from gaseous contaminant transport study with injection at 4E. As expected the results from this study were similar to the results found in study with injection at 2B. The largest CO₂ count was recorded at seat 4D which is right next to

the injection location, while the smallest CO₂ count occurred at seat 1B which is furthest away from the source. Figure 5.33 provides the lateral dispersion of tracer gas in the row of injection i.e. row 4 and in row 2. Figure 5.33 reveals that the dispersion of tracer gas within the row of injection decreases moving away from the source. The longitudinal dispersion of tracer gas is shown in Figure 5.34. In column E seats the CO₂ count decreased along the longitudinal direction from 1.65 at 3E which is close to the source to 0.57 at 1E which is away from the source. Similar trend was observed in column B seats, as the CO₂ count decreased from 0.89 at seat 4B, which is in the row of injection to 0.51 which is at the front end of the cabin. This shows that the risk of exposure to gaseous contaminants decreases moving away from the source in the longitudinal direction.

Table 5.17 Average Normalized CO₂ Count for Injection at 4E

	A	B	C	D	E	F
Row 1		0.51			0.57	
Row 2	0.94	0.67	0.68	0.73	0.88	1.25
Row 3		0.85			1.65	
Row 4	0.90	0.89	0.95	2.66	Injection	1.96
Row 5		0.81			0.89	

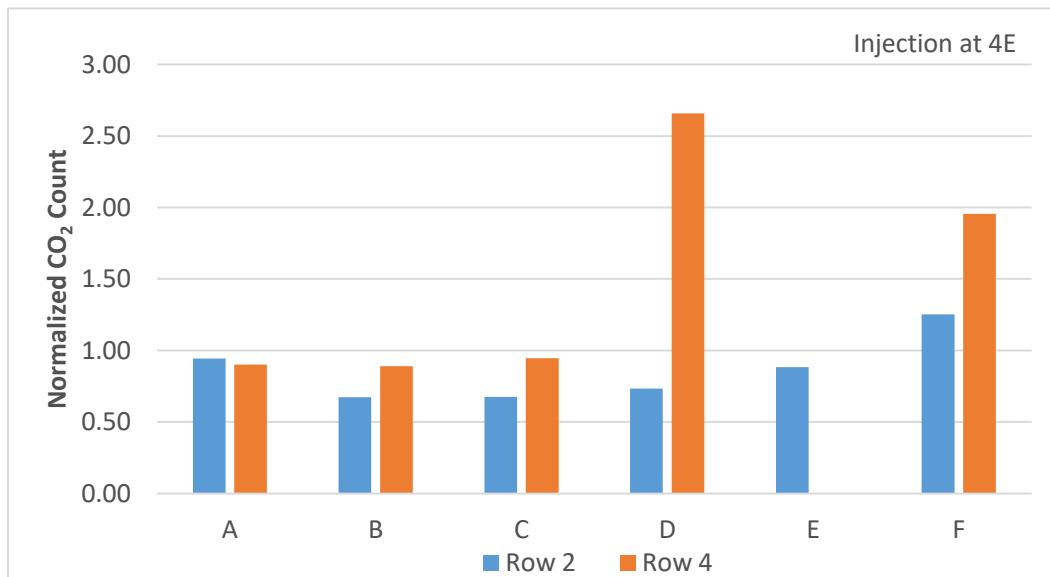


Figure 5.33 Lateral Dispersion of Tracer Gas

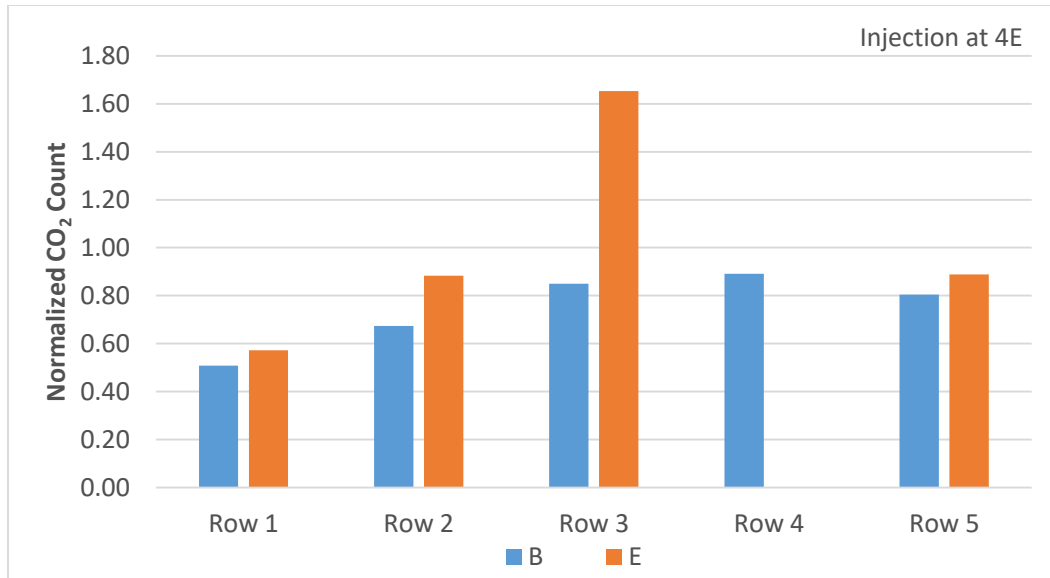


Figure 5.34 Longitudinal Dispersion of Tracer Gas

It is to be noted that, although the dispersion of tracer gas is intended to be dominant in the lateral direction, significant dispersion was observed in the longitudinal direction as well. This is expected as previous studies have shown that airflow inside the cabin is highly turbulent. Turbulence is three-dimensional in nature causing dispersion in all directions, including the longitudinal direction.

5.3 Dispersion of Tracer Gas with No Ventilation Air

Experiments are conducted inside the Boeing 737 mockup cabin to study the dispersion of tracer gas in the absence of ventilation air. A tracer gas mixture is injected at the centerline of aisle in row 3 and seat locations 2B and 4E to study tracer gas dispersion with no ventilation air supply. The experimental procedure used to conduct experiments for this study is explained in Chapter 4 of this thesis. The normalized CO₂ counts calculated using Equation 4.4 are analyzed to determine the dispersion pattern inside the cabin.

The results for dispersion of tracer gas in the absence ventilation air with injection at 2B are summarized in Table 5.18. Each value in this table is an average of data from two repeats. Similar to results from tracer gas dispersion study with ventilation air, it is observed that CO₂ concentrations are higher at seats in the row of injection than at seats in rows away from the source as shown in Figure 5.35. This suggests that the risk of exposure to gaseous contaminants is lower at seats in rows away from the source. For example, a person sitting in the same row as

an infected person has higher chances of being infected as compared to a person sitting in a row away from the source row/infected person. In addition, within the row of injection the tracer gas concentration decreases with increase in the distance from the source. Figure 5.36 shows the longitudinal dispersion of tracer gas inside the cabin. As can be seen from CO₂ counts in column B and column E seats the CO₂ concentration decreases moving away from the source in the longitudinal direction as well. This suggests that risk of exposure to gaseous contaminants decreases moving away from the source in the longitudinal direction. It is also to be noted that, although there was no ventilation air supplied to the cabin, significant dispersion of tracer gas occurred in both the lateral and longitudinal direction.

Table 5.18 Average Normalized CO₂ Count for Injection at 2B

	A	B	C	D	E	F
Row 1		1.41			0.92	
Row 2	1.57	Injection	1.98	1.25	0.99	0.76
Row 3		0.79			0.74	
Row 4	0.74	0.78	0.78	0.71	0.66	0.66
Row 5		0.72			0.68	

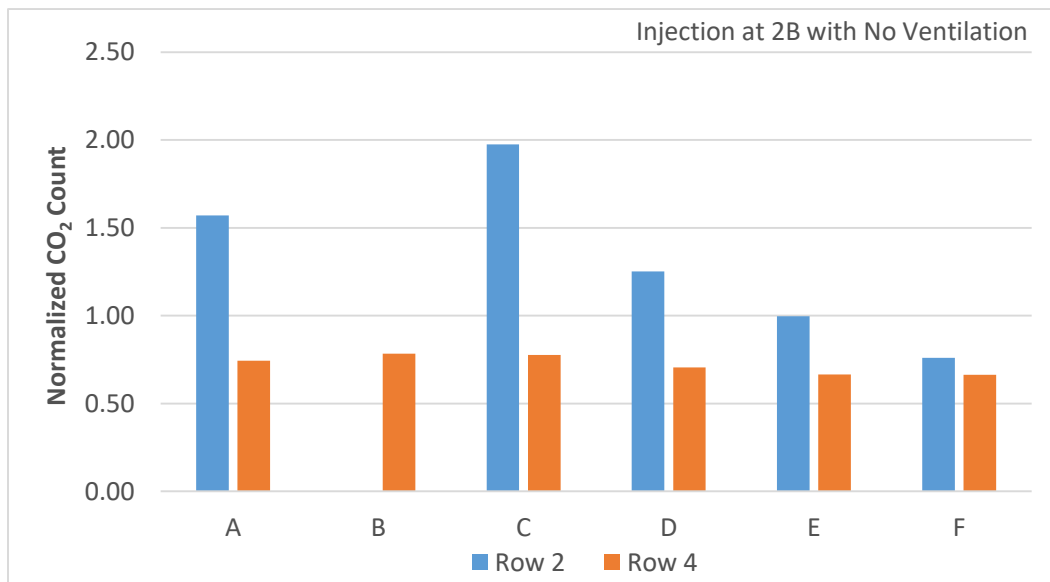


Figure 5.35 Lateral Dispersion of Tracer Gas

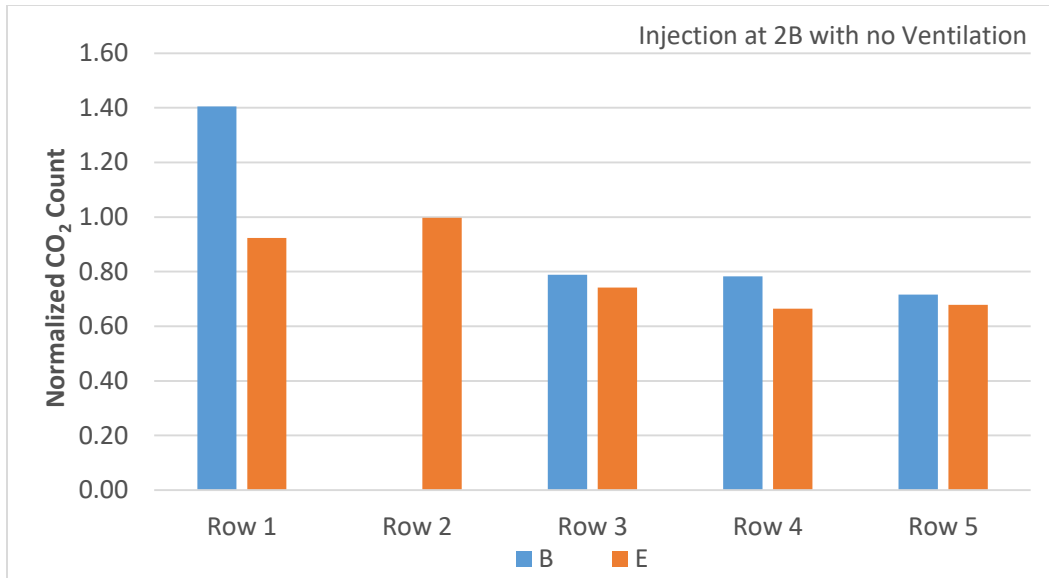


Figure 5.36 Longitudinal Dispersion of Tracer Gas

The results for average transient CO₂ counts for various sampling locations with injection at 2B are shown in Figures 5.37 to 5.41. As only limited data can be presented in this thesis, the results for injection at row 3 aisle and seat location 4E are provided in the Electronic Appendix attached with this thesis.

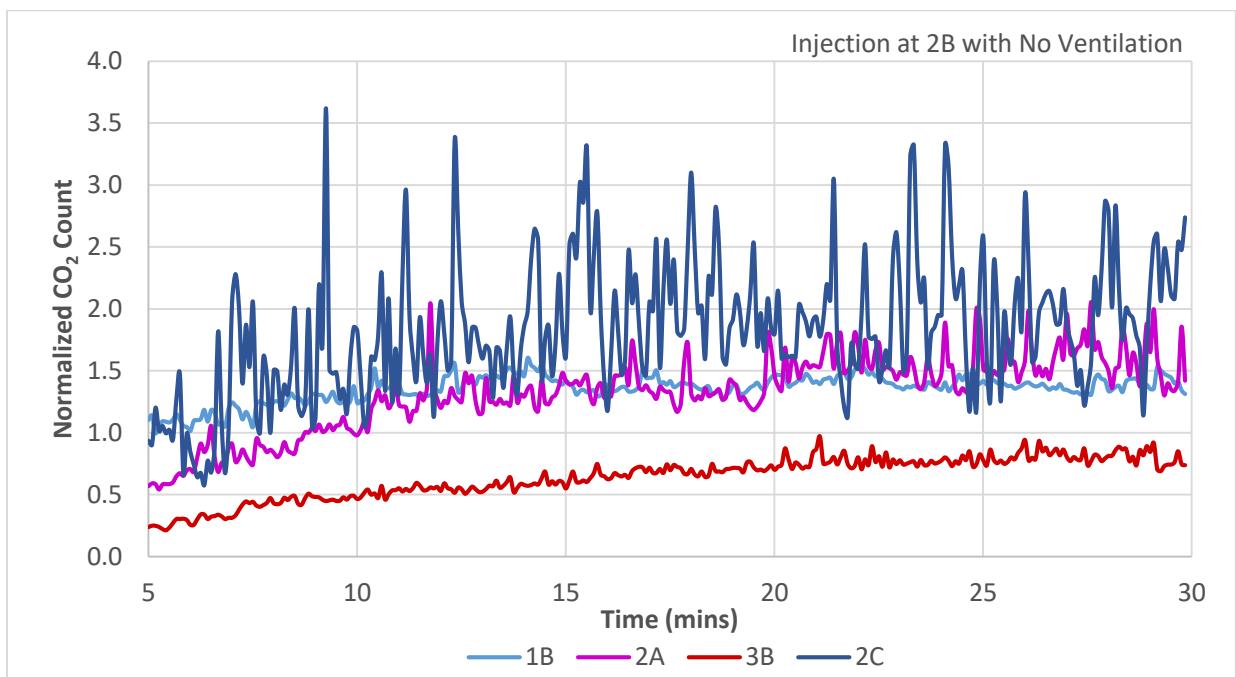


Figure 5.37 Average Normalized CO₂ Counts for Seats 1B, 2A, 3B and 2C

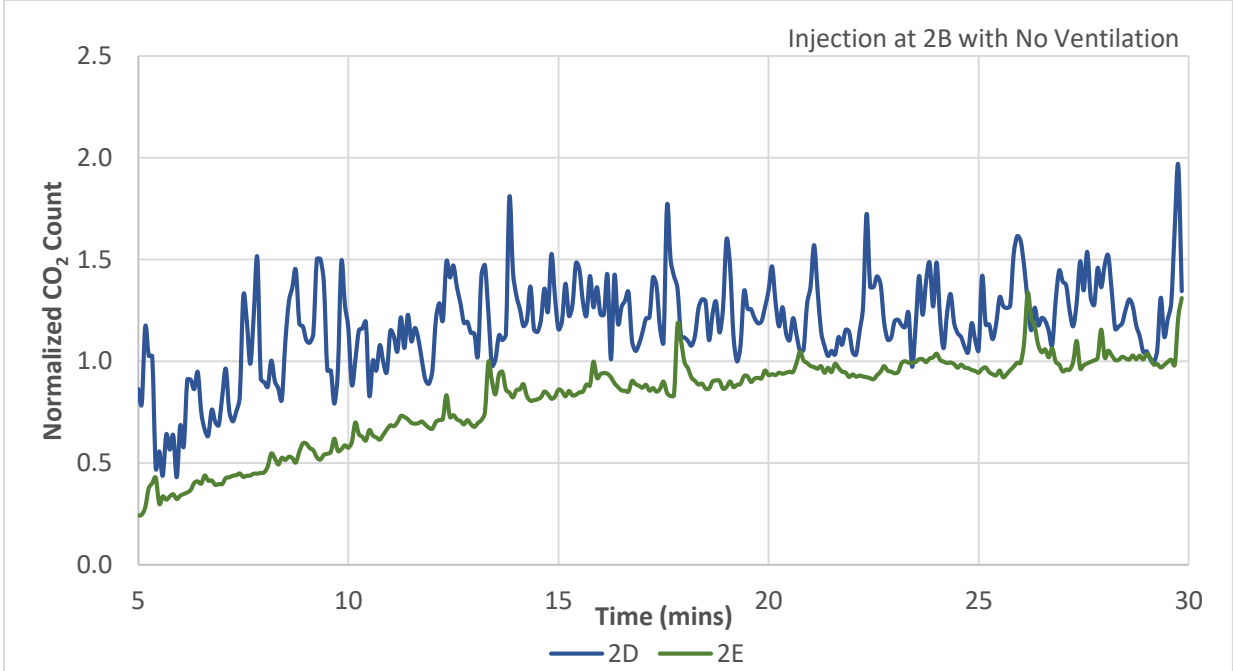


Figure 5.38 Average Normalized CO₂ Counts for Seats 2D and 2E

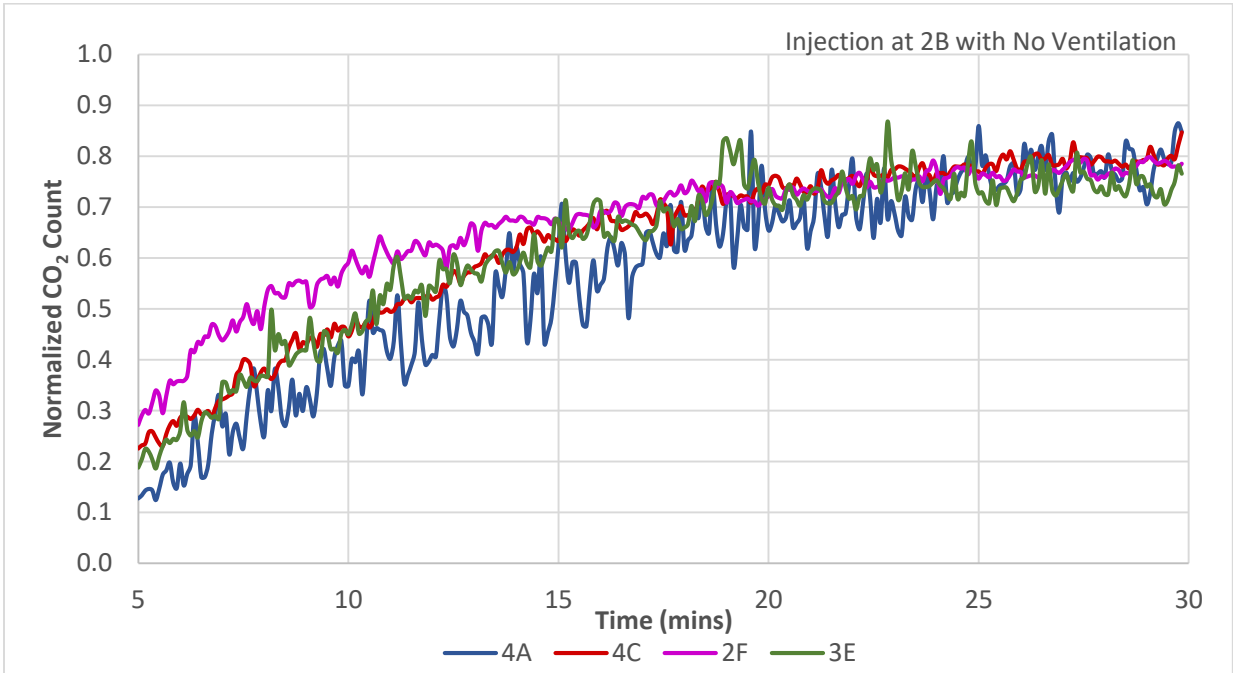


Figure 5.39 Average Normalized CO₂ Counts for Seats 4A, 4C, 2F and 3E

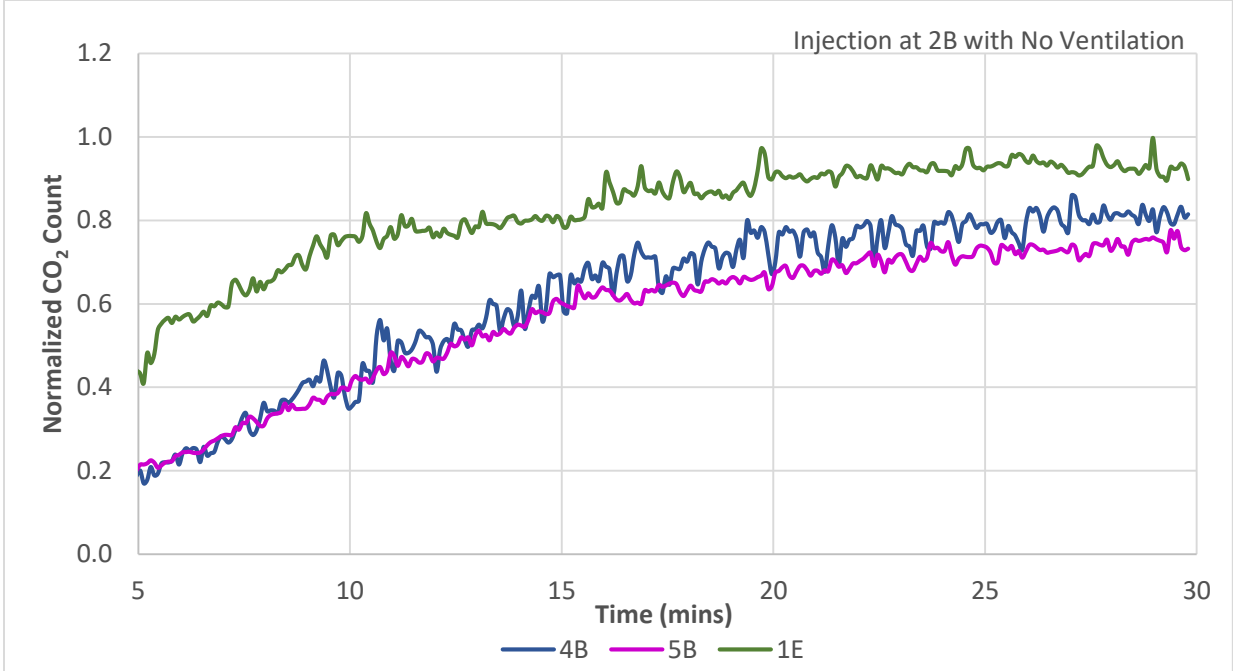


Figure 5.40 Average Normalized CO₂ Counts for Seats 4B, 5B and 1E

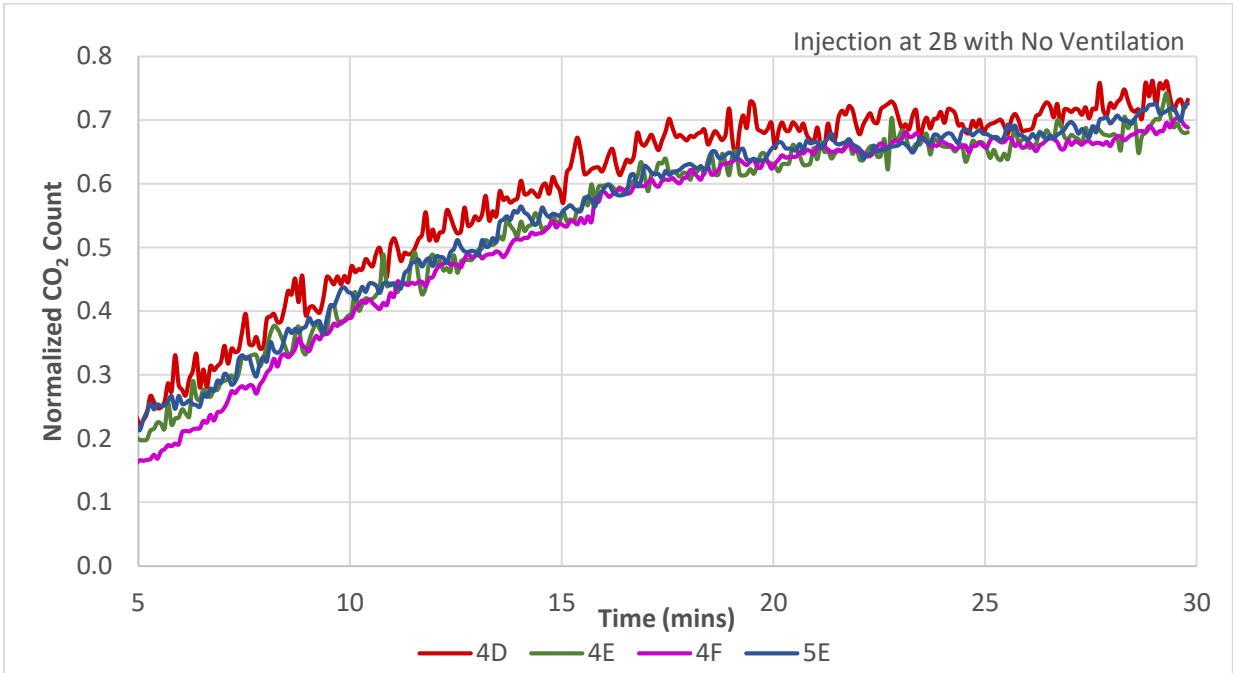


Figure 5.41 Average Normalized CO₂ Counts for Seats 4D, 4E, 4F and 5E

Results for no ventilation air study with injection at centerline of aisle in row 3 are summarized in Table 5.19. As expected, the CO₂ concentration was highest at seats in the row of injection i.e. row 3. Figure 5.42 shows that the CO₂ count decreases moving away from the

source in the longitudinal direction. For example, CO₂ count at seat 3C which is close to the source was calculated to be 1.47, while at seats 1C and 5C the CO₂ counts were 0.98 and 1.05 respectively. Figure 5.43 plots the lateral dispersion of tracer gas in various rows. As can be seen from Figure 5.43 within the row of injection i.e. row 3, the CO₂ concentration decreased as the distance between the source and the sampling point increased. In addition, symmetrical distribution of tracer gas about the two centerlines of the cabin was observed. This can be expected as injection occurred at the geometric center of the cabin and no ventilation air is supplied to the cabin to create movement of tracer gas in a particular direction.

Table 5.19 Average Normalized CO₂ Count for Injection at Centerline of Aisle at Row 3

	A	B	C	D	E	F
Row 1	0.92		0.98	0.97		0.84
Row 2						
Row 3	1.04		1.47	1.40		0.99
Row 4						
Row 5	1.01		1.05	0.99		1.02

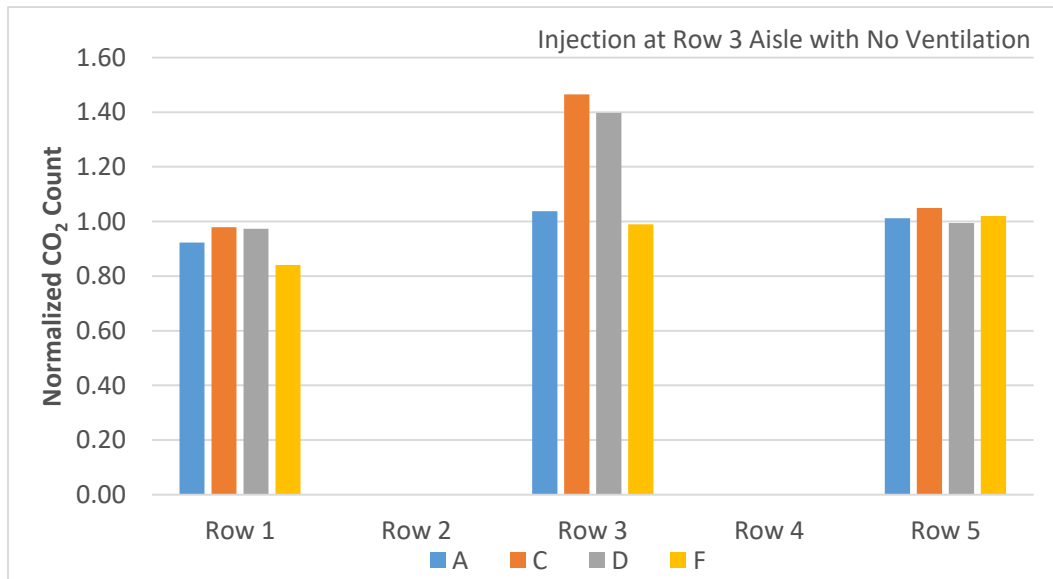


Figure 5.42 Longitudinal Dispersion of Tracer Gas

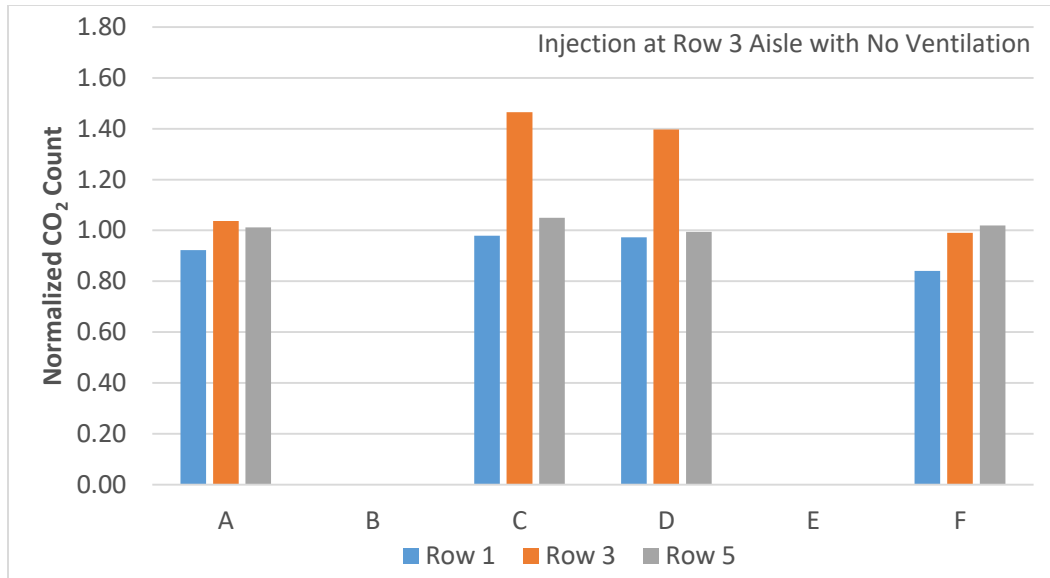


Figure 5.43 Lateral Dispersion of Tracer Gas

Table 5.20 shows the results from experiments with injection at 4E. The results are similar to the results from injection at 2B. Higher CO₂ concentrations were observed in the row of injection i.e. row 4, when compared to CO₂ concentrations at seats away from the source. The highest recorded CO₂ count was 1.68 at seat 4D, which is right next to the source, while the lowest CO₂ count of 0.65 was observed at seat 1B which is furthest away from the source. This shows the inverse relation of tracer gas transport to the relative distance between the source and sampling location. Figure 5.44 shows the lateral dispersion of tracer gas in the rows 2 and 4. It is observed that within the row of injection the CO₂ count decreased with increasing distance from the source. Figure 5.45 shows longitudinal dispersion of tracer gas. As can be seen from this figure, in column B and column E seats the CO₂ concentration decreased moving away from the source confirming exponential decay of tracer gas along the longitudinal direction.

Table 5.20 Average Normalized CO₂ Count for Injection at 4E

	A	B	C	D	E	F
Row 1		0.65			0.67	
Row 2	0.66	0.70	0.69	0.86	0.74	0.66
Row 3		0.77			0.82	
Row 4	0.84	1.08	1.25	1.68	Injection	1.36
Row 5		1.00			1.29	

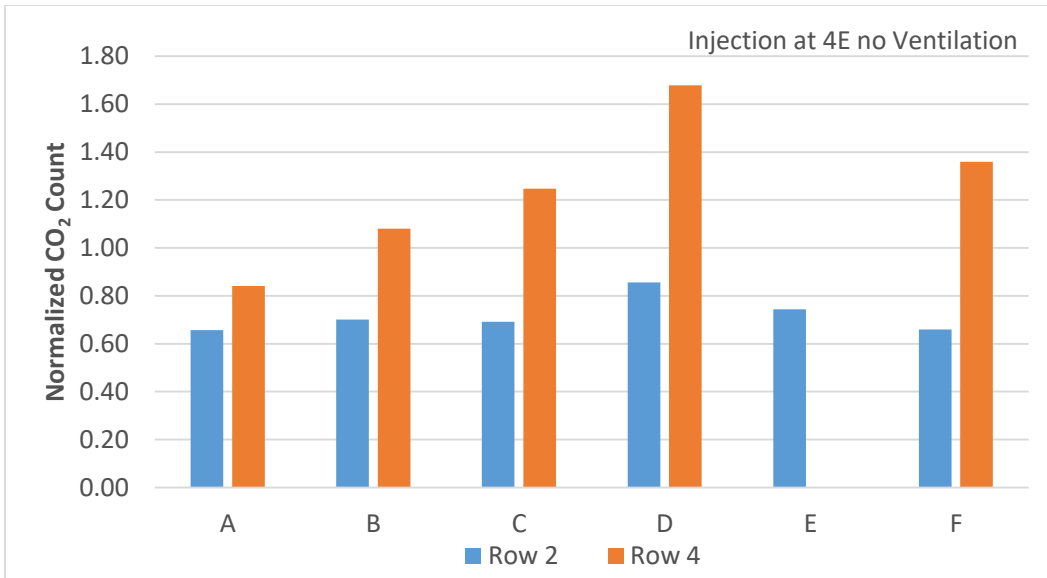


Figure 5.44 Lateral Dispersion of Tracer Gas

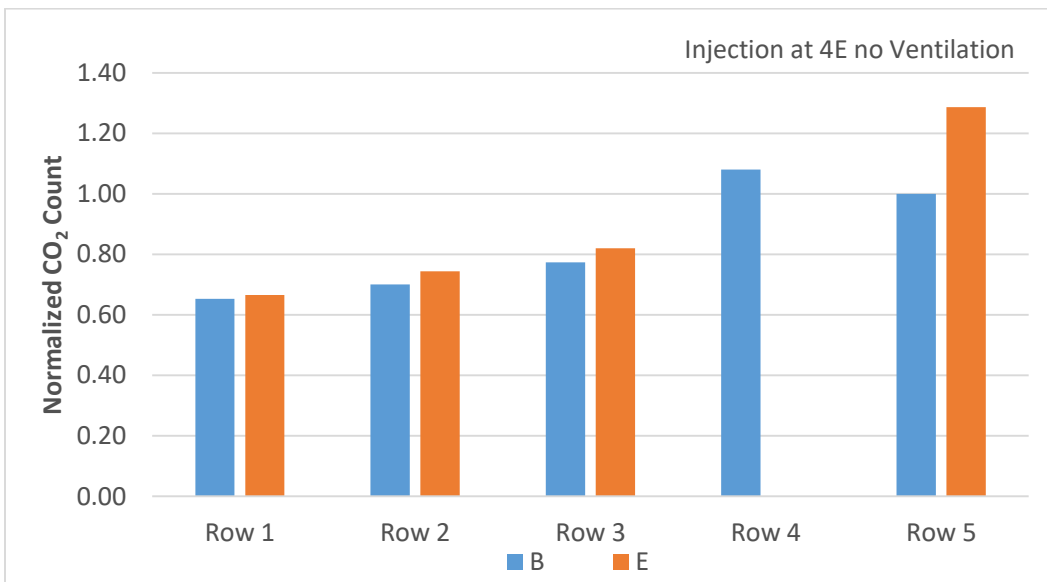


Figure 5.45 Longitudinal Dispersion of Tracer Gas

5.4 Verification Experiments

The data from transient decay of CO₂ concentration is used to evaluate the ventilation effectiveness inside the cabins. In addition, for the study of dispersion of tracer gas in the absence of ventilation air the transient CO₂ concentration data is analyzed to calculate the normalized CO₂ Count. Therefore, it was important to check if the sampling system and the

analyzers added a significant amount of error and if they had any effects on the results from these studies.

5.4.1 Experiment Repeatability

Results for experimental repeatability testing are summarized in Table 5.21. As can be seen from Table 5.21 for each analyzer the variations in e_L rates for all six experiments are slight but not insignificant when considering the variations in ventilation effectiveness at various locations inside the cabins. The mean standard deviation of the four analyzers is 0.018 min^{-1} , which is close to the calculated standard deviations in e_L rates for various cases studied inside both mockup cabins. The results from experimental repeatability testing suggests that experimental repeatability is likely an important factor in the ventilation effectiveness variations inside both mockups.

Table 5.21 Experimental Repeatability Testing Results (min^{-1})

Seat Location	8D	9D	7D	6D
	A-1 Sensor	A-2 Sensor	A-3 Sensor	A-4 Sensor
Repeat 1	0.46	0.44	0.41	0.43
Repeat 2	0.40	0.41	0.40	0.40
Repeat 3	0.42	0.44	0.43	0.45
Repeat 4	0.41	0.42	0.38	0.43
Repeat 5	0.41	0.43	0.45	0.41
Repeat 6	0.43	0.43	0.42	0.40
Standard Deviation	0.019	0.012	0.021	0.019

5.4.2 Effect of Transient Response of Sampling System

The sampling of tracer gas from various locations inside the cabin was carried out using sampling ports comprising of approximately 7.93 m (26 ft) long vinyl tubes. Thus, it was essential to check if the time delays due to the length of the tubes caused recording of incorrect data. Experiments were performed following the test procedure explained in Section 4.4 of this thesis. The results from experiments evaluating the effects of transient response of sampling system are summarized in Table 5.22. The results show that there are only slight variations in the

measured local effective ventilation rates for the three cases. These variations are likely due to experimental variations rather than an effect of the length of the sampling tubes. Thus, it can be safely concluded that the sampling tube length did not interfere with accurate measurement of transient CO₂ concentrations.

Table 5.22 Variation in e_L with Varying Sampling Tube Lengths (min^{-1})

Seat Location	4D	5B	4C	3A
	A-1 Sensor	A-2 Sensor	A-3 Sensor	A-4 Sensor
Short Tube	0.40	0.40	0.41	0.40
Without Tubes	0.42	0.42	0.42	0.44
With Long Tubes	0.47	0.43	0.43	0.43

5.4.3 Time Response of CO₂ Analyzers

Experiments were conducted to determine the time response of the CO₂ analyzers used for measurement of CO₂ concentrations. The experiments were performed following the test procedure mentioned in Chapter 4 of this thesis. Table 5.23 provides the details and results for these experiments. It was found from these experiments that three of the four sensors had a time response of approximately 15 seconds while the time response of the fourth analyzer was in the range of 10 to 12 seconds. These response times are very short compared to the 15 minutes of transient associated with the CO₂ decay inside the cabin. Thus, it is concluded that the analyzers by themselves are not a source of significant measurement error.

Table 5.23 Time Response of CO₂ Analyzers (seconds)

	A-1 Sensor	A-2 Sensor	A-3 Sensor	A-4 Sensor
Test 1	15	15	15	Inside Cabin
Test 2	15	Inside Cabin	15	10
Test 3	Inside Cabin	14	14	12

Chapter 6 - Summary and Conclusions

Experiments were conducted to evaluate the ventilation effectiveness inside a Boeing 767 mockup cabin. In addition, this thesis also presents results from ventilation effectiveness studies and study of dispersion of tracer gas for various scenarios inside a Boeing 737 mockup cabin. The ventilation effectiveness studies were carried out by injecting tracer gas directly into the supply air and collecting CO₂ concentration data from various locations inside the cabins. The tracer gas decay method was used to calculate the local effective ventilation rates and ventilation effectiveness for the cabins. For the transport of gaseous contaminant inside the mockup cabins, tracer gas mixture was injected at various point locations and sampled at multiple locations for each injection point. The CO₂ concentration data was normalized and analyzed using various equations for different scenarios.

6.1 Ventilation Effectiveness

Analysis of ventilation effectiveness results presented in Chapter 5 revealed that local effective ventilation rates were uniform throughout the Boeing 767 mockup cabin. The local effective ventilation rates inside the Boeing 767 mockup cabin ranged from 0.39 to 0.47 min⁻¹. Whereas the local ventilation effectiveness values ranged from 0.78 to 0.93 with the ventilation effectiveness value of 0.85 for the entire cabin. Results for Boeing 737 mockup cabin indicated that there were only slight variations in the local effective ventilation rates at various locations and heights inside the cabin. The local effective ventilation rates ranged from 0.49 to 0.53 min⁻¹, while the local ventilation effectiveness values ranged from 0.77 to 0.83. The ventilation effectiveness for the entire Boeing 737 cabin was found to be 0.80. The results from experiments conducted to check for analyzers repeatability and effects of the sampling system on results, confirmed that the variations in ventilation effectiveness values inside both the cabins are a result of experimental variations rather than ventilation effectiveness variations due to locations or heights inside the cabin. Therefore, it was concluded from the ventilation effectiveness studies that the ventilation system of both the aircraft cabin types efficiently and uniformly removed contaminants from the entire cabin with no particular regions of high or low ventilation identified. It is also to be noted that the local effective ventilation rates found for both the cabins are higher than those for other indoor applications. This result can be expected given the

relatively high air velocities inside aircraft cabins, which provides better mixing and thus efficient ventilation.

6.2 Dispersion of Tracer Gas with Ventilation Air

The Chapter 5 of this thesis also presents results from the study of tracer gas dispersion in the presence of ventilation air. The results show that transport of gaseous contaminants inside the aircraft cabin depends on the location of the source. For source locations along the centerline of the cabin, as expected within a particular row, transport of gaseous contaminants/tracer gas is roughly symmetrical in the two halves of the cabin. In addition, the study revealed that dispersion of tracer gas inside the cabin also depends on the relative distance between the source and the measurement location. Within the row of injection/source, CO₂ concentrations decreased moving away from the source location. In addition, measured CO₂ concentrations decreased moving away from the source in the longitudinal direction. Thus, it was concluded that the risk of exposure of gaseous contaminants decreases moving away from the source in both longitudinal and lateral direction. It is to be noted that although the dispersion of gaseous contaminants is intended to occur majorly in the lateral direction, significant dispersion occurs in the longitudinal direction as well.

6.3 Dispersion of Tracer Gas with No Ventilation Air

The results from dispersion of tracer gas with no ventilation study indicated that even in the absence of ventilation air, significant dispersion of tracer gas occurred in both the lateral and longitudinal directions. The dispersion of gaseous contaminants inside the cabin depends on the location of the source. As expected, for injection at the geometric center of the cabin, the dispersion was roughly symmetric about the lateral and longitudinal centerlines of the cabin. Experiments with injection at 2B and 4B indicated that majority of the dispersion of tracer gas occurred within the row of injection. The CO₂ count was higher at seats in row of injection than at seats in rows away from the source. This suggests that the CO₂ concentration decreases moving away from the source along the longitudinal direction. It was observed that within the row of injection the normalized CO₂ count decreased with the increase in the distance between the source and sampling location.

Chapter 7 - Recommendations

Gaspers were not operated for any of the testing conducted for this thesis. Thus, the ventilation effectiveness studies should be repeated with operational gaspers. This would help determine if the gaspers have any effect on the local ventilation effectiveness inside the cabins. The dispersion of tracer gas studies were carried out for only two scenarios: with ventilation air and without ventilation. It is recommended that similar tracer gas studies be conducted at different air supply rates, specifically at half and double the current air supply rate, to study the effects of air supply rate on the dispersion phenomenon inside the Boeing 737 cabin.

As mentioned previously, due to the time constraint, only selected injection locations were tested to study transport of gaseous contaminants in the presence and absence of ventilation air. More injection locations should be tested to give a more comprehensive and accurate picture of dispersion of gaseous contaminants. In particular, for the tracer gas study with ventilation air, similar experiments should be conducted to examine spread of gaseous contaminants from injection at locations in the front right section and rear left section of the cabin. For tracer gas study with no ventilation air, injection locations in the front right section, the rear left section, the centerline front and centerline rear sections should be tested. In addition, the number of sampling location for each injection location should also be increase to provide detailed and consistent results. Also as mentioned earlier, gaspers were not operated for all experiments conducted. Therefore, it is recommended to conduct experiments to study the effects of gaspers on the transport of gaseous contaminants inside the Boeing 737 mockup cabin.

The mockup cabins used are of relatively shorter length when compared to actual aircrafts. The Boeing 737 cabin is only five rows long and the Boeing 767 cabin is only eleven rows long. This limits the dispersion of tracer gas inside the cabin. In order to determine the extent of gaseous contaminants transport in the longitudinal direction from a particular source, similar tracer gas studies should be conducted inside elongated versions of these cabins. This can be done by either constructing longer mockup cabins or simply conducting experiments in an actual aircraft.

References

- BTS. 2016. http://www.rita.dot.gov/bts/press_releases/bts018_16. U.S. Department of Transportation, Washington, D.C.
- Air Transportation Center of Excellence (CoE) for Airliner Cabin Environment Research (ACER). 2007. Transport project.
- Shehadi, M. 2015. Airflow distribution and turbulence analysis in the longitudinal direction of a Boeing 767 Mockup Cabin. PhD diss., Kansas State University.
- Madden, M. 2015. The effects of passenger loading and ventilation air on airflow patterns within an aircraft cabin. Master's Thesis, Kansas State University.
- Anderson, M. 2012. Effect of gaspers on airflow patterns and the transmission of within an aircraft cabin environment. Master's Thesis, Kansas State University.
- Trupka, A. 2011. Tracer gas mapping of beverage cart wake in a twin aisle aircraft cabin simulation chamber. Master's Thesis, Kansas State University.
- Beneke, J. 2010. Small diameter particle dispersion in a commercial aircraft cabin. Master's Thesis, Kansas State University.
- Jones, B. 2009. Advanced models for predicting contaminants and infectious disease virus transport in the airliner cabin environment (part 2). *Proceedings of the Transportation Research Board, Research on the Transmission of Disease in Airports and Aircrafts, Washington, D.C.*
- Lebbin, P. 2006. Experimental and numerical analysis of air, tracer gas, and particulate movement in a large eddy simulation chamber. PhD diss., Kansas State University.
- FAA. 2010. Environmental control and life support systems for flight crew and space flight participants in suborbital space flight, Version 1, Guide for 14 CFR § 460.11. Federal Aviation Administration, Washington, D.C.
- Shehadi, M. 2010. Experimental investigation of optimal particulate sensor location in an aircraft cabin. Master's Thesis, Kansas State University.
- ASHRAE. 2007. Chapter 10, Aircraft. In *ASHRAE Handbook – Heating, Ventilating and Air-Conditioning Applications*. Atlanta: ASHRAE.
- Wang, A., Y. Zhang, J. Topmiller, J. Bennett, K. Dunn. 2006. Tracer study of airborne disease transmission in an aircraft cabin mock-up. *ASHRAE Transactions*, 112(2): 697-705.
- ASHRAE. 2013. Chapter 16, Ventilation and Infiltration. In *ASHRAE Handbook-Fundamentals*. Atlanta: ASHRAE.

- Wang, A., Y. Zhang, Y. Sun, and X. Wang. 2008. Experimental study of ventilation effectiveness and air velocity distribution in an aircraft cabin mockup. *Building and Environment* 43(3):337-343.
- Zhang, Z., X. Chen, S. Mazumdar, T. Zhang and Q. Chen. 2009. Experimental and numerical investigation of airflow and contaminant transport in an airliner cabin mockup. *Building and Environment* 44(1): 85-94.
- Singh, A., M.H. Hosni, R.H. Horstman, J.V. Gilder and R. May. 2002. Numerical simulation of airflow in an aircraft cabin section. *ASHRAE Transactions*, 108: 1005-1013.
- Mo, H. 2002. Experimental and computational study of interactions of airflow inside aircraft cabin with human body. Master's Thesis, Kansas State University.
- Coleman, H., W. Steele. 1989. *Experimentation and Uncertainty Analysis for Engineers*. New York: John Wiley & Sons Inc.
- Jones, B. 2016. The Effects of Recirculation on Local Ventilation Effectiveness. Unpublished article.

Appendix A - Uncertainty Analysis

Numerous instruments controlling and measuring various variables are simultaneously used for all experiments conducted for various studies reported in this thesis. Each of these instruments have considerable uncertainties associated with them. These errors/uncertainties propagate into the results through the various phases of testing. Therefore, it is imperative to carry out a general uncertainty analysis of each instrument to determine the goodness of the results found from the conducted experiments. The various instruments used to conduct all experiments are categorized into three subsystems which control the air conditioning and supply, the tracer gas injection and tracer gas sampling. The uncertainties related to each of these subsystems is calculated separately and combined to represent the overall uncertainty of the results for various studies. The detailed uncertainty analysis of each of the above mentioned subsystems is carried out in the following sections.

A.1 Supply Air Uncertainty

As mentioned earlier the air conditioning and supply system is used to provide air at 15.6 °C (60 °F) to the mockup cabins. The Boeing 767 cabin is supplied with 40 m³/min (1400 ft³/min) of conditioned air, while the Boeing 737 cabin is supplied with 17 m³/min (600 ft³/min) of conditioned air. The supply air temperature is measured using an Omega 3 wire-RTD at the duct near entrance to the cabins. The flowrate is measured using an Omega PX653 differential pressure transmitter along with a PCI FE-1500 flow meter. Data from the temperature sensor, flow meter and pressure sensor is collected by an Agilent DAQ system. Details of instruments used for the air supply and conditioning are provided in Table A.1 (Madden, 2015).

Table A.1 Supply Air Instruments Uncertainties

Instrument	Uncertainty	Range
Agilent 34970 DAQ	0.06 °C (RTD)	49 – 2.1
NI Filed Point AI-110	0.07% of reading + 0.007% of range	0 - 5 V
PCI FE-1500 Flow Meter	2%	100 – 10000 fpm
Omega PX 653	0.25% F.S	1” Water Column
	0.05% F.S. Repeatability	0 – 5 V
Omega 3-wire RTD	$\pm (0.30 + 0.005 * T) ^\circ$	-50 – 250, Class B

The uncertainty in the velocity/flow rate of the supply air is the desired result. Temperature and pressure are the measured variables whose uncertainties are used to calculate the uncertainty related to the velocity of the supply air. The uncertainty related to the temperature variable is calculated using Equation A.1 through A.4 as shown below (Madden, 2015). The nomenclature ‘U’ for uncertainty is used throughout. The uncertainty associated with the temperature remains essentially the same for both flow rates.

$$\left(\frac{U_{temp}}{T_{supply}}\right)^2 = \left(\frac{U_{RTD}}{T_{supply}}\right)^2 + \left(\frac{U_{DAQ}}{T_{supply}}\right)^2 \quad (A.1)$$

$$\left(\frac{U_{temp}}{T_{supply}}\right)^2 = \left(\frac{(0.30 + 0.005 * 15.6) \text{ }^\circ\text{C}}{288.8 \text{ K}}\right)^2 + \left(\frac{0.06 \text{ }^\circ\text{C}}{288.8 \text{ K}}\right)^2 \quad (A.2)$$

$$\frac{U_{temp}}{T_{supply}} = 0.134\% \quad (A.3)$$

$$U_{temp} = T_{supply} * 0.134 \% = 0.39 \text{ }^\circ\text{C} = 0.70 \text{ }^\circ\text{F} \quad (A.4)$$

The next calculation for the overall supply air uncertainty is the uncertainty related to the pressure. Uncertainty for the flow rate of 40 m³/min (1400 ft³/min) was already calculated by Trupka (2011) and is reproduced here. The Equations A.5 and A.6 were used to calculate the pressure uncertainty as shown.

$$U_{press} = \sqrt{U_{PCI}^2 + U_{\omega}^2 + U_{NI}^2} \quad (A.5)$$

$$U_{press@1400cfm} = \sqrt{2 \%^2 + 0.803 \%^2 + 0.08 \%^2} = 2.16 \% \quad (A.6)$$

For 17 m³/min (600 ft³/min) of flow through the duct section, the velocity was calculated to be 2.19 m/s (430 ft/min). Using the Engineering Reference Table by Pentagon Controls, the velocity pressure corresponding to the velocity of 2.19 m/s (430 ft/min) is found to be 0.29 mm of H₂O column (0.012 in. of H₂O). Based on this, the uncertainty for the Omega PX 653 pressure transducer is calculated to be 0.0029%. In addition, assuming linear nature of the pressure transducer, the voltage reading recorded by the NI Field Point AI-110 module for a velocity of 2.19 m/s (430 ft/min) is found to be 1.5 V. This voltage reading is used with the repeatability of

the module provided in Table A.1 to give the module uncertainty of 0.14%. The uncertainty for the flow rate of 17 m³/min (600 ft³/min) is calculated using Equations A.5 and A.7.

$$U_{press@600cfm} = \sqrt{2 \%^2 + 0.0029 \%^2 + 0.14 \%^2} = 2.0 \% \quad (A.7)$$

The overall uncertainty for the supply air is calculated using the root sum squared method. As we know from the Bernoulli's Equation, the pressure is related to the square of the velocity. The principle of partial derivatives thus requires that the temperature and pressure uncertainties be reduced by a factor of two before being squared. The overall uncertainty for the two flowrates are calculated as shown in Equations A.8 through A.11.

$$U_{supply\ air@1400cfm} = \sqrt{\left(\frac{1}{2}U_{temp}\right)^2 + \left(\frac{1}{2}U_{press@1400cfm}\right)^2} \quad (A.8)$$

$$U_{supply\ air@1400cfm} = \sqrt{\left(\frac{1}{2} * 0.134 \%\right)^2 + \left(\frac{1}{2} * 2.16\%\right)^2} = 1.08 \% \quad (A.9)$$

$$U_{supply\ air@600cfm} = \sqrt{\left(\frac{1}{2}U_{temp}\right)^2 + \left(\frac{1}{2}U_{press@600cfm}\right)^2} \quad (A.10)$$

$$U_{supply\ air@600cfm} = \sqrt{\left(\frac{1}{2} * 0.134\%\right)^2 + \left(\frac{1}{2} * 2\right)^2} = 1.0 \% \quad (A.11)$$

A.2 Tracer Gas Injection Uncertainty

The CO₂ analyzers produce voltage outputs, which need to be converted to ppm of CO₂. This is achieved by calibrating the CO₂ analyzers using calibration gases. The calibration gases have specific uncertainties associated with them. In addition, the CO₂ and He gases used as tracer gas have a certain level of purity. The Table A.2, provides the various purities and uncertainties associated with each of the gases used (Trupka, 2011).

Table A.2 Calibration Gas and Tracer Gas Mixture Uncertainty

Gas	Uncertainty/Purity
CO ₂	0.5% / 99.5% pure
He	0.003% / 99.997% pure
500 ppm CO ₂ – Air Mixture	2%
1000 ppm CO ₂ – Air mixture	1%
2000 ppm CO ₂ – Air Mixture	1%

The total uncertainty related to the calibration gases is calculated using the root sum squared method. The Equations A.12 and A.13 are used to calculate the total calibration gas uncertainty.

$$U_{calib} = \sqrt{U_{500}^2 + U_{1000}^2 + U_{2000}^2} \quad (\text{A.12})$$

$$U_{calib} = \sqrt{2\% ^2 + 1\% ^2 + 1\% ^2} = 2.45\% \quad (\text{A.13})$$

The tracer gas injection system also consists of two mass flow controllers for CO₂ and He gases and a PR 4000 power supply, which has a 16-bit uncertainty. These mass flow controllers have uncertainties, which add to the total uncertainty of the tracer gas injection system, which in turn adds to the overall uncertainty of the results. The Table A.3 summarizes the uncertainties related to the mass flow controllers (Trupka, 2011).

Table A.3 Mass Flow Controllers Uncertainty

Instrument	Uncertainty	Rated Flow
CO ₂ Mass Flow Controller	1.0% F.S. (accuracy)	100 SLM
	0.2% F.S. (repeatability)	
	0.1% F.S. (resolution)	
	15 to 40 °C (operation)	
He Mass Flow Controller	1.0% F.S. (accuracy)	10,000 SCCM
	0.2% F.S. (repeatability)	
	0.1% F.S. (resolution)	
	0 to 50 °C (operation)	

As mentioned previously different studies are conducted for this research, which utilize different injection rates. The tracer gas injection details for each study is listed in Table A.4. The

repeatability values from Table A.3 along with injection rates from Table A.4 are used to calculate the tracer gas injection uncertainty for various studies.

Table A.4 Tracer Gas Injection Repeatability

Study	Tracer Gas	Injection Rate (LPM)
Dispersion Study with Ventilation Air	CO ₂	5 LPM
	He	3.1 LPM
Dispersion Study with No Ventilation Air	CO ₂	2 LPM
	He	1.2 LPM

For dispersion of tracer gas study with ventilation air the CO₂ injection uncertainty is calculated using Equations A.14 and A.15, while the He injection uncertainty is calculated using Equations A.16 and A.17.

$$U_{rep,CO_2,DispVent} = \frac{0.2\% * 100 \text{ LPM}}{5 \text{ LPM}} = 4.00 \% \quad (\text{A.14})$$

$$U_{CO_2,DispVen} = \sqrt{U_{rep,CO_2,DispVent}^2 + U_{CO_2,purity}^2} = 4.03 \% \quad (\text{A.15})$$

$$U_{rep,He,DispVent} = \frac{0.2\% * 10 \text{ LPM}}{3.01 \text{ LPM}} = 0.66\% \quad (\text{A.16})$$

$$U_{He,DispVen} = \sqrt{U_{rep,He,DispVent}^2 + U_{He,purity}^2} = 0.66 \% \quad (\text{A.17})$$

Similarly, the tracer gas injection uncertainty for dispersion study with no ventilation air is calculated using equations A.18 and A.19.

$$U_{CO_2,DispNoVen} = \sqrt{U_{rep,CO_2,DispVent}^2 + U_{CO_2,purity}^2} = 10 \% \quad (\text{A.18})$$

$$U_{He,DispNoVen} = \sqrt{U_{rep,CO_2,DispVent}^2 + U_{CO_2,purity}^2} = 1.67 \% \quad (\text{A.19})$$

A.3 Tracer Gas Sampling Uncertainty

As mentioned previously, four infrared CO₂ gas analyzers are used to measure CO₂ concentrations at various locations. An Agilent 34970 DAQ system collects data from the analyzers and transfers it to the computer. The DAQ system and each of the analyzers have certain measurable range and uncertainties associated with them. The details of the four analyzers are as shown in Table A.5 (Anderson, 2012).

Table A.5 Tracer Gas Sampling System Uncertainty

Model/Instrument	Uncertainty	Range
Edinburgh Gas card NG	2% of Range (accuracy)	0 – 3000 ppm
	0.3@zero, 1.5% @span (repeatability)	
PP Systems WMA-4	<1% @span (repeatability)	0 – 2000 ppm
	20 ppm (accuracy)	
Agilent 34970A DAQ	0.0035% of reading + 0.0005% of range	10V

Table A.6, provides the root mean squared values and average linearity of each analyzer for all the calibrations performed during the testing period. As can be seen from the values, the four analyzers are extremely linear in nature. Thus, the repeatability of the analyzers is calculated by linearly interpolating between zero and the span of the analyzers.

Table A.6 R-Squared and Linearity Values of Analyzers

Calibration Date	A-1 Sensor	A-2 Sensor	A-3 Sensor	A-4 Sensor
08-24-2016	0.99998517	0.99998970	0.99999411	0.99999995
09-13-2016	0.99998001	0.99998207	0.99999840	0.99997675
10-24-2016	0.99998980	0.99999964	0.99999992	0.99999977
Average R-Squared Values	0.99998499	0.99999047	0.99999748	0.99999216
Linearity Uncertainty	0.00150%	0.00095%	0.00025%	0.00078%

In order to avoid overestimation of the uncertainty by choosing worst-case scenario, a distance of four seats between the injection location and sampling location is used to calculate the uncertainty of various analyzers. For dispersion of tracer gas with supply of ventilation air, the uncertainties for A-1 and A-3 sensors are determined with the injection location at 2B and sampling location at 5E, while for A-2 sensor sampling at seat 4E is utilized, for the purpose of this study the A-4 sensor always measured the inlet CO₂ concentration. For dispersion study in

absence of ventilation air, the uncertainties for all four sensors is determined by utilizing the injection location at 2B and sampling at 2A or 2C. The average CO₂ concentrations for the two studies measured by the analyzers at locations as mentioned and the associated repeatability are provided in Table A.7 and A.9. The overall uncertainty associated with each of the sensors for the two separate dispersion studies are summarized in Tables A.8 and A.10. As can be seen from Table A.8, for dispersion study with ventilation air the uncertainties of the analyzers A-1, A-2 and A-3 are fairly similar with the worst case of 2.47 for A-2 sensor. This uncertainty is used in the calculation for the overall uncertainty of the results from tracer gas dispersion with ventilation air. Similarly, for dispersion study with no ventilation air the sensor uncertainties related to A-4 sensor are used to calculate the overall uncertainty of results.

Table A.7 Sampling Uncertainty for Dispersion Study With Ventilation Air

Sensor	CO ₂ Concentration(ppm)	Output Voltage (V)	Repeatability (%)
A-1	518.56	1.28	0.26
A-2	608.63	1.52	0.30
A-3	500.13	0.51	0.25
A-4	398.97	0.61	0.50

Table A.8 CO₂ Analyzers Total Uncertainty for Dispersion Study With Ventilation Air

Sensor	U _{calibration}	U _{linearity}	U _{repeatability}	U _{DAQ}	U _{sensor}
A-1	2.45	0.00150	0.26	0.0095	2.46
A-2	2.45	0.00095	0.30	0.0103	2.47
A-3	2.45	0.00025	0.25	0.0068	2.46
A-4	2.45	0.00078	0.50	0.0071	2.50

Table A.9 Sampling Uncertainty for Dispersion Study With No Ventilation Air

Sensor		CO ₂ Concentration(ppm)	Output Voltage (V)	U _{repeatability}
A-1	Start	527	0.50	0.26
	Final	1550	1.10	0.78
A-2	Start	538.2	1.33	0.27
	Final	1176.6	2.91	0.59
A-3	Start	500.5	1.10	0.25
	Final	1105.5	3.84	0.55
A-4	Start	530	0.81	0.51
	Final	1240	1.99	0.80

Table A.10 CO₂ Analyzers Total Uncertainty for Dispersion Study With No Ventilation Air

Sensor		U _{calibration}	U _{linearity}	U _{repeatability}	U _{DAQ}	U _{sensor}
A-1	Start	2.45	0.00150	0.26	0.0068	2.46
	Transient	2.45	0.00150	0.78	0.0089	2.57
A-2	Start	2.45	0.00095	0.27	0.0097	2.47
	Transient	2.45	0.00095	0.59	0.0152	2.52
A-3	Start	2.45	0.00025	0.25	0.0089	2.46
	Transient	2.45	0.00025	0.55	0.018	2.51
A-4	Start	2.45	0.00078	0.51	0.0078	2.51
	Transient	2.45	0.00078	0.80	0.012	2.58

A.4 Overall Uncertainty

After the uncertainties of all the subsystems are calculated, the uncertainties are combined to give the overall uncertainty of the results found. The overall uncertainty is calculated using the general Equation A.20, where ‘U’ stands for uncertainty, ‘X’ stands for a variable and ‘r’ stands for the desired result.

$$U_r = \left[\left(\frac{\partial r}{\partial X_1} U_{X_1} \right)^2 + \left(\frac{\partial r}{\partial X_2} U_{X_2} \right)^2 + \dots + \left(\frac{\partial r}{\partial X_j} U_{X_j} \right)^2 \right]^{1/2} \quad (\text{A.20})$$

For the purpose of demonstration, only the steps for overall uncertainty for results from dispersion study with ventilation air are shown. The overall uncertainty for the dispersion study with ventilation air is calculated using Equation A.21. The partial differentials of Equation A.21 are separately solved using Equation A.22 through A.26.

$$U_N^2 = \left(\frac{\partial N}{\partial C_{sample}} * U_{sample} \right)^2 + \left(\frac{\partial N}{\partial C_{inlet}} * U_{inlet} \right)^2 + \left(\frac{\partial N}{\partial \dot{V}_{CO_2}} * U_{inject,CO_2} \right)^2 + \left(\frac{\partial N}{\partial \dot{V}_{supplyair@600cfm}} * U_{supplyair@600cfm} \right)^2 \quad (\text{A.21})$$

$$N = \frac{C_{sample} - C_{inlet}}{\dot{V}_{CO_2} / \dot{V}_{supply}} \quad (\text{A.22})$$

$$\frac{\partial N}{\partial C_{sample}} = \frac{\dot{V}_{supplyair@600cfm}}{\dot{V}_{CO_2}} \quad (A.23)$$

$$\frac{\partial N}{\partial C_{inlet}} = -\frac{\dot{V}_{supplyair@600cfm}}{\dot{V}_{CO_2}} \quad (A.24)$$

$$\frac{\partial N}{\partial \dot{V}_{CO_2}} = \frac{\dot{V}_{supplyair@600cfm}}{\dot{V}_{CO_2}} * (C_{inlet} - C_{sample}) \quad (A.25)$$

$$\frac{\partial N}{\partial \dot{V}_{supplyair@600cfm}} = \frac{(C_{sample} - C_{inlet})}{\dot{V}_{CO_2}} \quad (A.26)$$

The values of the partial differentials are plugged into Equation A.21 and the equation is divided by the desired result i.e. the normalized CO₂ count to provide percentage uncertainty as shown in Equation A.27.

$$\begin{aligned} \left(\frac{U_N}{N}\right)^2 &= \left(\frac{U_{sample}}{C_{sample} - C_{inlet}}\right)^2 + \left(\frac{U_{inlet}}{C_{sample} - C_{inlet}}\right)^2 + \left(\frac{U_{inject,CO_2}}{\dot{V}_{CO_2}}\right)^2 \\ &+ \left(\frac{U_{supplyair@600cfm}}{\dot{V}_{supplyair@600cfm}}\right)^2 \end{aligned} \quad (A.27)$$

It is to be noted that the uncertainties related to supply air and injection of CO₂ are already in terms of percentages i.e. the air supply rate and injection rate have already been utilized. Thus the two flow rates should be removed from the Equation A.27. In addition, the uncertainty of the sampling analyzer and inlet analyzer are also in terms of percentages, which need to be converted to absolute uncertainties to maintain consistency of the equation. Doing this gives the reduced Equation A.28.

$$\begin{aligned} \left(\frac{U_N}{N}\right)^2 &= \left(\frac{U_{sample}}{C_{sample} - C_{inlet}}\right)^2 + \left(\frac{U_{inlet}}{C_{sample} - C_{inlet}}\right)^2 + U_{inject,CO_2}^2 \\ &+ U_{supplyair@600cfm}^2 \end{aligned} \quad (A.28)$$

The values of the individual uncertainties calculated previously are plugged into Equation A.28 to give the overall uncertainty of the results from tracer gas study with ventilation air. Note

that only the uncertainty of A-2 sensor is utilized for this calculation as the rest of the analyzers have similar uncertainties.

$$U_{N,vent} = \sqrt{\left(\frac{608.63 * 2.47 \%}{608.63 - 398.97}\right)^2 + \left(\frac{398.97 * 2.50 \%}{608.63 - 398.97}\right)^2 + 4.03^2 + 1^2} \quad (\text{A.29})$$

$$U_{N,vent} = 10 \% \quad (\text{A.30})$$

The overall uncertainty for dispersion of tracer gas study in the absence of ventilation air is calculated using Equation A.31. As the supply air is eliminated for this study, the uncertainties related to the supply air and inlet air are not included. The partial derivatives of Equation A.31 are calculated as done previously to give the reduced Equation A.32. The final uncertainty in results is calculated by plugging in various individual uncertainties into Equation A.32. For the tracer gas dispersion study with no ventilation air, the uncertainty is calculated to be as shown in Equations A.33 and A.34.

$$U_N^2 = \left(\frac{\partial N}{\partial C_{sensor,start}} * U_{sensor,start}\right)^2 + \left(\frac{\partial N}{\partial C_{sensor,transient}} * U_{sensor,transient}\right)^2 + \left(\frac{\partial N}{\partial \dot{V}_{CO_2}} * U_{inject,CO_2}\right)^2 \quad (\text{A.31})$$

$$\left(\frac{U_N}{N}\right)^2 = \left(\frac{U_{sensor,start}}{C_{sensor,transient} - C_{sensor,start}}\right)^2 + \left(\frac{U_{sensor,start}}{C_{sensor,transient} - C_{sensor,start}}\right)^2 + U_{inject,CO_2}^2 \quad (\text{A.32})$$

$$U_{N,vent} = \sqrt{\left(\frac{530 * 2.51 \%}{1240 - 530}\right)^2 + \left(\frac{1240 * 2.58 \%}{1240 - 530}\right)^2 + 10^2} \quad (\text{A.33})$$

$$U_{N,Novent} = 11 \% \quad (\text{A.34})$$

Appendix B - Electronic Appendix Manual

The electronic appendix contains data for all experiments conducted for various studies reported in this thesis. The electronic appendix is attached with this thesis in a file named “Electronic Appendix.zip”. It is recommended to extract the entire file locally as Excel spreadsheets to retain the links between various files present in the electronic appendix. The electronic appendix folder contains three subfolders. The folders are named “Ventilation Effectiveness”, “Dispersion of Tracer Gas with Ventilation Air” and “Dispersion of Tracer Gas with No Ventilation Air”. Instructions for each of these folders is provided in the sections following.

B.1 Ventilation Effectiveness Folder Instructions

The “Ventilation Effectiveness” folder contains two subfolders namely “Boeing 737 Cabin” and “Boeing 767 Cabin”. This was done to distinguish between the ventilation effectiveness studies conducted inside the two separate cabin mockups.

The “Boeing 737 Cabin” folder contains four subfolders: “At Breathing Level of Adult Passengers Standing at Aisle Locations”, “At Breathing Level of Adult Passengers Standing at Seat Locations”, “At Breathing Level of Seated Adult Passengers” and “At Breathing Level of Seated Infant Passengers” to present data from various locations analyzed inside the Boeing 737 cabin. Inside each of these folders, there are numerous subfolders for various sampling locations analyzed along with an Excel file named “Overall Result” which summarizes data from all sampling locations for that particular scenario. Each of these subfolders contains Excel spreadsheet files for the experiment repeats and average of the repeats. The excel files for repeats of an experiment are named using the format “(row number) (seat column) - (row number) (seat column) - ... _R (repeat number)”. For example, for repeat one experiments to analyze seats 1A, 2B and 3C the file is named “1A-2B-3C_R1”. The excel file for average of repeats is named similarly excluding the indication for the repeat number i.e. “_R (repeat number)”.

The folder “Boeing 767 Cabin” contains two subfolders named “Repeat 1” and “Repeat 2”. The folder “Repeat 1” contains multiple subfolders for sampling at various seat columns and a subfolder “CORRECTION DATA” along with an Excel spreadsheet file named “Repeat 1 Data Result”. Each folder for various seat columns contains numerous subfolders named using

the convention “(row number) (seat column) - (row number) (seat column) – (row number) (seat column) Seats Sampling” which in turn contain Excel spreadsheet files for the experiment repeats and average of the repeats. The excel files are named using the convention used for the Boeing 737 cabin data. The folder “CORRECTION DATA” contains various subfolders containing the correction data folders for faulty and incomplete values from Repeat 1 data. The naming convention for these folders is same as mentioned previously. Similar to the folder “Repeat 1”, the “Repeat 2” folder also contains subfolders for sampling for various seat columns. The instructions for “Repeat 2” folder are similar to that of “Repeat 1” folder.

B.2 Dispersion of Tracer Gas with Ventilation Air Folder Instructions

The “Dispersion of Tracer Gas with Ventilation Air” folder contains six subfolders for various injection locations and calibration of analyzers details. The folder “Calibration” contains two subfolders for calibrations carried out at various dates. Each of these folders contains four subfolders named after the four CO₂ analyzers along with an Excel file “Result” which contains the summarized calibration result. Each CO₂ analyzer folder contains three Excel files, named using the convention “(Analyzer name) _ (Concentration of Calibration Gas)” to present data from the calibration process. Each folder for various injection locations contain multiple subfolders for various sampling locations analyzed along with an Excel file named “Injection at (injection location) – Overall Result” which summarizes data from all sampling locations for that particular injection location. The subfolders are named using the format “(row number) (column letter) - (row number) (column letter) ... Seats Sampling”. Each of these subfolders contains Excel spreadsheet files for the experiment repeats and average of the repeats. The excel files use the same naming convention as the folder they belong to along with an addition of “_R (repeat number)” to represent the experiment repetition number. The excel file for average of repeats is named similarly excluding the indication for the repeat number i.e. “_R (repeat number)”.

B.3 Dispersion of Tracer Gas with No Ventilation Air Folder Instructions

The folder “Dispersion of Tracer Gas with No Ventilation Air” contains four subfolders. Three of these folders are named according to the injection locations used for this study, while the fourth folder is named “Calibration”. Instructions of each of these folders is similar to the instructions given in section B.2 of this Appendix.

Appendix C - The Effect of Recirculation on Local Ventilation

Effectiveness¹

Introduction

There are (at least) two definitions of local ventilation effectiveness. The first definition refers to the effectiveness with which supply air is distributed to a given location and the second definition refers to the effectiveness with which outside air is distributed to a given location. When the space is ventilated with 100% outside air, these two ventilation effectiveness measures are one and the same. However, if the supply air is composed, in part, of recirculated air, the two values most likely will not be the same.

Measurements have been conducted for aircraft cabins where the ventilation effectiveness is measured using 100% outside air with ventilation flow rates representative of the cabin supply flow rates of operating aircraft. The resulting ventilation effectiveness values are then representative of the supply air ventilation effectiveness. Since the supply air in most aircraft is composed of a mixture of outside air and recirculated air, the question arises as to how the measured values apply to the ventilation effectiveness with respect to outside air in an operating aircraft.

Derivation

There are several different, equivalent ways of defining ventilation effectiveness. To keep the mathematics simple for this discussion, it will be defined as the concentration of a uniformly generated contaminant that would result divided by the perfectly mixed concentration of that same uniformly generated contaminant. To further simplify the calculations, the hypothetical contaminant will have near zero concentration in the outside air. The end result is the same whether or not there is a significant level in the outside air but this simplification makes the mathematics less messy.

¹ The information in this appendix was provided to the author by Byron W. Jones and is included here as it is not published elsewhere.

Consider the ventilated space shown in Figure 1. Inside this space, a contaminate is generated uniformly at the rate $(Q_C / V)_{\text{gen}}$ which has the units of m^3/s of contaminant per m^3 of space or s^{-1} and is the contaminant generation rate per unit volume. If the space is ventilated with outside air, and the concentration of the contaminant is much less than one, the steady state perfectly mixed concentration of the contaminant, C_p , in the space will be

$$C_p = (Q_C / V)_{\text{gen}} / (Q_S / V_S) \quad (1)$$

where Q_S is the supply air flow rate and V_S is the volume of the ventilated space. The local supply air ventilation effectiveness VE_{SL} is then defined as

$$VE_{\text{SL}} = C_p / C_{\text{L100}} \quad (2)$$

where C_{L100} is the local contaminant concentration with 100% outside air.

Now consider ventilation with recirculation as shown in Figure 2. The perfectly mixed concentration will be

$$C_p = (Q_C/V)_{\text{gen}} / (Q_O/V_S)$$

The concentration of the contaminant in the exhaust airflow will also necessarily be C_p .² Now, consider the contaminant concentration at some local space. The effective amount of supply air going to this space, Q_L , will be

$$Q_L = Q_S VE_{\text{SL}} V_L/V_S \quad (3)$$

The contaminant concentration in the supply air, C_S , will be

$$C_S = C_p (Q_R/Q_S) = [(Q_C/V)_{\text{gen}} / (Q_O/V_S)] (Q_R/Q_S) \quad (4)$$

² For simplicity, this discussion utilizes a single return air path. If there are multiple exhausts and those exhausts are not fully mixed for the recirculation air, the result may be different depending upon whether the recirculated air comes preferentially from locations of high or low contaminant concentration.

The contaminant mass balance for the local space is then

$$(C_L - C_S) Q_L / V_L = (Q_C/V)_{gen}$$

Or

$$C_L = C_S + (Q_C/V)_{gen} / (Q_L / V_L) \quad (5)$$

Substituting for Q_L and C_S gives the following expression

$$C_L = [(Q_C/V)_{gen} / (Q_O / V_S)] (Q_R/Q_S) + (Q_C/V)_{gen} / [(Q_S VE_{SL} V_L / V_S) / V_L] \quad (6)$$

The local ventilation effectiveness with respect to outside air, VE_{OL} , will be

$$VE_{OL} = C_p / C_L \quad (7)$$

Substituting from previous equations gives

$$VE_{OL} = \{ (Q_C/V)_{gen} / (Q_O / V_S) \} / \{ [(Q_C/V)_{gen} / (Q_O / V_S)] (Q_R/Q_S) + (Q_C/V)_{gen} / [(Q_S VE_{SL} V_L / V_S) / V_L] \} \quad (8)$$

Defining the recirculation fraction, f , as

$$f = Q_R / Q_S \quad (9)$$

and simplifying the expression in Equation 8 gives the final relationship between the local ventilation effectiveness with respect to outside air and the local ventilation effectiveness with respect to supply air.

$$VE_{OL} = VE_{SL} / [1 + f (VE_{SL} - 1)] \quad (10)$$

Discussion

It may not be immediately obvious from this expression but the net effect of recirculation is to drive VE_{OL} towards unity. A couple of examples with $f=0.5$ will demonstrate this effect.

First, with $VE_{SL} = 0.70$:

$$VE_{OL} = 0.7 / [1 + 0.5 (0.70 - 1)] = 0.82$$

Generally, VE_{SL} values are less than unity but there is no theoretical upper limit on its value and it is certainly possible that aircraft systems could be designed to give values of VE_{SL} greater than one. Thus, the second example with $VE_{SL} = 1.30$:

$$VE_{OL} = 1.30/[1 + 0.5 (1.30 - 1)] = 1.13$$

As long as $VE_{SL} < 1$, which is case with current aircraft environmental control system designs, then recirculation improves the ventilation effectiveness with respect to outside air.

These results may lead one to believe that recirculation improves local ventilation. It all depends upon the point of reference. The effective outside air ventilation rate for the local space, is

$$\text{Local Outside Air Ventilation Rate} = (Q_o/V_s) VE_{OL} \quad (11)$$

If Q_o is kept constant and recirculation is added, then the increased ventilation effectiveness results in improved outside air ventilation. However, if the recirculation is used to decrease the amount of outside air, the increased ventilation effectiveness will not offset the decrease flow of outside air. In the end, it is the Local Outside Air Ventilation Rate that is important and the emphasis should be on the this value and not focused only on (Q_o/V_s) or VE_{OL} .

This analysis is based on no cleaning of the recirculation air and contaminant control is achieved only by ventilation with outside air. For aircraft, this basis is correct for gaseous contaminants with most commercial aircraft. Most commercial aircraft employ high grade particulate filtration of recirculation air and the recirculation air is free of particulate contamination, including pathogens. From the point of view of particulate contaminants, the supply air is equivalent to and possibly better than outside air. The applicable local ventilation rate for particulates is then

$$\text{Local Supply Air Ventilation Rate} = (Q_s/V_s) VE_{SL} \quad (12)$$

Again, it is the product of the two terms that is important and undo emphasis should not be placed on either individual term.

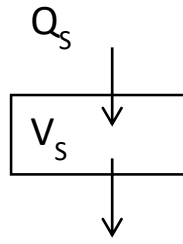


Figure 1. Ventilation of a Space

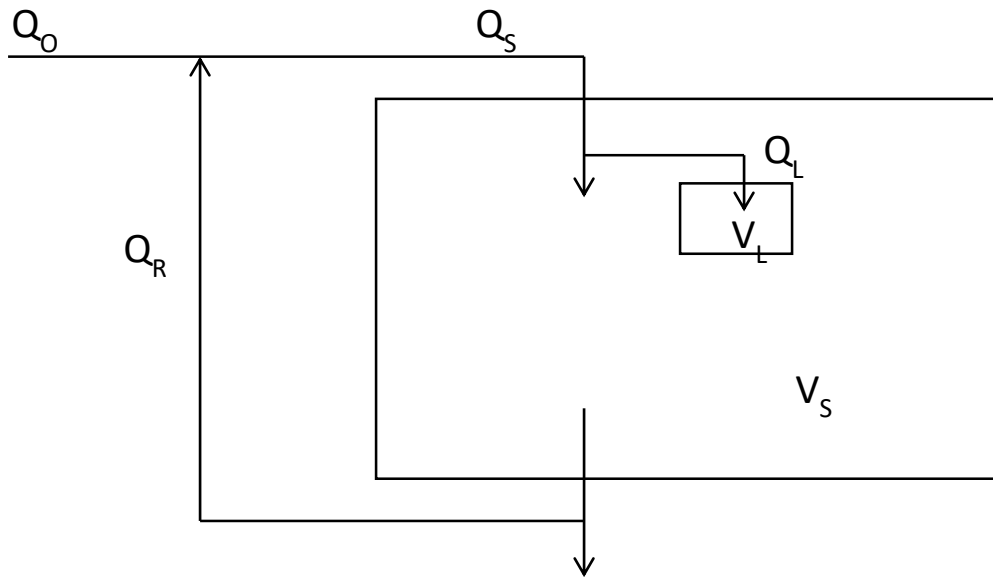


Figure 2. Ventilation with Recirculation